Geochemical Evaluation of the BirTlacsin Formation at Ghat Area Murzuq Basin, SW Libya.

By

Yousef Muftah Bokereis

Supervisor

Dr. Osama Shaltami

This Thesis was Submitted in Partial Fulfillment of the Requirements for Master's Degree of Science in Geology.

University of Benghazi

Faculty of Science

May 2018

Student Name: Yousef Muftah Bokereis El- Oshabi

Faculty: Faculty of Science

Title of Thesis: Geochemical Evaluation of the Bir Tlacsin Formation at Ghat Area Murzuq Basin, SW Libya

Defended and Approved date: ……/……/……

Examination Committee Signature:

Dr. Osama Shaltami (Supervisor)

Dr. Mohamed El-Faitouri Member (Internal Examiner)

Dr. Hamed El-Werfalli Member (External Examiner)

Hussein Elbarasi

(Dean of Faculty)

ACKNOWLEDGMENT

I would like to express my sincere gratitude to my supervisor Dr. Osama Shaltami, for his help and advice in the preparation of this thesis.

I would also like to thank the laboratories of StratoChem and the Nuclear Materials Authority of Egypt for preparing and analyzing samples.

Special thanks must go to all Staff Members of the Department of the Earth Sciences, Faculty of Science, Benghazi University, for their help during the academic years of my study at this department .

Yousef Muftah Bokereis

TABLE (List) OF CONTENTS

List of Tables

LIST OF FIGURES

Geochemical Evaluation of the BirTlacsin Formation at Ghat Area Murzuq Basin, SW Libya.

By

Yousef muftah bokereis

Supervisor

Dr. Osama Shaltami

ABSTRACT

The objective of the present study is the geochemical assessment of the Bir Tlacsin Formation at Ghat area, SW Libya. This assessment includes the depositional environment, paleo-oxygenation, paleoclimate, paleosalinity, provenance, tectonic setting, organic matter richness, kerogen type and thermal maturity. The field trips included five surface sections for the formation (Wadi Maghidat, Wadi Tashat, Wadi Anlakm, Wadi Iggiten, and Wadi Awzarq). This formation consists of sandstone and shale units. The sandstones are mainly greywackes. The observed clay minerals in the studied shales are smectite, kaolinite, gibbsite and chlorite. These minerals are the main carrier of TOC. The Th/Cr, Th/Sc and Th/Co ratios and the provenance discrimination diagrams indicated that the felsic (granitic) rocks found in the Air Mountains, central Niger, may be the possible source of the Bir Tlacsin Formation. Based on the ICV values, the shales are thermally immature whereas the sandstones are thermally submature to mature. Moreover, the organic geochemical data showed that the organic matter are thermally immature. The organic matter are essentially of marine origin. The Zr/Hf, Hf/Ta, Zr/Ta and B/Ga ratios indicated that the Bir Tlacsin Formation was deposited in a high salinity marine environment. Based on the trace element, Pr/Ph, Pr/n-C_{17} and Ph/n-C_{18} ratios the anoxic conditions were prevalent during deposition. The paleoclimate prevailing in the source area was almost semi-arid to semi-humid. The tectonic environment is essentially continental (active continental margin (C) and passive continental margin (D)). Generally, the shales are good source rocks. The discrimination diagrams showed that kerogen type II is the basic type in the shale samples. The hydrocarbons are mainly migrated (nonindigenous).

CHAPTER ONE
INTRODUCTION

1.1. General

Bir Tlacsin Formation is important from a petroleum point of view because it forms a barrier between the Mamuniyat reservoir and the Tanzuft source rock (Hallett, 2002).

The Bir Tlacsin Formation has been not defined as a formal unit and it not appear in the lithostratigraphic lexicon of Libya (Mamgain, 1980). It was firstly defined in the subsurface on the Tlacsin field (A1-70) in the Ghadamis Basin (Hallett, 2002), where it is well developed. Probably it will be equivalent to the Iyadhar Formation (Hallett, 2002) and many authors (e.g., Shalbak, 2015) consider that this unit could be equivalent to the Argilles microconglomeratique from southern Tunisia and Algeria. The Bir Tlacsin Formation has been correlated throughout the Ghadamis Basin (Echikh, 1992; Hallett, 2002; Deepender and Siddharth, 2015), and several wells drilling in the Murzuq Basin interstratified between the Mamuniyat and Tanezzuft formations, thin sequences attributed to the Bir Tlacsin Formation. It is well developed in the subsurface of blocks NC58, NC101, NC115, NC151 and NC186, but it is poorly exposed in surface outcrops (Shalbak, 2015). McDougall *et al.*, (2005) reported Bir Tlacsin sequences few meters thick cropping out near Ghat. The unit has been also reported from outcrops in western Gargaf.

1.2. Regional Geology

The roughly triangular Murzuq Basin in SW Libya is located between 21°- 29° N and 10°- 17° E. It is one of the several endorheic Basins of the North African platform, and covers an area over 350000 km^2 (Davidson *et al.*, 2000). The borders of the basin are the Gargaf Uplift to the North, the Tassili Plateau to the west, the Haruj and Tibesti Uplifts to the East. To the South the basin extends into the Djado Basin in Niger (Fig.1.1). The shape of the basin reflects a Variscan and Mesozoic overprint on an older

structural relief (Klitzsch, 2000). Strata on the basin flanks generally dip towards the basin center, exposing Cambrian to Quaternary rock units in a concentric pattern. A comprehensive and detailed geological map of Murzuq Basin is provided in (Fig. 1.2).

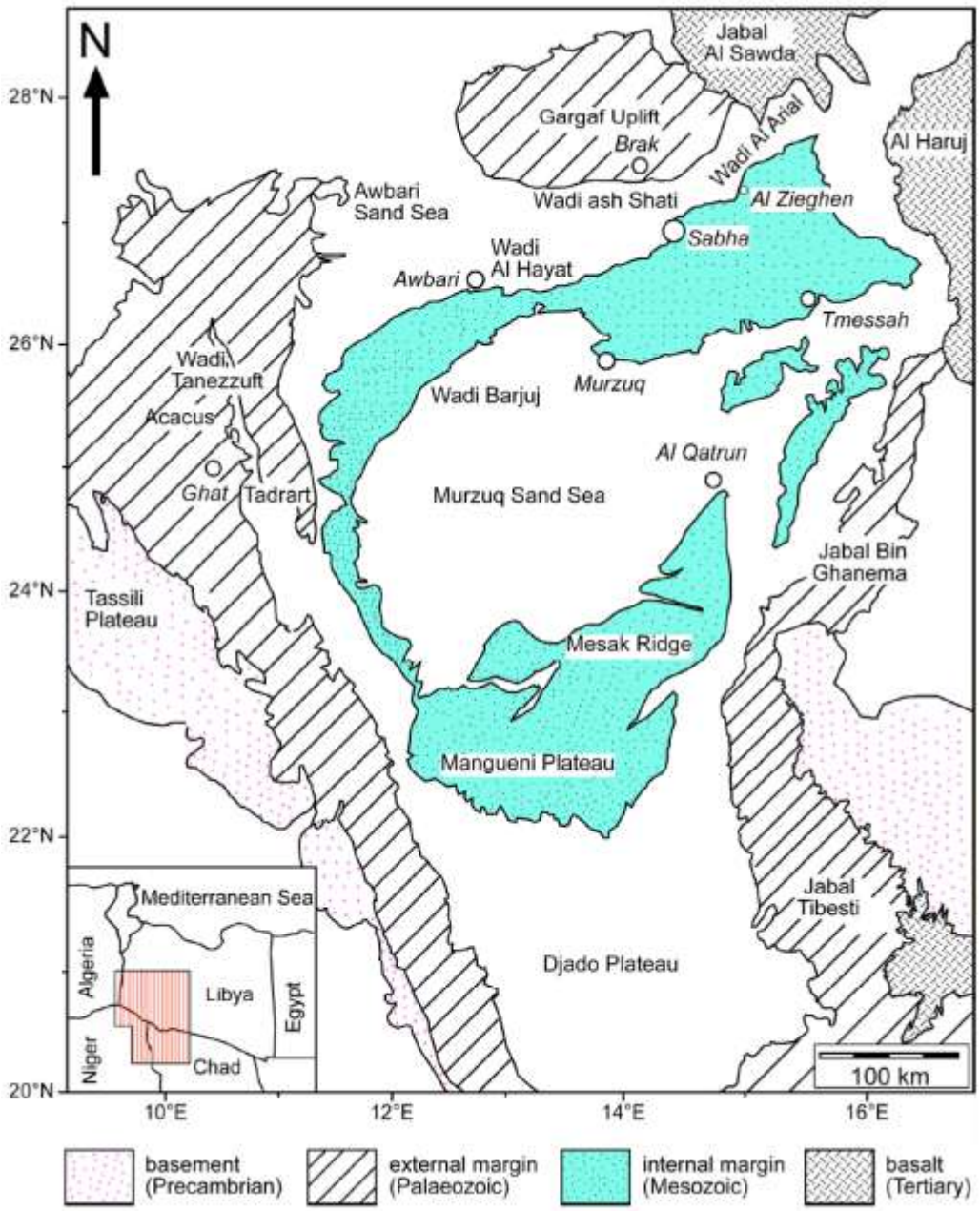

Fig. 1.1: Location map of the Ghat area showing the location of the sampled stations (after Abdullah, 2010)

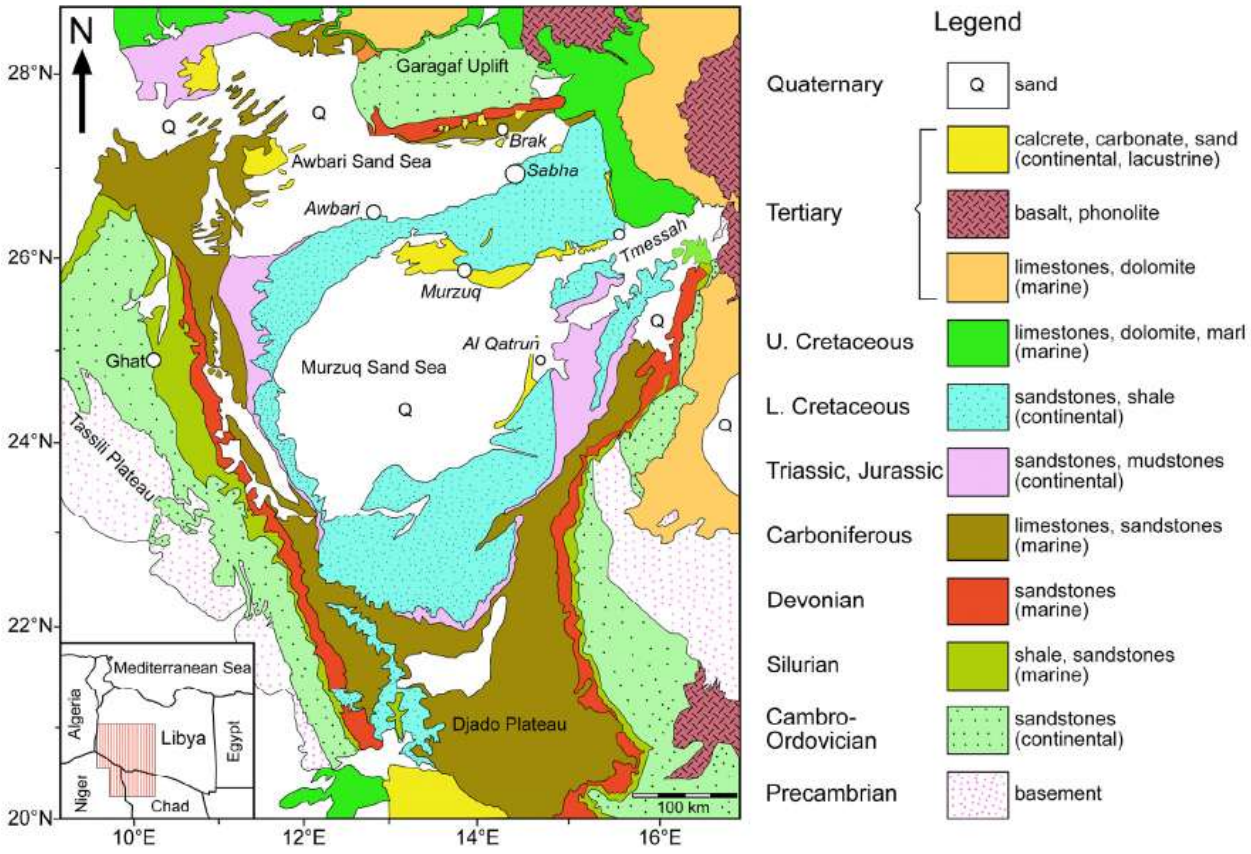

Fig. 1.2: Geological map of the Murzuq Basin showing the main stratigraphic units (after Abdullah, 2010)

Current knowledge of the geology of the Murzuq Basin, together with the important information obtained by mapping project of large areas of Murzuq Basin allows us to outline its geological history as follows: In the Paleozoic periods, large repeated NW-SE sea transgressions took place in the central Sahara. These transgressions occurred in different stages and reached different points in the south of the recent Sahara. Because of the variations in the range and duration of the transgressions in the Sahara, thick marine sedimentary successions were formed in the northern part of Sahara, which gradually decrease in thickness towards the southern part of the Sahara. During the Late Cambrian, the highly weathered Pan-African Basement was gradually covered by a shallow sea. The next and largest transgression in the Murzuq Basin was in the Ordovician, which was intense enough to reach as far south as the location of present-day Lake Chad (Grunert, 1983). It left fine-grained marine

sandstones and claystones, which usually cover the coarse-grained fluvial sandstones from the Middle to Late Cambrian (Hasawnah Formation). These Cambro-Ordovician Formations form the outer edge of the Murzuq Basin. The third largest sea transgression occurred during the Silurian; it also reached the southern central Sahara and again resulted in the deposition of clay and sandstones the claystones generally represent the flooding phase (transgression), whereas the sandstones are assigned to the regression phase. These deposits are the marine graptolite-bearing Tanezzuft Formation and the younger Acacus Formation, which are overlain by the Tadrart Formation of Lower Devonian age. After a temporary retreat in the Early Devonian, the sea over flooded the central Sahara again in the Middle Devonian time and reached as far south as latitude 15° N, whereby it submerged Acacus and Tadrart mountains and deposited the Ounkasa Formation, which consists of marine sandstones and minor clay, siltstones. The enormous transgressions of Silurian and Middle Devonian Sea into the area of today's central Sahara was possible only due to large NW-SE trending troughs and uplifts structures, whose formation probably started in the Cambrian age, and reached its maximum range in the Upper Devonian/Lower Carboniferous periods. The Murzuq Basin was situated on the axis of the broad Murzuq-Djado Trough at that time, which can be followed to the present latitude 18° N in Republic of Chad (Klitzsch, 2000). It was bordered by the Tihemboka Uplift in the West, and by Tripoli-Tibesti Uplift in the East. The evidence for formation of uplifts and trough structures can be deduced from the presence of unconformity surfaces and variations in the thickness of different sediments. For instance, in case of the Tihemboka Uplift at the northwest edge of the Murzuq Basin, where Carboniferous sediments directly superimpose the Cambro-Ordovician formations, their Silurian and Devonian sediment covers were entirely weathered due to elevation during a tectonic uplift (Klitzsch, 2000). On the other hand, the sediments in the center of the trough have a much greater thickness of more than 1000 m in the deep protected areas. Even in the western margin of the Murzuq-Djado Trough, for example in the Acacus Mountains, the Silurian and Devonian deposits reach about 1200 m in thickness (El Chair, 1984). According to Klitzsch (1970) the structural orientation gradually changed in the Lower Carboniferous from NW-SE direction to NE-SW direction caused by the Hercynian orogeny. Hence, in the Lower Carboniferous, the

sea transgression overflooded the Al Hamada Basin in the North and extended southward to approximately latitude 20° N in the middle Sahara. The Gargaf Uplift prevented the later transgressions into Murzuq Basin (Seidl and Rohlich, 1984). Therefore, the continental conditions prevailed in the Murzuq Basin and have continued until present time. The east edge of the Murzuq Basin was occupied by a shallow sea in the Upper Cretaceous/Lower Tertiary period, which originated from the Sirte Basin and extended to the northern edge of the Tibesti Mountains (Furst and Klitzsch, 1963). Subsidence in the basin increased progressively from the Late Palaeozoic to Mesozoic, while the basin was continuously being filled with continental sediments (clay-, silt- and sandstones). During the Late Tertiary and Quaternary, sand dunes were developed under arid climate conditions, which continued with short interruptions during the middle Miocene and Pleistocene periods, when the dry desert climate changed to a humid climate with heavy rainfall, which led to the creation of several freshwater lakes in many locations in the Central Sahara (Pachur and Altmann, 2006).

1.3. Geomorphology of the Murzuq Basin

Morphologically, the Murzuq Basin is one of the principal features of the central Sahara, and can be described as an enormous, flat dish of approximately 1000km long and 600km wide, surrounded by an outward-turned cuesta landscape. Strata on the flanks dip gently towards the basin centre, exposing all rock units around the flanks in a concentric pattern . According to Thiedig *et al.*, (2000), the present shape of the continental endorheic Murzuq Basin was formed during the Tertiary, by deflation and fluvial erosion during humid intervals. These processes carved out the Mesak Ridge between the present large sand Sea areas. The main morphological units of this basin consist of plateaus, bench lands (cuestas), planation, wadies and sand dunes cover. On the basis of morphological features, the Murzuq Basin can be subdivided into external and internal margins. This basin margins are separated from each other by low lands covered mostly by gravelly sand and sand dunes .

1.4. Current Climate of the Murzuq Basin

The Murzuq Basin lies presently in a completely arid climatic area. The current climate of western North Africa is influenced by Atlantic currents; that of southeastern North Africa is affected by the Indian monsoonal circulation. According to Abdullah (2010) stable isotope analysis of speleothems from different locations in North Africa, Namibia, and northern Oman in the southern part of the Arabian Peninsula indicate that during the peaks of interglacial periods, the limit of the monsoon rainfall shifted far north of it is present location, and each pluvial period coincided with an interglacial stage of the marine oxygen isotope record. In the early decades of the 20th century a numerous of meteorological stations were established in the Murzuq Basin such as Sabha, Brak, Murzuq, Awbari, Al Qatrun and Ghat etc, which measured daily temperature, rainfall and relative air humidity of Murzuq Basin.

1.5. Objectives

The main objective of the present work is to evaluate the surface sections of the Bir Tlacsin Formation at Ghat area in terms of organic and inorganic geochemical characteristics. Using geochemical data we can discuss the following:

1) Depositional environment, paleo-oxygenation, paleoclimate, paleosalinity, provenance and tectonic setting.

2) Organic matter richness, kerogen types, and thermal maturation of the Bir Tlacsin Formation.

1.6. Previous Studies

Most previous studies on the Bir Tlacsin Formation were focused on the subsurface rocks of this formation, while there are very few studies of the exposed rocks. In general, there is no geochemical study of the surface rocks of the Bir Tlacsin Formation. However, the following is a summary of some prior studies on the Bir Tlacsin Formation. Echikh and Sola (2000) found that the core samples of the Bir

Tlacsin Formation show that the unit was originated as debris flow deposits in marine paleoenvironments varying from very proximal to distal. However, many authors are in disagreement with this interpretation. For example, Blanpied *et al.,* (2000) consider the Bir Tlacsin Formation as wave dominated shoreface deposits accumulated during the basal Silurian transgression.

Miles (2001) studied the Bir Tlacsin Formation in the subsurface of block NC115. He found that the palynological assemblages suggest that the Bir Tlacsin Formation was deposited during the Hirnantian stage of the Ordovician.Hallett (2002) found that in the Ghadamis Basin the Bir Tlacsin Formation reaches 100m in thickness in well Cl-NC100 and in the Murzuq Basin it has a thickness of 130m in well Dl-NC115.McDougall *et al.,* (2005) defined the Bir Tlacsin Formation cropping out in the Ghat zone as a broadly coarsening-up thin sequence, composed of interbedded mud and silt or fine grained sandstone. In this zone, the top of the formation is marked by iron-rich burrowed sandstone lag forming a hard ground and directly overlain by the Tanezzuft shales. Shalbak (2015) found that the areal extent of the Bir Tlacsin Formation is limited to the western Libya. It is present in the subsurface of the Ghadamis and Murzuq basins and also is sparsely present in thin sequences cropping in the Ghat and western Gargaf zones. He also found that the Bir Tlacsin Formation has not been reported from the Cyrenaica nor Kufrah basins.

1.7. Stratigraphy

A stratigraphic column for the Murzuq Basin is depicted in (Fig. 1.3). The sedimentary deposits in the basin range from the Cambrian to the Quaternary in age, and can be subdivided into different sedimentary units (Mamgain, 1980; Abugares and Ramaekers, 1993; Aziz, 2000; El Hawat and Ben Rahuma, 2008; Abdullah, 2010; Shalbak, 2015).

The field work was done by Shaltami (2013). The field trips included five surface sections for the Bir Tlacsin Formation at Ghat area, SW Libya (Figs. 1.5-12). These sections are Wadi Maghidat area (25° 23' 46.11"N, 10° 3' 8.96" E), Wadi Tashat

area (25° 23' 45" N, 11° 2' 00" E), Wadi Anlakm area (24° 1' 00" N, 10° 3' 8" E), Wadi Iggiten area (23° 21' 22" N, 11° 00' 00" E), and Wadi Awzarq area (23° 5' 00" N, 10° 9' 15" E, Fig. 1.1).

In the studied sections the lower boundary of the Bir Tlacsin Formation is conformable with the underlying Mamuniyat Formation (Late Ordovician rocks), while the upper boundary is conformable with the overlying Tanezzuft Formation (Early Silurian rocks).

The lithostratigraphic correlation was made between the studied sections; the datum is the top of the pebbly shale unit (Fig. 1.9). This correlation shows that the shale units (shale and pebbly shale) are present in all sections (except for unit 5 in the Wadi Anlakm). Moreover, the author made a correlation between the surface composite columnar section and the idealized lithological log for the Bir Tlacsin Formation in the subsurface of the Murzuq Basin (designed by Shalbak, 2015); the datum is the top of the sandstone unit (Fig. 1.10). Clearly, there are four shale units in the subsurface log, while only three units are present in the surface sections.

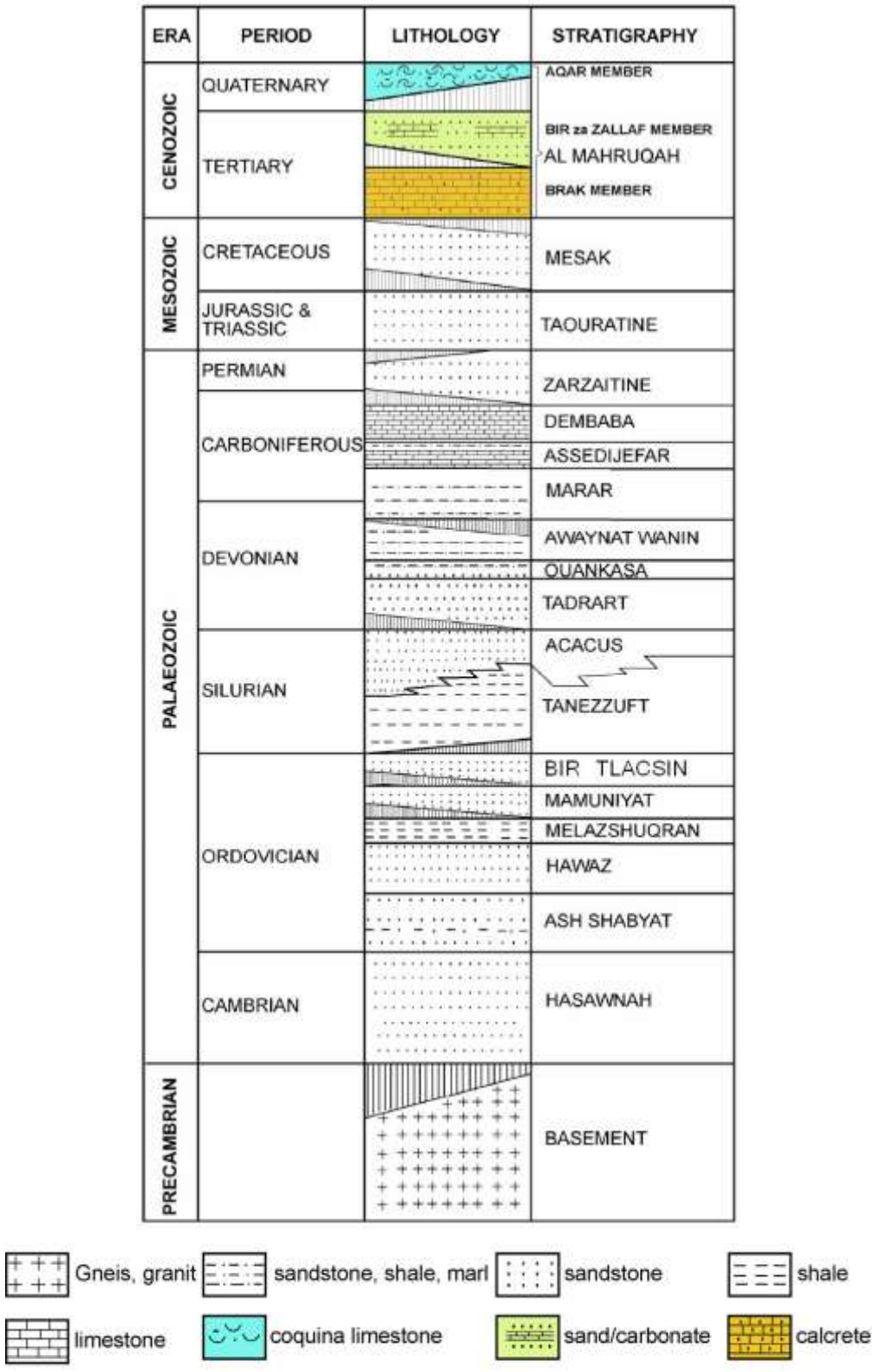

Fig. 1.3: Stratigraphic chart of the exposed rocks in the Murzuq Basin (modified after Abdullah, 2010)

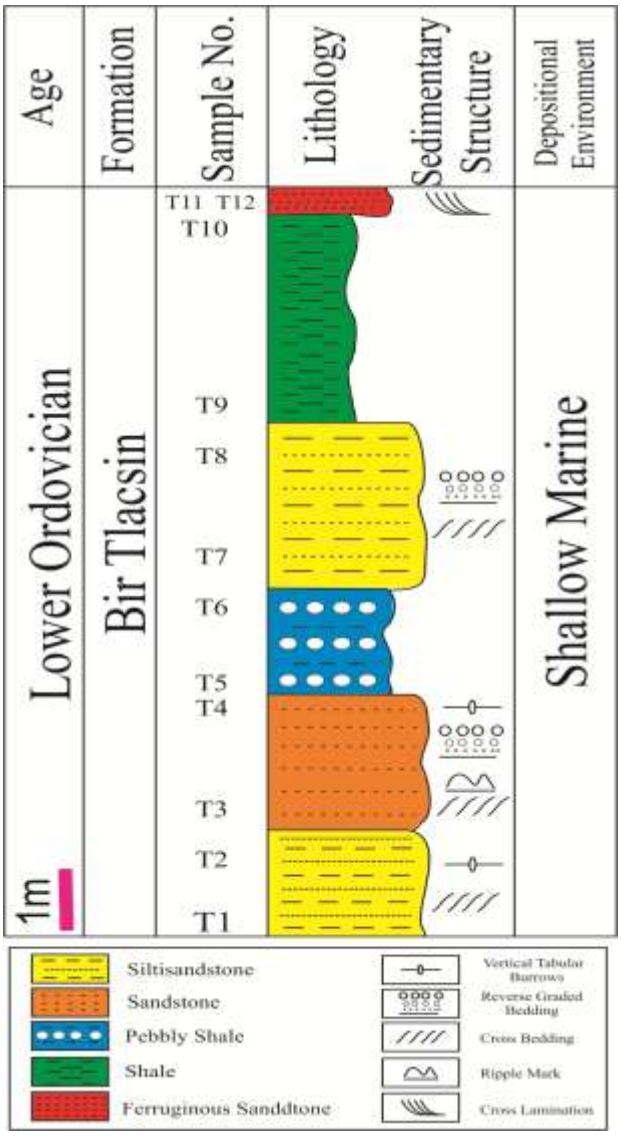

Fig. 1.4: Lithostratigraphic column of the Bir Tlacsin Formation at Wadi Maghidat

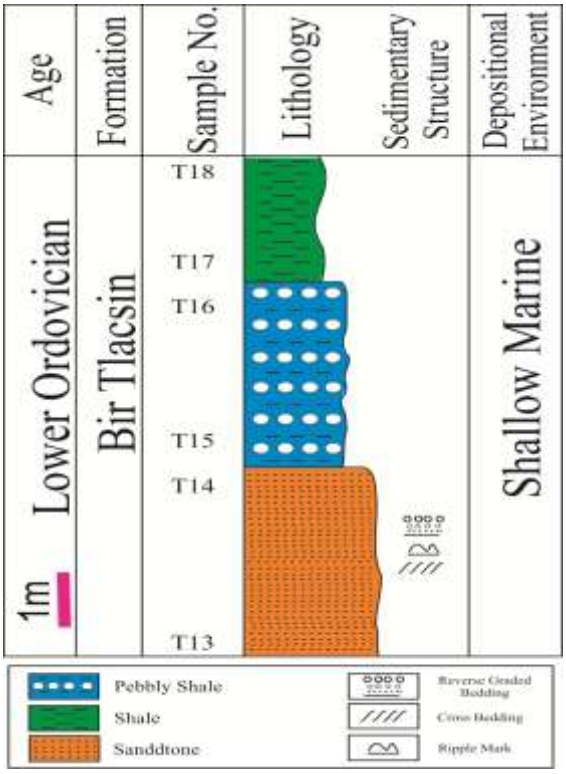

Fig. 1.5: Lithostratigraphic column of the Bir Tlacsin Formation at Wadi Tashat

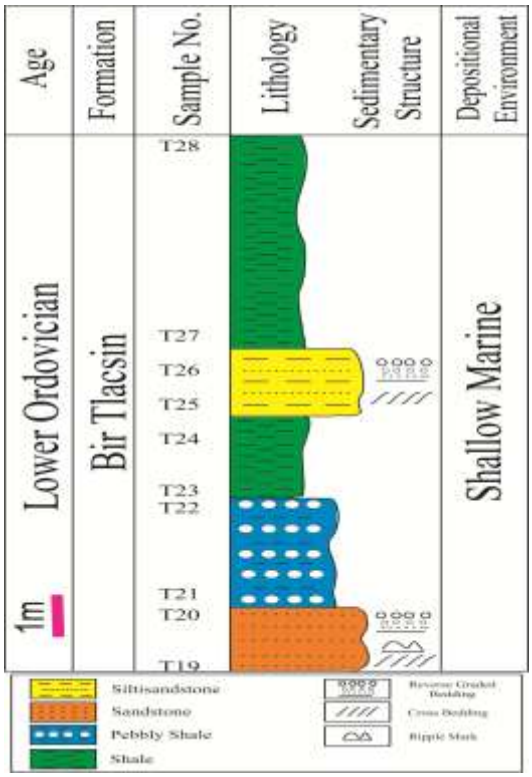

Fig. 1.6: Lithostratigraphic column of the Bir Tlacsin Formation at Wadi Anlakm

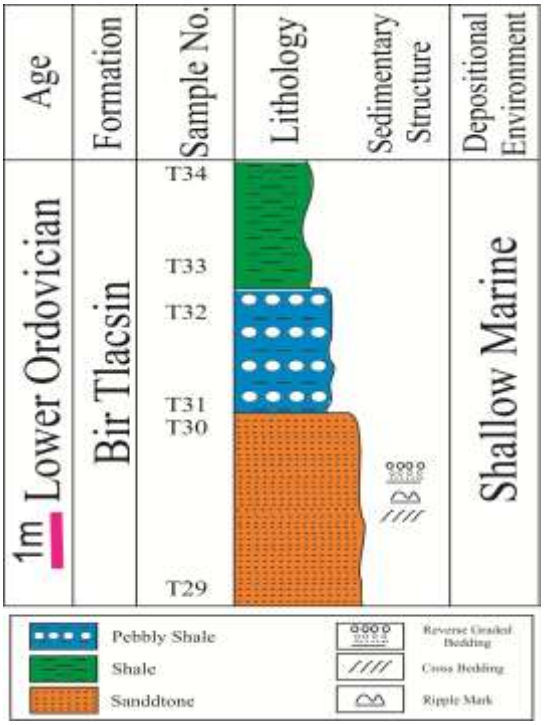

Fig. 1.7: Lithostratigraphic column of the Bir Tlacsin Formation at Wadi Iggiten

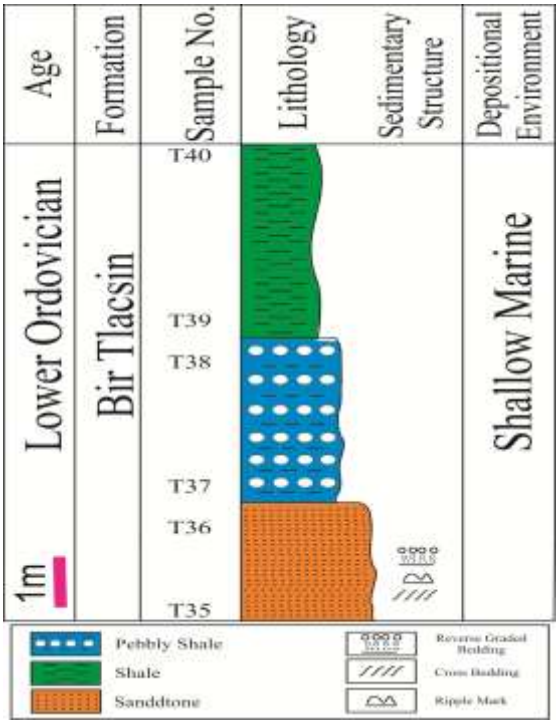

Fig. 1.8: Lithostratigraphic column of the Bir Tlacsin Formation at Wadi Awzarq

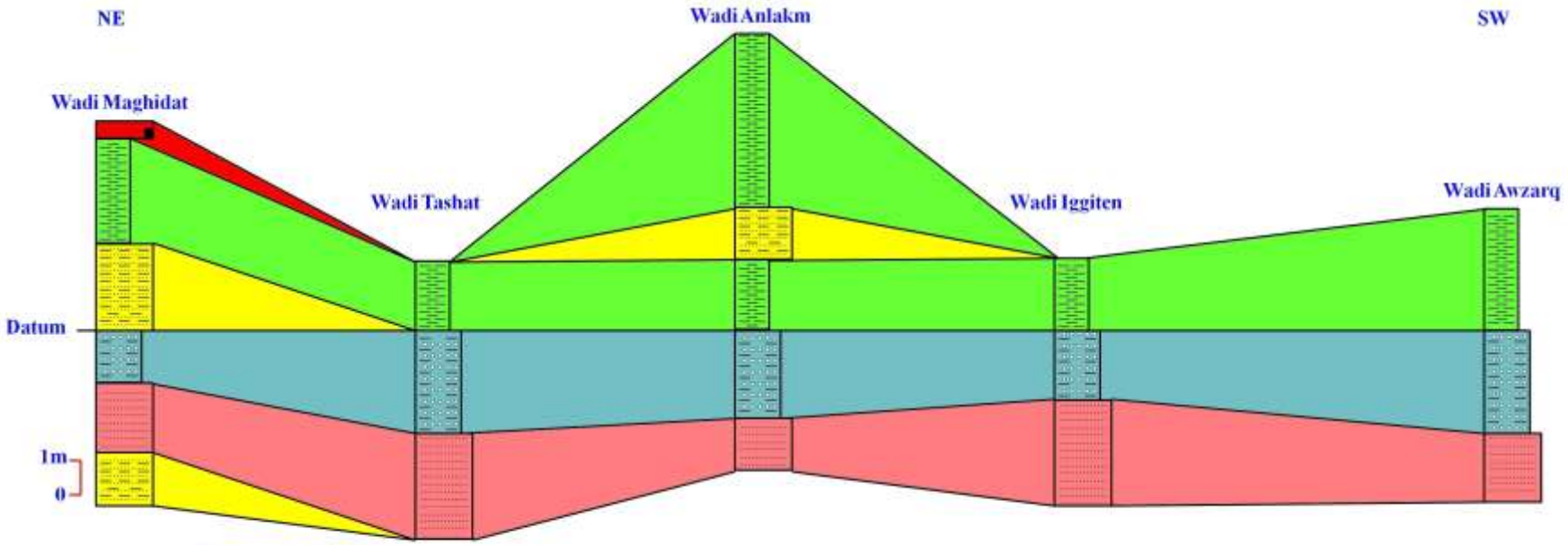

Fig.1.9: Lithostratigraphic correlation between the surface sections of the Bir Tlacsin Formation.

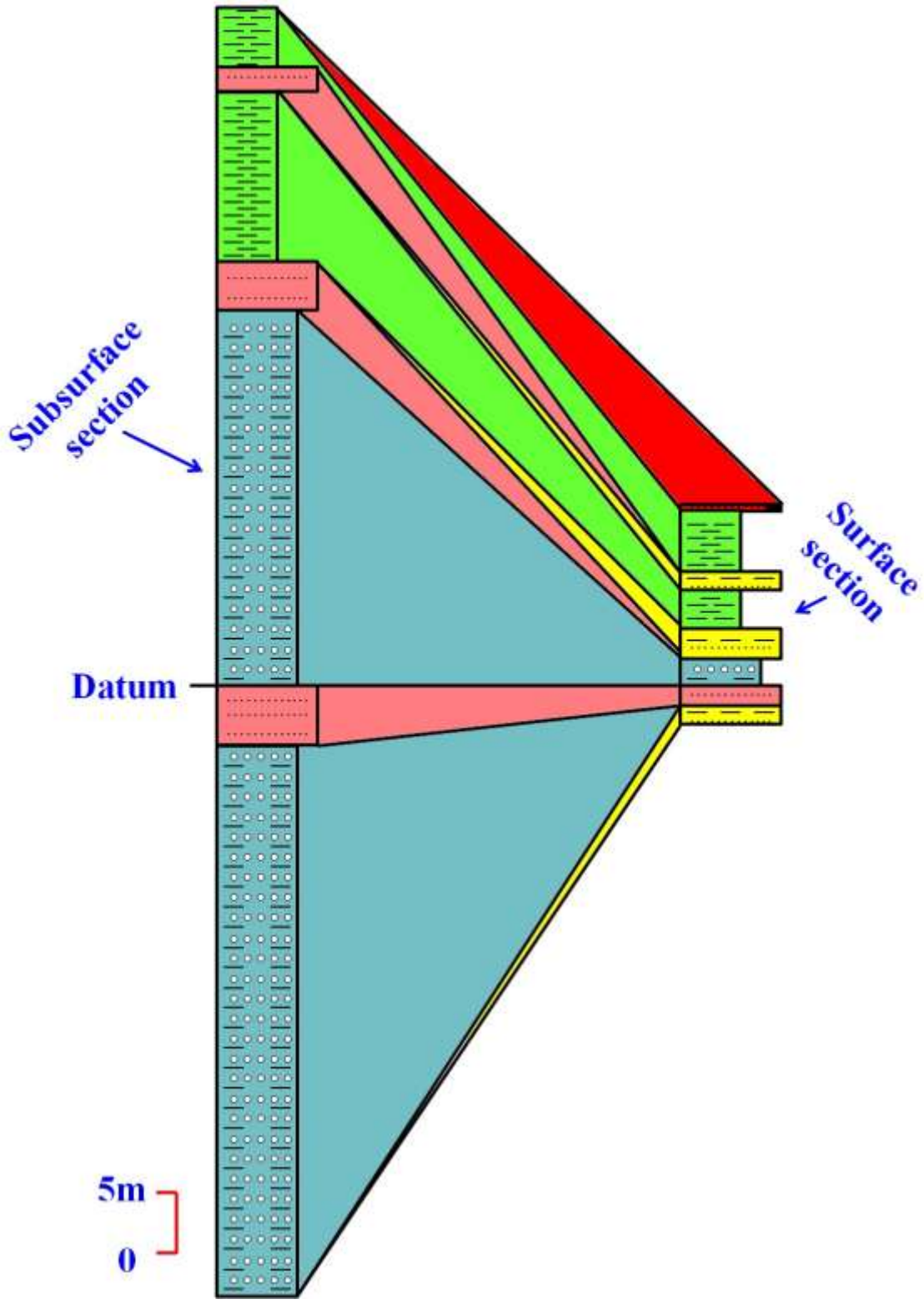

Fig. 1.10: Lithostratigraphic correlation between the surface composite columnar section and the idealized lithological log for the Bir Tlacsin Formation in the subsurface of the Murzuq Basin

1.8. Methodology

1.8.1. Sampling

Samples were collected by Shaltami in (2013). About 40 samples were collected from the Bir Tlacsin Formation at Ghat area (two samples of each unit), from 5 stations (Wadi Maghidat, Wadi Tashat, Wadi Anlakm, Wadi Iggiten, and Wadi Awzarq, Fig. 1.1).

1.8.2. Analytical Techniques

1.8.2.1. Inductively Coupled Plasma-Mass Spectrometry (ICP-MS)

The studied rock samples were grinded in an agate mortar and sieved through a 200 ASTM (American Society for Testing and Materials) mesh for chemical analysis. About 0.2 g of samples were digested with 4ml HNO_3 and 1ml of $HClO_4$ for 24 hours in a tightly closed Teflon vessel on a hot plate at 150°C, heated to dryness, and then digested with a mixture of 4 ml of HF and 1ml of $HClO_4$. Later, the solution was evaporated to dryness, and extracted with 10ml of 1% HNO_3. The digested samples were measured for major oxides and trace elements by Inductively Coupled Plasma-Mass Spectrometry (Fig. 1.11) technique (ICP-MS Plasma QUAD 3). This analysis was done the Nuclear Materials Authority of Egypt.

1.8.2.2. Rock-Eval Pyrolysis and Total Organic Carbon (TOC) Measurements

Rock-Eval Pyrolysis and TOC measurements were performed only for shale samples. To minimize the effects of surface weathering, surface materials were removed before sampling at approximately 0.5 m. The shale samples were washed with doubly distilled water and dried at room temperature prior to analysis. The samples were crushed to less than 200 mesh. These samples were ground to a fine powder (particle size of <150 μm) using a ring-mill (Rocklabs). Rock-Eval pyrolysis of powdered rock (10-50 mg) was carried out on a Rock-Eval 6 instrument (Fig. 1.12), while the TOC was measured on a Leco instrument (Fig. 1.13). These analyses were done in the laboratories of StratoChem in Egypt.

1.8.2.3. Gas Chromatography-Mass Spectrometry (GC-MS)

A Gas Chromatography-Mass Spectrometry (Fig. 1.14), housed at the laboratories of StratoChem in Egypt, was used in this study to analyze the shale samples. About 30 g of ground sediment was extracted in an ultrasonic bath for two hours using a 9:1 mixture of dichloromethane (DCM) and methanol (MeOH). The solvent extract was then filtered and excess solvent removed by carefully heating on a sand bath (60°C) to obtain the bitumen. Asphaltenes were precipitated by mixing the bitumen with an excess of chilled n-heptane. Maltenes were fractionated using a small- scale column chromatographic method (Bastow *et al.,* 2007). In brief, the sample (maltenes, about 10 - 20 mg) was applied to the top of a small column (5.5 cm × 0.5 cm i.e.) of activated silica gel (120°C, 8 h). The aliphatic hydrocarbon (saturated) fraction was eluted with n-pentane (2 mL); the aromatic hydrocarbon fraction with a mixture of n-pentane and DCM (2 mL, 7:3 v/v,); and the polar (NSO) fraction with a mixture of DCM and MeOH (2 mL, 1:1 v/v). Aliphatic and aromatic fractions were analyzed by (Gas Chromatography-Mass Spectrometry) GC-MS using a Hewlett Packard (HP) 5973 mass-selective detector (MSD) interfaced to a HP6890 gas chromatograph (GC). A HP5MS (J and W Scientific) GC column (5% phenylmethylsiloxane stationary phase) was used with helium as the carrier gas. The GC oven was programmed from 40°C to 310°C at 3°C/min, after which it was held isothermal for 30 min. Samples were dissolved in nhexane and introduced by the HP6890 auto-sampler into a split-splitless injector operated in the pulsed-split- less mode. Biomarker data were acquired in a full-scan mode (m/z 50 -500). The ion source was operated in electron ionization (EI) mode at 70 eV. Selected ion monitoring (SIM) was used to identify the terpanes, steranes and triaromatic steroids by monitoring m/z 85 and 217 ions.

Fig. 1.11: Inductively Coupled Plasma-Mass Spectrometry (ICP-MS) instrument

Fig. 1.12: Rock-Eval 6 instrument

Fig. 1.13: Leco instrument

Fig. 1.14: Gas Chromatography-Mass Spectrometry (GC-MS) instrument

CHAPTER TWO
INORGANIC GEOCHEMISTRY

2.1. Introduction

Clastic sedimentary rocks have vital information about the composition, tectonic setting and evolution of continental crust, mainly when the traditional petrographic methods are unclear (Baiyegunhi *et al.,* 2017). Nonetheless, their chemical and mineralogical composition can be influenced by factors like source rock characteristics, weathering, sorting processes during transportation, sedimentation and diagenetic processes to an extent (Nesbitt and Young, 1996; Armstrong-Altrin, 2009; Beygi and Jalali, 2018). Trace elements such as high field strength elements (HFSE) and rare earth elements (REE) are thought to be useful indicators of provenance, geological processes and tectonic setting due to their relatively low mobility and insolubility during sedimentary processes (McLennan *et al.,* 1993; Shaltami *et al.,* 2016). Hence, the geochemistry of clastic sediments (i.e. sandstone and shale) reflects a combination of provenance, chemical weathering, hydraulic sorting, and abrasion (Nesbitt *et al.,* 1997; Yan *et al.,* 2007; Shaltami *et al.,* 2018).

In geochemical provenance studies, fine grained sedimentary rocks like shales are considered to be the most useful rock because of their homogeneity before deposition, post-depositional impermeability and higher abundance of trace elements (Condie, 1993; Bracciali *et al.,* 2007). Some relatively immobile elements like some HFSE and REE show very low concentrations in natural waters and are transported almost quantitatively throughout the sedimentary process from parent rocks to clastic sediments (Condie, 1991). The relative distribution or enrichment of these immobile elements in felsic and basic rocks have been used to infer the relative contribution of felsic and basic sources in shales from different tectonic environments (Wronkiewicz and Condie, 1990; Baiyegunhi *et al.,* 2017). For example, La and Th are enriched in felsic rocks, whereas Sc, Cr, and Co are more concentrated in basic rocks relative to

felsic rocks (Cullers and Podkovyrov, 2000). These elements are relatively immobile during weathering (Cullers *et al.,* 1987). Hence, the ratios of La or Th to Co, Sc, or Cr are sensitive indicators of source rock compositions (Cullers and Podkovyrov, 2000). Similarly, felsic igneous rocks contain negative Eu anomalies, whereas basic igneous rocks have little or no Eu anomalies, and the size of the negative anomalies in the provenance seems to be preserved in fine grained sediment (Baiyegunhi *et al.,* 2017). Furthermore, some major elements such as alkali and alkali earth elements, which are water mobile elements and very sensitive to climatic change, can be used as a proxy of paleoclimate evolution (Nesbitt and Young, 1984; Wei *et al.,* 2004). Geochemical data on sandstones of unmetamorphosed sedimentary sequences deposited in epicratonic or intracratonic basins also give important clues on paleoweathering conditions, variations in provenance composition and tectonic settings (Condie *et al.,* 2001; Araujo *et al.,* 2010).

Several researchers (e.g., Bhatia, 1983) have proposed K_2O/Na_2O versus SiO_2 tectonic setting discrimination diagrams for sedimentary rocks in order to identify tectonic setting of unknown basins. These diagrams are still commonly used to deduce the tectonic setting of ancient basins. However, more detailed results can be obtained using the calc-alkaline oxide ternary diagram ($CaO-Na_2O-K_2O$) of Bhatia (1983) and modified by Toulkeridis *et al.,* (1999). Nesbitt and Young (1984) documented that the index of compositional variability (ICV), K_2O/Al_2O_3 ratio, chemical index of alteration (CIA) and Al_2O_3-(CaO^*+Na_2O)-K_2O (A-CN-K) ternary plots are useful geochemical parameters for the study of provenance and maturity of the rocks. In addition, Roser and Korsch (1986) and McCann (1991) used alkali metal oxides to reveal information about the provenance of clastic sediments. Recent geochemical investigations on sandstones and shales have focused on deciphering the provenance and tectonic evolution of sedimentary basins (e.g., Shaltami *et al.,* 2016).

All the samples show high concentration of SiO_2 and Al_2O_3. The Na_2O, CaO, MgO and Fe_2O_3 contents are moderately high. The concentrations of TiO_2, MnO, K_2O and P_2O_5 are faintly low. Generally, the SiO_2, TiO_2 and CaO contents in the sandstones

are slightly higher than the shales. On the other hand, shales contain more Al_2O_3 content than the sandstones, which reflect, in agreement with Madhavaraju and Lee (2010), its association with clay-sized phases. In general, the difference in the concentration of high field strength elements (Zr, Hf, Nb, Ta, Th and U) and heavy metals (Ga, B, V, Cr, Ni, Co, Cu and Zn) between sandstones and shales has no geochemical significance.

Table 2.1: Chemical analysis data (major oxides in wt%, trace elements in ppm) of the Bir Tlacsin Formation at Wadi Maghidat

Sample No.	T1	T2	T3	T4	T5	T6	T7	T8	T9	T10	T11	T12
SiO_2	52.59	52.68	61.23	60.21	51.74	50.94	58.79	59.25	53.86	53.51	57.09	57.00
TiO_2	0.57	0.50	0.67	0.74	0.33	0.46	0.89	0.52	0.30	0.20	0.91	0.93
Al_2O_3	24.25	24.34	15.51	15.19	26.67	25.50	12.07	13.19	24.84	24.28	14.07	13.98
Fe_2O_3	4.32	4.32	6.17	6.38	4.93	5.06	6.77	3.00	5.36	5.66	10.11	10.00
MnO	0.03	0.03	0.06	0.08	0.05	0.05	0.08	0.08	0.05	0.05	0.09	0.09
MgO	1.41	1.39	2.83	3.45	1.53	1.49	1.57	1.80	1.58	1.69	4.57	4.48
CaO	1.11	1.09	2.61	2.96	1.49	1.32	7.15	8.95	1.00	1.19	4.08	3.99
Na_2O	7.13	7.09	4.52	3.88	7.26	7.58	3.44	3.79	6.96	6.85	2.76	2.67
K_2O	0.27	0.28	1.74	1.65	0.31	0.20	1.78	2.01	0.45	0.46	0.53	0.44
Cl	0.04	0.04	0.06	0.09	0.03	0.03	0.07	0.08	0.03	0.03	0.09	0.09
P_2O_5	0.18	0.16	0.26	0.27	0.21	0.19	0.29	0.21	0.14	0.27	0.22	0.26
Ga	21.33	22.00	17.09	18.41	7.92	6.65	15.29	17.05	6.22	5.54	22.25	21.09
B	110.88	111.55	106.64	107.96	97.47	96.20	104.84	106.60	95.77	95.09	117.17	117.44
V	158.67	154.62	249.32	188.21	157.44	166.42	138.63	146.14	155.21	181.50	187.09	185.00
Cr	70.56	72.90	109.18	80.08	66.83	59.72	58.34	59.17	71.90	58.26	84.96	80.87
Ni	46.67	60.10	62.44	54.93	51.63	59.97	22.27	30.79	54.50	51.84	53.81	53.72
Co	8.96	11.42	10.41	10.52	9.23	10.29	4.10	5.39	10.37	9.79	10.40	9.31
Cu	80.36	78.39	81.59	81.19	87.18	87.45	48.32	75.36	91.72	87.26	80.07	79.98
Zn	33.71	36.58	27.21	26.37	37.39	33.89	19.61	29.00	33.35	34.27	25.25	25.16
Zr	168.37	172.05	129.53	128.26	156.96	157.98	141.53	115.86	157.78	154.92	128.42	128.61
Hf	2.92	2.53	1.60	1.39	2.47	2.40	1.83	1.88	2.52	2.11	1.55	1.74
Nb	8.51	7.80	5.87	6.22	7.63	8.17	6.48	5.89	7.74	6.60	6.38	6.57
Ta	1.19	1.22	0.90	0.93	1.07	1.14	0.93	0.97	1.05	1.10	0.69	0.78
Th	6.60	5.48	3.88	3.82	5.60	5.71	2.88	2.64	5.41	5.80	3.98	4.17
U	8.72	8.18	5.41	5.25	7.73	7.83	4.65	4.96	7.80	8.39	5.41	6.60
Sc	16.81	16.10	17.84	17.76	17.09	17.18	13.17	12.85	16.79	18.96	17.92	18.11

Table 2.2: Chemical analysis data (major oxides in wt%, trace elements in ppm) of the Bir Tlacsin Formation at Wadi Tashat

Sample No.	T13	T14	T15	T16	T17	T18
SiO_2	61.09	61.15	52.57	52.00	52.26	51.70
TiO_2	0.81	0.75	0.16	0.22	0.25	0.46
Al_2O_3	15.37	15.43	24.17	24.11	24.29	26.18
Fe_2O_3	6.31	6.25	6.57	6.67	6.78	4.85
MnO	0.05	0.09	0.05	0.05	0.05	0.05
MgO	2.69	2.75	1.50	1.67	1.59	1.54
CaO	2.47	2.53	1.25	1.50	1.37	1.23
Na_2O	4.38	4.44	6.28	6.58	6.33	7.08
K_2O	1.60	1.66	0.57	0.39	0.50	0.32
Cl	0.07	0.08	0.03	0.03	0.03	0.03
P_2O_5	0.19	0.25	0.26	0.25	0.25	0.17
Ga	18.11	17.21	8.17	9.09	6.71	6.52
B	107.66	106.76	97.72	98.64	96.26	96.07
V	249.18	249.24	153.65	145.41	167.50	164.12
Cr	110.64	115.70	68.66	60.00	65.11	58.96
Ni	62.30	62.36	32.21	29.82	52.00	54.81
Co	11.27	11.33	6.22	5.16	9.95	10.61
Cu	81.45	81.51	88.62	89.14	101.37	105.56
Zn	27.07	27.13	36.27	32.39	45.60	41.80
Zr	129.67	129.61	143.55	144.27	161.32	160.68
Hf	1.74	1.68	2.09	1.92	2.81	2.52
Nb	6.00	5.95	7.22	7.00	8.08	7.79
Ta	0.73	0.77	0.89	0.81	1.17	1.08
Th	4.00	3.96	3.58	4.89	6.08	4.76
U	7.55	7.49	5.37	6.81	8.94	6.66
Sc	17.98	17.92	16.57	15.09	18.00	17.27

Table 2.3: Chemical analysis data (major oxides in wt%, trace elements in ppm) of the Bir Tlacsin Formation at Wadi Anlakm

Sample No.	T19	T20	T21	T22	T23	T24	T25	T26	T27	T28
SiO_2	60.30	61.36	52.05	52.27	55.33	56.66	59.00	59.37	53.55	51.98
TiO_2	0.65	0.56	0.40	0.33	0.19	0.32	0.61	0.49	0.33	0.41
Al_2O_3	15.28	15.64	23.31	23.35	21.70	24.00	13.00	13.31	25.00	25.67
Fe_2O_3	6.29	6.00	8.52	8.42	8.65	6.23	3.11	2.90	5.22	4.48
MnO	0.05	0.04	0.05	0.05	0.05	0.05	0.09	0.06	0.05	0.05
MgO	3.54	2.96	2.21	2.17	2.62	1.84	1.61	1.92	1.44	1.60
CaO	3.05	2.74	1.10	1.07	1.55	1.43	8.76	9.07	1.10	1.20
Na_2O	3.97	4.65	5.82	5.70	3.85	3.48	3.60	3.91	6.88	7.28
K_2O	1.74	1.87	0.47	0.44	0.29	0.41	1.82	2.13	0.42	0.40
Cl	0.06	0.05	0.03	0.03	0.03	0.03	0.09	0.07	0.04	0.04
P_2O_5	0.13	0.09	0.22	0.20	0.20	0.24	0.24	0.29	0.29	0.30
Ga	17.00	16.92	6.64	8.13	12.25	13.17	20.06	18.00	8.92	10.00
B	106.55	106.47	96.19	97.68	101.80	102.72	109.61	107.55	98.47	99.55
V	188.30	249.45	162.95	155.80	167.84	175.35	145.95	146.26	137.06	132.20
Cr	86.17	108.91	58.54	57.71	72.07	81.05	58.98	59.20	55.57	61.65
Ni	55.02	62.57	25.95	26.57	52.11	51.52	30.60	30.91	44.34	46.08
Co	10.61	11.54	4.44	4.92	10.12	9.86	5.20	5.51	8.14	8.35
Cu	81.28	81.72	73.80	78.90	83.38	84.00	75.17	75.48	107.41	106.09
Zn	26.46	27.34	24.23	23.06	36.86	38.43	28.83	29.14	42.58	46.49
Zr	128.17	129.40	186.49	185.85	160.00	158.44	115.95	115.78	198.54	193.46
Hf	1.30	1.47	2.71	2.59	2.44	2.53	1.97	1.80	3.07	3.14
Nb	6.13	5.74	7.89	7.95	7.84	7.73	5.98	5.81	9.98	9.47
Ta	0.84	0.76	1.15	1.11	1.05	1.12	0.96	0.89	1.31	1.38
Th	3.73	3.75	4.18	4.08	5.58	5.55	2.73	2.56	5.62	5.56
U	5.16	5.28	5.59	5.29	7.65	7.23	1.05	0.88	7.93	7.29
Sc	17.67	17.71	17.60	16.77	15.19	15.45	12.94	12.77	14.81	13.63

Table 2.4: Chemical analysis data (major oxides in wt%, trace elements in ppm) of the Bir Tlacsin Formation at Wadi Iggiten

Sample No.	T29	T30	T31	T32	T33	T34
SiO_2	61.00	61.10	52.52	52.05	52.21	51.68
TiO_2	0.83	0.77	0.18	0.24	0.27	0.48
Al_2O_3	15.35	15.41	24.15	24.09	24.27	26.16
Fe_2O_3	6.33	6.27	6.59	6.69	6.80	4.87
MnO	0.05	0.05	0.05	0.05	0.05	0.05
MgO	2.67	2.73	1.48	1.65	1.57	1.52
CaO	2.49	2.55	1.27	1.52	1.39	1.25
Na_2O	4.36	4.42	6.26	6.56	6.31	7.06
K_2O	1.62	1.68	0.59	0.41	0.52	0.34
Cl	0.06	0.06	0.03	0.03	0.03	0.03
P_2O_5	0.17	0.23	0.24	0.23	0.23	0.15
Ga	18.93	19.56	7.00	6.24	11.12	9.97
B	108.48	109.11	96.55	95.79	100.67	99.52
V	249.20	249.26	153.67	145.43	167.52	164.14
Cr	110.60	115.66	68.62	58.97	65.07	58.92
Ni	62.33	62.39	32.24	29.85	52.05	54.84
Co	11.23	11.29	6.18	5.12	9.91	10.57
Cu	81.48	81.54	88.66	89.17	101.40	105.59
Zn	27.10	27.16	36.30	32.42	45.63	41.83
Zr	129.63	129.57	143.51	144.23	161.28	160.64
Hf	1.78	1.72	2.13	1.96	2.85	2.56
Nb	6.05	6.00	7.26	7.04	8.12	7.83
Ta	0.70	0.74	0.86	0.78	1.14	1.05
Th	4.05	4.00	3.61	4.92	6.11	4.79
U	7.51	7.45	5.33	6.77	8.90	6.62
Sc	18.00	17.94	16.59	15.11	18.00	17.29

Table 2.5: Chemical analysis data (major oxides in wt%, trace elements in ppm) of the Bir Tlacsin Formation at Wadi Awzarq

Sample No.	T35	T36	T37	T38	T39	T40
SiO_2	61.19	61.25	52.67	52.09	52.36	51.80
TiO_2	0.79	0.73	0.14	0.20	0.23	0.44
Al_2O_3	15.40	15.47	24.20	24.14	24.33	26.21
Fe_2O_3	6.29	6.23	6.56	6.65	6.76	4.83
MnO	0.05	0.05	0.05	0.05	0.05	0.05
MgO	2.71	2.77	1.52	1.69	1.61	1.56
CaO	2.45	2.51	1.23	1.48	1.35	1.21
Na_2O	4.40	4.46	6.30	6.61	6.35	7.10
K_2O	1.58	1.64	0.55	0.37	0.48	0.30
Cl	0.05	0.05	0.03	0.03	0.03	0.03
P_2O_5	0.21	0.27	0.28	0.28	0.27	0.19
Ga	17.59	16.00	5.86	5.43	9.23	7.94
B	107.14	105.55	95.41	94.98	98.78	97.49
V	249.16	249.20	153.61	145.39	167.48	164.10
Cr	110.68	115.74	68.70	60.05	65.15	60.00
Ni	62.27	62.33	32.18	29.79	52.00	54.78
Co	11.31	11.37	6.26	5.20	9.98	10.65
Cu	81.42	81.48	88.59	89.11	101.34	105.53
Zn	27.04	27.09	36.24	32.36	45.57	41.77
Zr	129.71	129.65	143.59	144.31	161.36	160.72
Hf	1.70	1.64	2.05	1.88	2.77	2.48
Nb	5.97	5.91	7.18	6.96	8.05	7.75
Ta	0.76	0.80	0.92	0.84	1.21	1.11
Th	3.98	3.94	3.55	4.86	6.05	4.74
U	7.59	7.53	5.41	6.85	8.98	6.70
Sc	17.96	17.90	16.55	15.07	17.98	17.25

2.2. Statistical Analysis

In the present chapter, the chemical data were processed statistically using the SPSS© program. The statistical analysis includes descriptive statistics (Table 2.6), Pearson's correlation coefficient (correlation analysis, Table 2.7 and Figs. 2.1-3) and factor analysis (Table 2.8 and Fig. 2.4).

Table 2.6: Descriptive statistics of the studied samples (major oxides in wt %, trace elements in ppm)

Oxides and elements	N	Minimum	Maximum	Mean	Std. Deviation
SiO_2	40	50.94	61.36	55.59	3.90
TiO_2	40	0.14	0.93	0.48	0.24
Al_2O_3	40	12.07	26.67	20.57	5.06
Fe_2O_3	40	2.90	10.11	6.11	1.60
MnO	40	0.03	0.09	0.06	0.02
MgO	40	1.39	4.57	2.12	0.82
CaO	40	1.00	9.07	2.48	2.19
Na_2O	40	2.67	7.58	5.46	1.49
K_2O	40	0.20	2.13	0.88	0.66
Cl	40	0.03	0.09	0.05	0.02
P_2O_5	40	0.09	0.30	0.22	0.05
Ga	40	5.43	22.25	12.82	5.65
B	40	94.98	117.44	102.67	6.27
V	40	132.20	249.45	177.92	38.58
Cr	40	55.57	115.74	75.25	20.29
Ni	40	22.27	62.57	47.72	13.06
Co	40	4.10	11.54	8.81	2.47
Cu	40	48.32	107.41	86.23	11.48
Zn	40	19.61	46.49	32.90	7.13
Zr	40	115.78	198.54	147.99	21.25
Hf	40	1.30	3.14	2.16	0.50
Nb	40	5.74	9.98	7.11	1.05
Ta	40	0.69	1.38	0.97	0.18
Th	40	2.56	6.60	4.53	1.05
U	40	6.05	8.98	7.29	0.78
Sc	40	12.77	18.96	16.59	1.69

2.2.1. Descriptive Statistics

Descriptive statistics are used to describe the basic features of the data in a study. They provide simple summaries about the sample and the measures. Together with simple graphics analysis, they form the basis of virtually every quantitative analysis of data. Table (2.6) shows that the studied samples contain high concentrations of some trace elements such as B (117.44), V (249.45ppm), Cr (115.74ppm), Cu (107.41ppm) and Zr (198.54ppm).

2.2.2. Pearson's Correlation Coefficient

Pearson's correlation coefficient is a statistical measure of the strength of a linear relationship between paired data. The correlation coefficient can range from -1 to +1, with -1 indicating a perfect negative correlation, +1 indicating a perfect positive correlation, and 0 indicating no correlation at all. (A variable correlated with it will always have a correlation coefficient of 1). The correlation analysis (Table 2.7 and Figs. 2.1-3) shows that SiO_2 is negatively correlated with Al_2O_3 (r = -0.92). This reflects the occurrence of SiO_2 in both silicate and free silica modes. Quite the contrary, SiO_2 has a strong correlation with K_2O (r = 0.91) which indicates their presence in potash feldspar and clay minerals. The Al_2O_3 content is negatively correlated with TiO_2 and Ga (r = -0.8 and -0.78, respectively), which indicates that aluminosilicates are not the sole carrier of TiO_2 and Ga. Since CaO is negatively correlated with Al_2O_3 (r = -0.76), therefore the enrichment of CaO can be attributed to the presence of diagenetic calcite cement. The weak correlations between most of the major oxides with trace elements (high field strength elements and heavy metals) indicate that accessory minerals are the main carriers of trace elements. Furthermore, each of the heavy metals and high field strength elements are definitely present in different minerals.

2.2.3. Factor Analysis

Factor analysis is a statistical procedure used to identify a small number of factors that can be used to represent relationships among sets of interrelated variables. In this chapter, three factors were extracted to explain approximately 76.41% of the total

variables (Table 2.8). Fig (2.4) shows the distribution of the analyzed major oxides and trace elements in factors 1, 2 and 3. However, the following is a brief explanation of the three factors:

Factor one (F1):

It accounts for about 49.4% of the total variables. It shows positive loading for SiO_2, TiO_2, MnO, MgO, CaO, K_2O, Cl, Ga, B, V and Cr. It also displays negative loading for Al_2O_3, Na_2O, Cu, Zn and high field strength elements (except for U). This factor is important in the interpretation of the minerals carrying the major oxides and trace elements.

Factor two (F2):

It accounts for 19.1% of the total variables. It loads positively for V, Cr, Ni, Co, U and Sc. This factor may be important in identifying accessory minerals bearing trace elements.

Factor three (F3):

It accounts for 7.91% of the total variables. It has only negative loading for Fe_2O_3. This factor is practically insignificant.

Table 2.7: Correlation matrix of the studied samples

Oxides and elements	SiO_2	TiO_2	Al_2O_3	Fe_2O_3	MnO	MgO	CaO	Na_2O	K_2O	Cl	P_2O_5	Ga	B	V	Cr	Ni	Co	Cu	Zn	Zr	Hf	Nb	Ta	Th	U	Sc
SiO_2	1.00																									
TiO_2	0.75	1.00																								
Al_2O_3	-0.92	-0.80	1.00																							
Fe_2O_3	-0.01	0.10	-0.08	1.00																						
MnO	0.42	0.50	-0.63	0.19	1.00																					
MgO	0.63	0.69	-0.67	0.59	0.48	1.00																				
CaO	0.55	0.45	-0.76	-0.31	0.65	0.19	1.00																			
Na_2O	-0.81	-0.66	0.89	-0.32	-0.65	-0.74	-0.65	1.00																		
K_2O	0.91	0.62	-0.88	-0.24	0.40	0.38	0.70	-0.68	1.00																	
Cl	0.76	0.81	-0.90	0.02	0.79	0.67	0.74	-0.79	0.71	1.00																
P_2O_5	-0.05	-0.13	-0.05	0.09	0.35	-0.10	0.18	-0.09	0.01	0.12	1.00															
Ga	0.74	0.81	-0.78	-0.03	0.37	0.60	0.52	-0.70	0.61	0.80	-0.14	1.00														
B	0.69	0.82	-0.77	0.10	0.45	0.69	0.51	-0.73	0.52	0.82	-0.11	0.98	1.00													
V	0.74	0.60	-0.53	0.20	0.04	0.59	-0.05	-0.43	0.55	0.35	-0.24	0.48	0.45	1.00												
Cr	0.78	0.62	-0.57	0.19	0.06	0.61	-0.01	-0.49	0.57	0.41	-0.20	0.58	0.54	0.95	1.00											
Ni	0.36	0.42	-0.12	0.01	-0.14	0.40	-0.30	-0.07	0.12	0.13	-0.40	0.36	0.34	0.71	0.67	1.00										
Co	0.31	0.37	-0.06	0.02	-0.17	0.37	-0.34	-0.05	0.06	0.08	-0.43	0.33	0.31	0.66	0.62	0.99	1.00									
Cu	-0.56	-0.51	0.69	-0.14	-0.38	-0.34	-0.58	0.64	-0.55	-0.54	-0.03	-0.54	-0.51	-0.19	-0.26	0.24	0.29	1.00								
Zn	-0.66	-0.65	0.76	-0.28	-0.44	-0.60	-0.47	0.66	-0.61	-0.63	0.08	-0.52	-0.52	-0.42	-0.44	0.10	0.17	0.85	1.00							
Zr	-0.74	-0.52	0.79	0.05	-0.52	-0.50	-0.64	0.68	-0.75	-0.69	0.01	-0.55	-0.54	-0.48	-0.51	-0.12	-0.07	0.49	0.57	1.00						
Hf	-0.76	-0.57	0.78	-0.17	-0.45	-0.66	-0.46	0.67	-0.71	-0.65	0.04	-0.50	-0.50	-0.56	-0.59	-0.14	-0.09	0.56	0.75	0.89	1.00					
Nb	-0.80	-0.56	0.82	-0.04	-0.45	-0.55	-0.57	0.69	-0.80	-0.65	0.07	-0.54	-0.52	-0.61	-0.60	-0.13	-0.08	0.61	0.73	0.93	0.93	1.00				
Ta	-0.65	-0.50	0.67	-0.31	-0.36	-0.60	-0.32	0.59	-0.56	-0.51	0.09	-0.41	-0.44	-0.58	-0.62	-0.10	-0.05	0.45	0.67	0.83	0.89	0.85	1.00			
Th	-0.62	-0.45	0.74	0.04	-0.54	-0.35	-0.71	0.63	-0.75	-0.63	-0.09	-0.38	-0.36	-0.21	-0.25	0.30	0.34	0.58	0.68	0.69	0.71	0.73	0.63	1.00		
U	-0.20	-0.17	0.34	-0.04	-0.47	-0.20	-0.45	0.37	-0.27	-0.35	-0.11	-0.07	-0.11	0.11	0.05	0.46	0.50	0.32	0.44	0.42	0.47	0.41	0.45	0.77	1.00	
Sc	0.06	0.18	0.08	0.45	-0.19	0.40	-0.57	0.08	-0.13	-0.11	-0.31	0.00	0.04	0.62	0.49	0.66	0.67	0.22	-0.02	0.00	-0.12	-0.11	-0.18	0.28	0.40	1.00

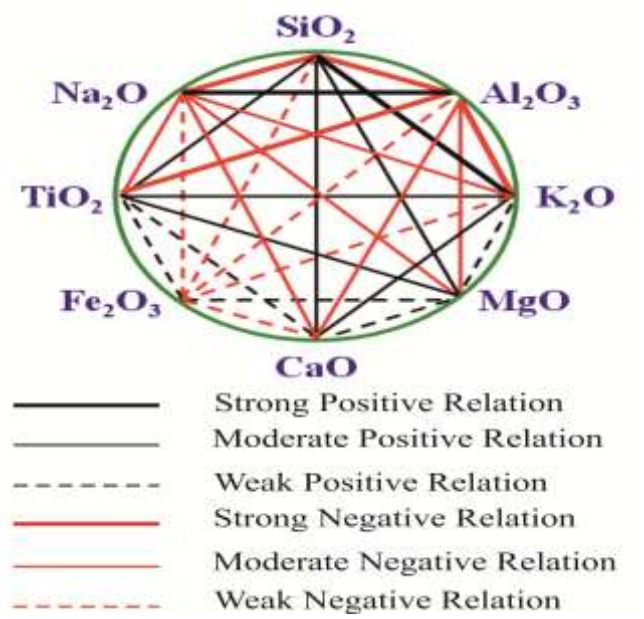

Fig. 2.1: Correlations among the major oxides in the studied samples (intensity of lines corresponds to the strength of the correlation coefficient (< 0.4 to > 0.8)) (red line means inverse relation)

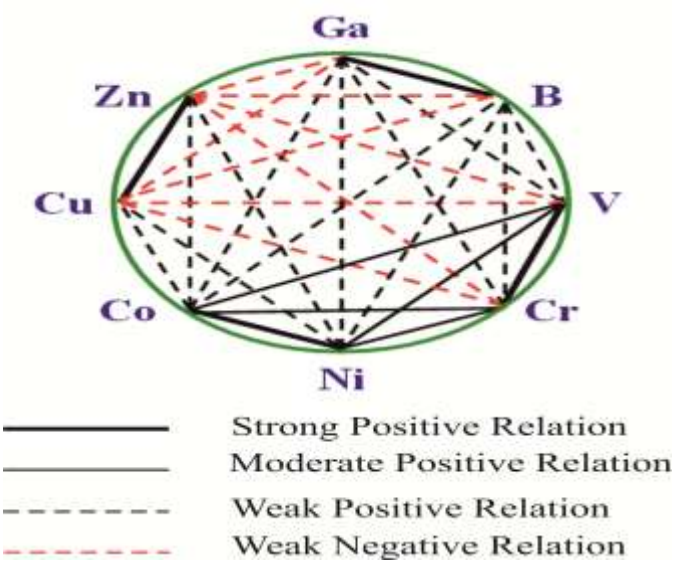

Fig. 2.2: Correlations among the heavy metals in the studied samples (intensity of lines corresponds to the strength of the correlation coefficient (< 0.4 to > 0.8)) (red line means inverse relation)

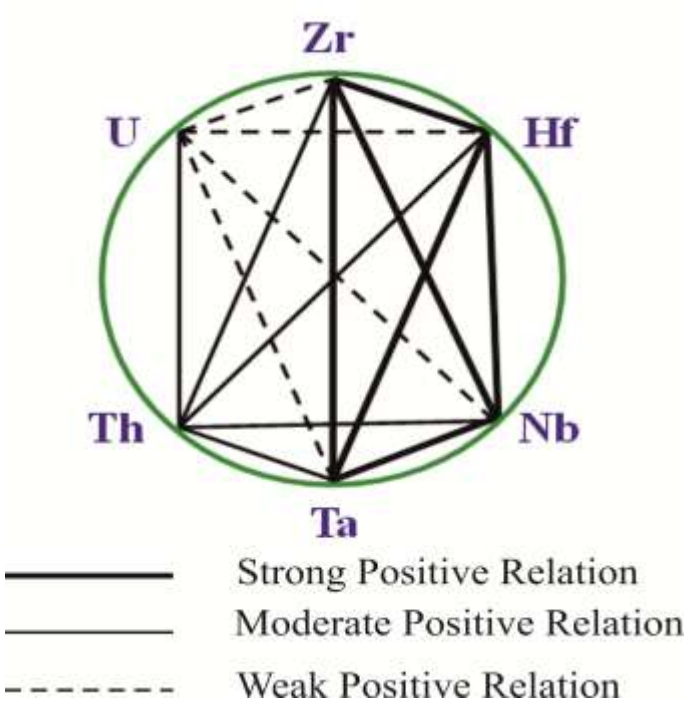

Fig. 2.3: Correlations among the high field strength elements in the studied samples (intensity of lines corresponds to the strength of the correlation coefficient (< 0.4 to > 0.8)) (red line means inverse relation)

Factor two (F2):

It accounts for 19.1% of the total variables. It loads positively for V, Cr, Ni, Co, U and Sc. This factor may be important in identifying accessory minerals bearing trace elements.

Factor three (F3):

It accounts for 7.91% of the total variables. It has only negative loading for Fe_2O_3. This factor is practically insignificant.

2.3. Normalization to Post Archean Australian Shale (PAAS)

The average chemical composition of the shale samples was normalized using PAAS values (Taylor and McLennan, 1985, Fig. 2.5). This normalization shows the following:

1) There are notable enrichments in Na_2O, Al_2O_3, P_2O_5, Cu and U.

2) The concentrations of CaO, V and Sc almost like the PAAS values.

3) There are obvious depletions in most major oxides and trace elements.

Table 2.8: Factor analysis of the studied samples

Eigenvalue	12.84	4.97	2.06
% of Variance	49.40	19.10	7.91
Cumulative %	49.40	68.51	76.41
Factor	1	2	3
SiO_2	0.92	0.15	0.15
TiO_2	0.82	0.22	0.21
Al_2O_3	-0.97	0.11	-0.12
Fe_2O_3	0.14	0.21	-0.74
MnO	0.60	-0.38	0.00
MgO	0.74	0.33	-0.27
CaO	0.65	-0.59	0.38
Na_2O	-0.88	0.11	0.02
K_2O	0.84	-0.11	0.23
Cl	0.88	-0.14	0.25
P_2O_5	-0.03	-0.45	-0.06
Ga	0.79	0.17	0.42
B	0.78	0.17	0.33
V	0.63	0.67	-0.12
Cr	0.67	0.62	-0.07
Ni	0.21	0.91	0.23
Co	0.15	0.92	0.23
Cu	-0.68	0.33	0.06
Zn	-0.80	0.17	0.28
Zr	-0.85	0.10	0.06
Hf	-0.87	0.02	0.30
Nb	-0.89	0.04	0.17
Ta	-0.78	-0.04	0.45
Th	-0.74	0.49	0.14
U	-0.40	0.60	0.32
Sc	0.05	0.82	-0.38

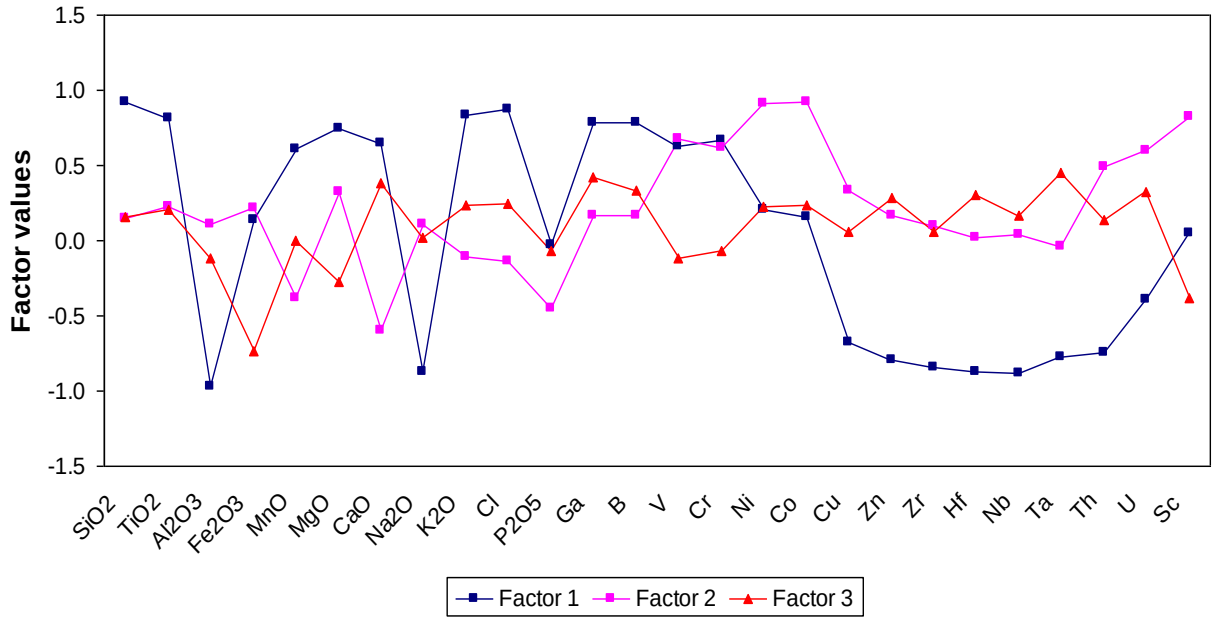

Fig. 2.4: Distribution of the analyzed major oxides and trace elements in factors 1, 2 and 3

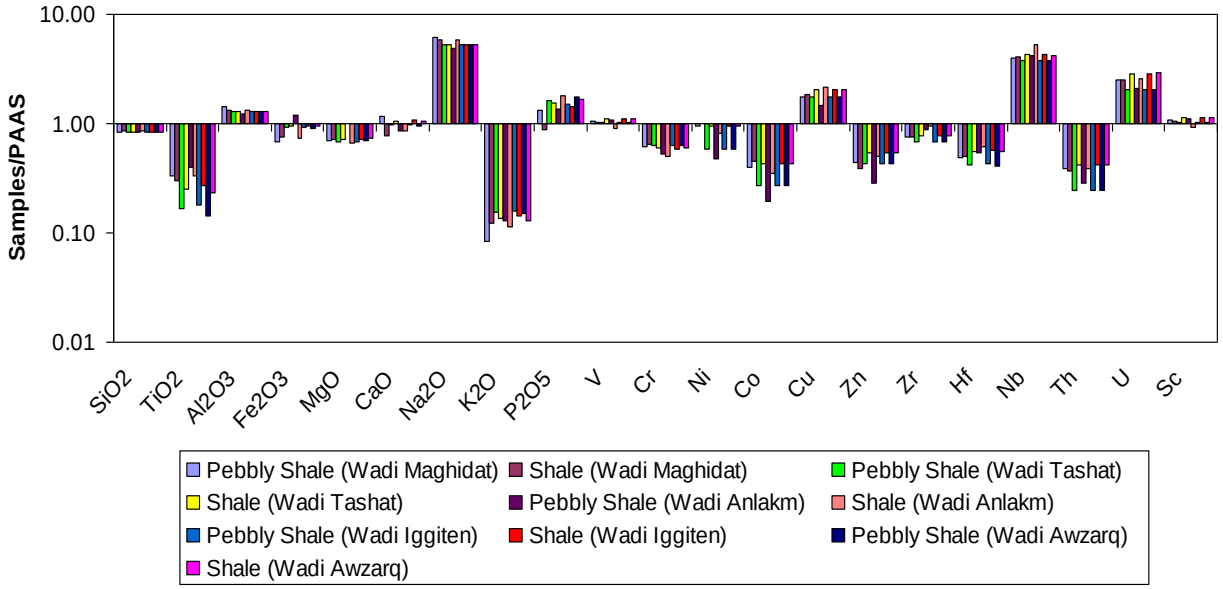

Fig. 2.5: Major oxides and trace elements content of the studied shale samples normalized to the PAAS (Taylor and McLennan, 1985)

2.4. Chemical Classification of Sandstone

There are two chemical classifications for sandstone: Pettijohn *et al.,* (1972) and Herron (1988). According to Shalbak (2015) in the subsurface sections, the sandstones of the Bir Tlacsin Formation were classified as greywackes. In the studied surface sections, the author found the same result (Figs. 2.6-7). Moreover, Fig (2.8) shows that the Bir Tlacsin Formation data plot in the Quartz-intermediate field (except for the ferruginous sandstone unit). The enrichment of Na_2O in the studied sandstones can be attributed to a relatively higher amount of Na-rich plagioclase in them. This assumption is further supported by the low K_2O/Na_2O (<1), which revealed that Na-feldspar dominates over K-feldspar.

2.5. Provenance

The composition of major oxides and trace elements in clastic rocks has been used to determine sedimentary provenance by the application of discriminant function analysis (Armstrong-Altrin *et al*., 2004; Shaltami *et al.,* 2016). Many authors (e.g., Cox *et al*., 1995; Baiyegunhi *et al.,* 2017) used Th/Cr, Th/Sc and Th/Co ratios to determine the source of the sediments. Table (2.9) shows that felsic rocks must be the probable source rocks for the Bir Tlacsin Formation. This assumption is further supported by the Zr versus TiO_2 and Ni versus TiO_2 plots (Figs. 2.9-10). The granitic rocks found in the Air Mountains (18° 16' 22.20" N, 7° 59' 34.79" E), central Niger, may be the possible source of the Bir Tlacsin Formation.

2.6. Paleosalinity

According to Fulai *et al.,* (2009) the B concentration in salt water (80-125ppm) is higher than in fresh water (<60ppm). The B/Ga ratio is an important index to infer the paleosalinity of sediments (Jun *et al.,* 2015). According to Deng and Qian (1993) salt water is expected to contain high B/Ga ratio (>4.2), while low values of B/Ga ratio (<3.3) indicate fresh water, and values between 3.3 and 4.2 suggest brackish water. The studied samples show high B/Ga ratio (5.07-17.49), thus, the Bir Tlacsin Formation was deposited in a high salinity marine environment.

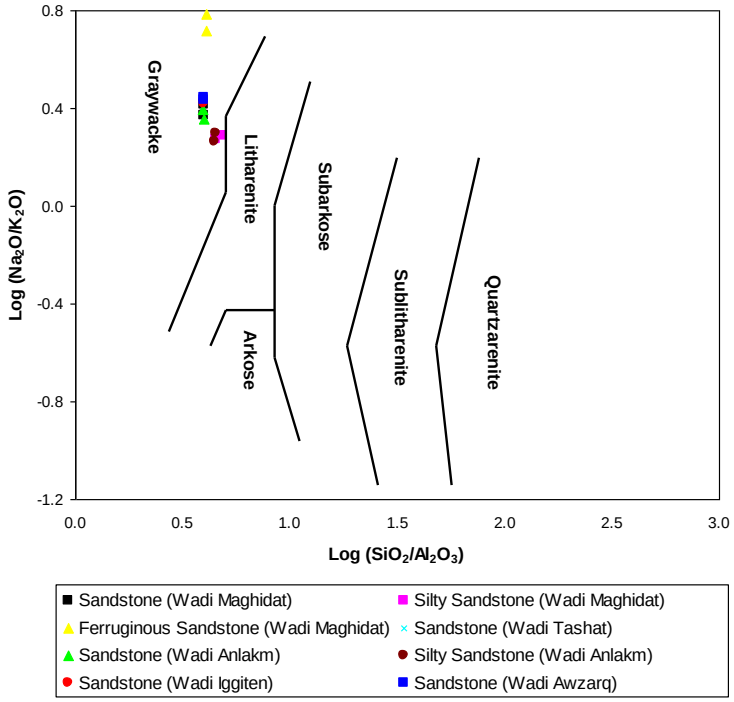

Fig. 2.6: Chemical classification of the Bir Tlacsin Formation using log(SiO_2/Al_2O_3) vs. log(Na_2O/K_2O) diagram (fields after Pettijohn et al., 1972)

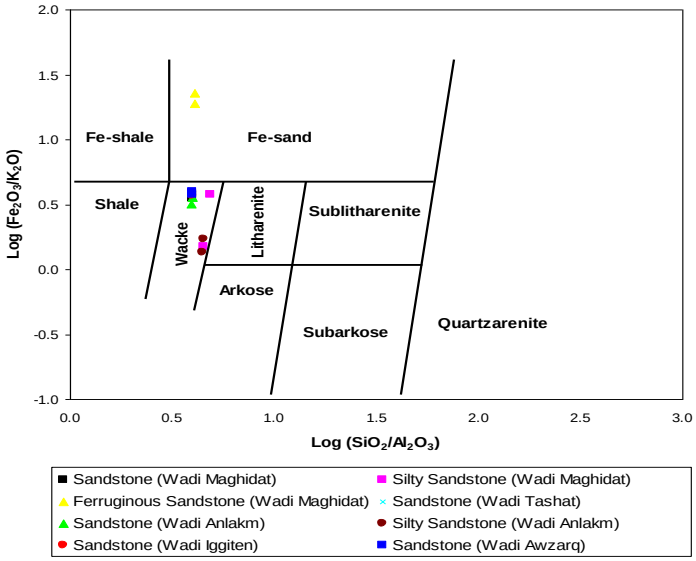

Fig. 2.7: Chemical classification of the Bir Tlacsin Formation using log(SiO_2/Al_2O_3) vs. log(Fe_2O_3/K_2O) diagram (fields after Herron, 1988)

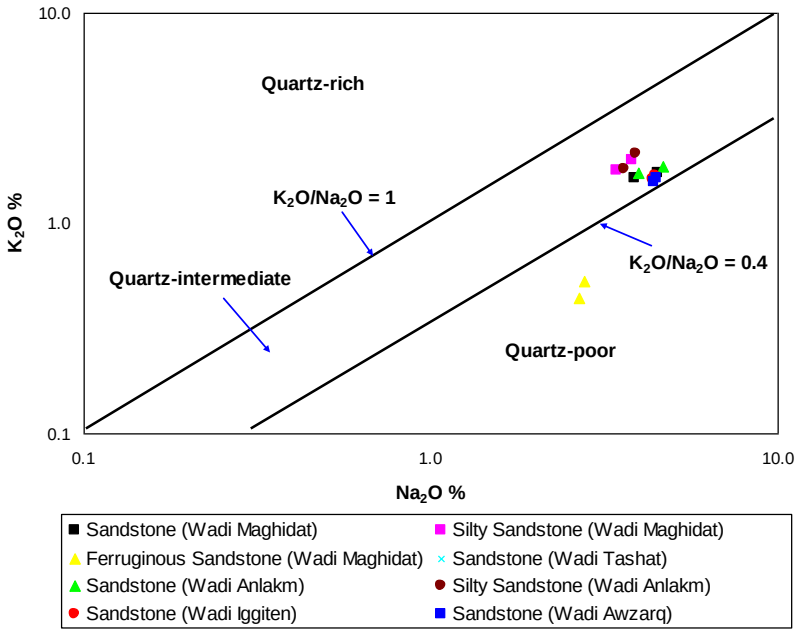

Fig. 2.8: Plot of Na_2O vs. K_2O showing the quartz richness in the Bir Tlacsin Formation (fields after Crook, 1974)

Table 2.9: Range of elemental ratios of the studied samples compared to the ratios derived from felsic rocks, mafic rocks (after Cullers and Podkovyrov (2000) and Post-Archean Australian shale after Taylor and McLennan (1985))

Rocks	Th/Cr	Th/Sc	Th/Co
Felsic rocks	0.13 - 2.7	0.84 - 20.5	0.67 - 19.4
Mafi c rocks	0.43 - 0.86	0.02 - 0.05	0.04 - 0.4
PAAS	0.13	0.90	0.63
Present study	0.06	0.27	0.55

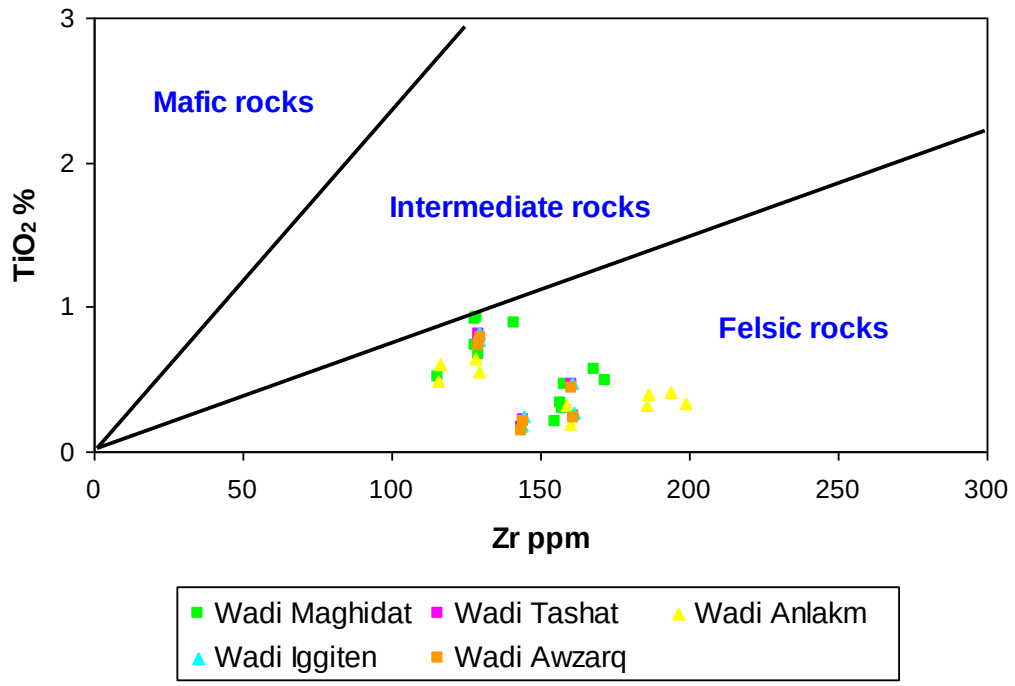

Fig. 2.9: Plot of Zr vs. TiO_2 showing the provenance for the Bir Tlacsin Formation (fields after Hayashi et al., 1997)

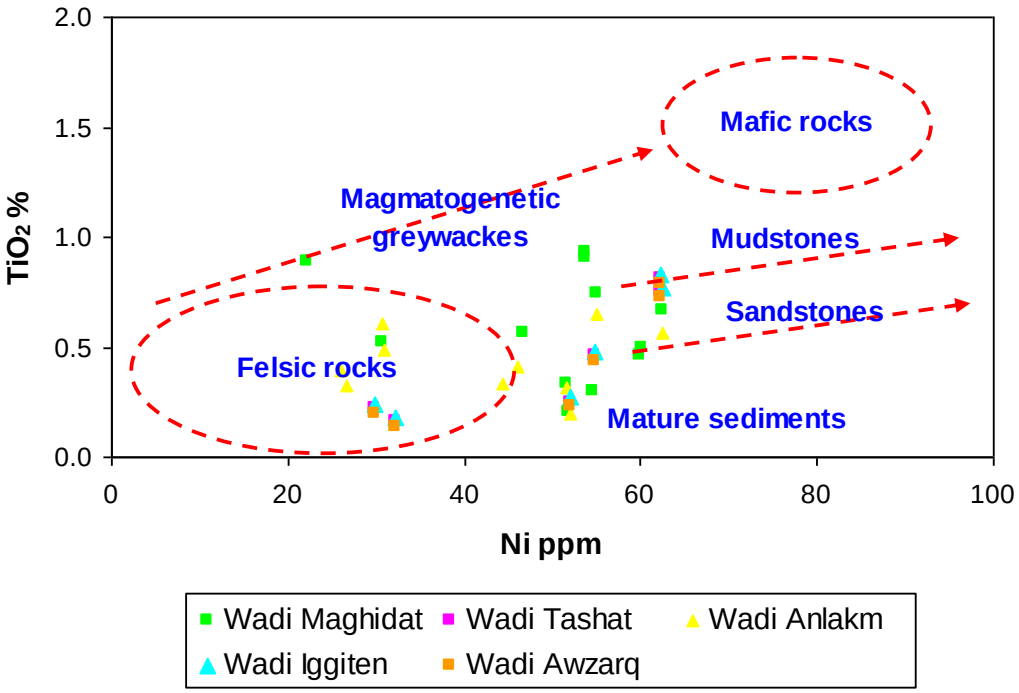

Fig. 2.10: Plot of Ni vs. TiO_2 showing the provenance for the Bir Tlacsin Formation (fields after Floyd et al., 1989)

2.7. Paleoweathering

Intensity of chemical weathering of source rocks are mainly controlled by the composition of the source rock, duration of weathering, climatic conditions and rates of tectonic uplift of source region (Wronkiewicz and Condie, 1987). Many authors (e.g., Taylor and McLennan, 1985; Lindsey, 1999) have documented that about 75% of labile materials in the upper crust are composed of feldspars and volcanic glass. Chemical weathering of these materials resulted in the formation of clay minerals. During chemical weathering, Ca, Na and K are largely removed from source rocks and the amount of these elements surviving in sediments derived from the rocks served as indicator of the intensity of chemical weathering (Nesbitt *et al.,* 1997). According to Lindsey (1999), if siliciclastic sedimentary rocks are free from alkali related post-depositional modifications, then their alkali contents (K_2O + Na_2O) and K_2O/Na_2O ratios should be considered as reliable indicators of the intensity of source material weathering. In order to determine the degree of source rock weathering, a few indices of weathering have been proposed based on the molecular proportions of mobile and immobile element oxides (Na_2O, CaO*, K_2O and Al_2O_3). Thus, the chemical composition of weathering products in a sedimentary basin is expected to reveal the mobility of various elements during weathering (Singh, 2005). The indices of weathering/alteration include chemical index of alteration (CIA), chemical index of weathering (CIW) and plagioclase index of alteration (PIA). Chemical index of alteration (CIA) proposed by (Nesbitt and Young, 1982) is the most widely used chemical index to determine the degree of source area weathering. For quantifying source weathering of carbonate-bearing siliciclastic rocks, a modified version of CIW (CIW´) is also considered (Cullers, 2000). The value of CIA gives a measure of the ratio of original/primary minerals and secondary products such as clay minerals. CIA values range from almost 50 in case of fresh rocks to 100 for completely weathered rocks. Thus, CIA values increase with increasing weathering intensity, reaching 100 when all the Ca, Na and K have been leached from weathering residue (Baiyegunhi *et al.,* 2017). In comparison to other weathering indices, the CIW is a superior method involving restricted number of components that are well-known with consistent geochemical

behavior during weathering. As documented by (Fedo *et al.,* 1995), source area weathering and elemental redistribution during diagenesis also can be assessed using the plagioclase index of alteration (PIA). PIA monitors and quantifies progressive weathering of feldspars to clay minerals (Armstrong-Altrin *et al.,* 2004). The maximum value of PIA is 100 for completely altered materials (i.e. kaolinite and gibbsite) and weathered plagioclase has PIA value of 50. These indices were calculated as:

$$CIA = \{Al_2O_3 / (Al_2O_3 + CaO^* + Na_2O + K_2O)\} \times 100$$

$$CIW = \{Al_2O_3 / (Al_2O_3 + CaO^* + Na_2O)\} \times 100$$

$$PIA = \{(Al_2O_3 - K_2O) / ((Al_2O_3 - K_2O) + CaO^* + Na_2O)\} \times 100$$

$$CIW' = \{Al_2O_3 / (Al_2O_3 + Na_2O)\} \times 100$$

Where CaO* is the content of CaO incorporated in silicate fraction. In the present study, the CIA, CIW, PIA and CIW´ range from 47.32 to 82.53, 51.19 to 83.71, 46.84 to 83.47 and 77.08 to 87.34, respectively. These values point to relatively moderate to high degree of chemical weathering in the source area.

During the initial stages of weathering, Ca is quickly leached than Na and K. With increasing weathering, the total alkali content ($K_2O + Na_2O$) decreases with increase in K_2O/Na_2O ratio. This is due to destruction of feldspars among which plagioclase is more favorably removed than K-feldspars (Nesbitt and Young, 1984). Feldspathic materials in the sandstones and shales were subjected to variable intensities of weathering during the different evolution stages. The individual bivariate plots of K_2O/Na_2O, $K_2O + Na_2O$, Na_2O, K_2O and CaO against PIA can be used to unravel the mobility of elements during the final stage of chemical weathering of previously altered feldspars. In this study, there is negative correlation between the K_2O/Na_2O ratio and PIA ($r = -0.88$, Fig. 2.11). Furthermore, the total alkalis ($K_2O + Na_2O$) is weakly correlated with PIA ($r = 0.31$, Fig. 2.12). Figs (2.13-15) show the behavior of Na, Ca and K during progressing weathering of feldspars in the studied samples.

2.8. Clay Minerals

According to Nesbitt and Young (1982) the ternary plot of A-CN-K (Al_2O_3-($CaO+Na_2O$)-K_2O) can be used to assess the composition of original source rock as well as the mobility of elements during the process of chemical weathering of source material and post-depositional chemical modifications. This ternary plot is also useful for identifying clay minerals in shale. Fig (2.16) shows that the detected clay minerals are mainly smectite, kaolinite, gibbsite and chlorite. This interpretation is further supported by the K versus Th plot (Fig. 2.17).

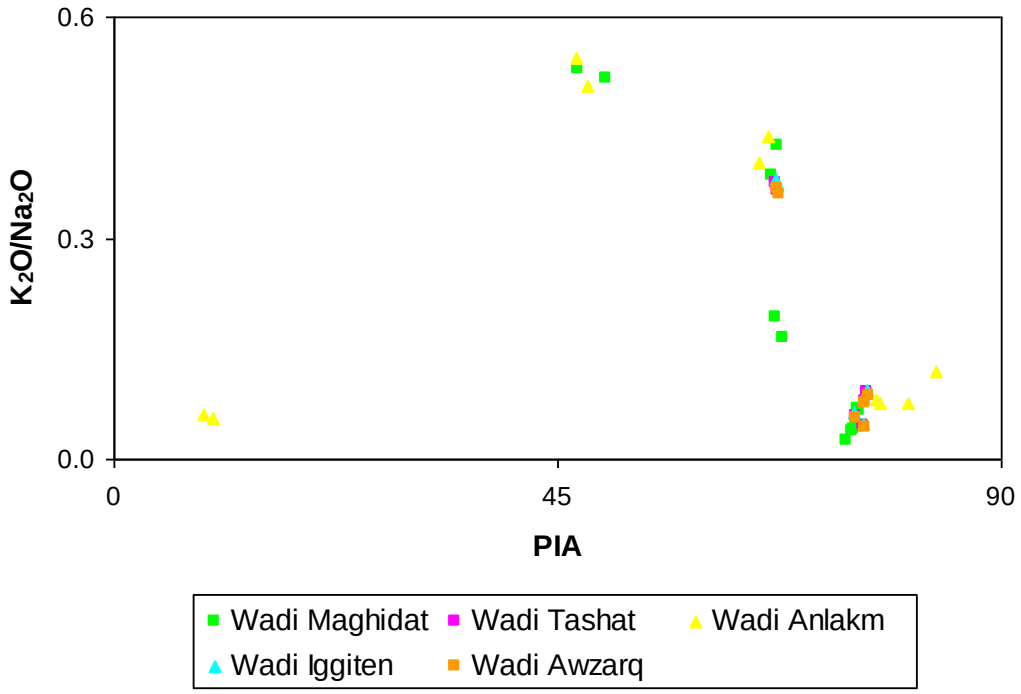

Fig. 2.11: Relationship between K_2O/Na_2O ratio and PIA in the studied samples

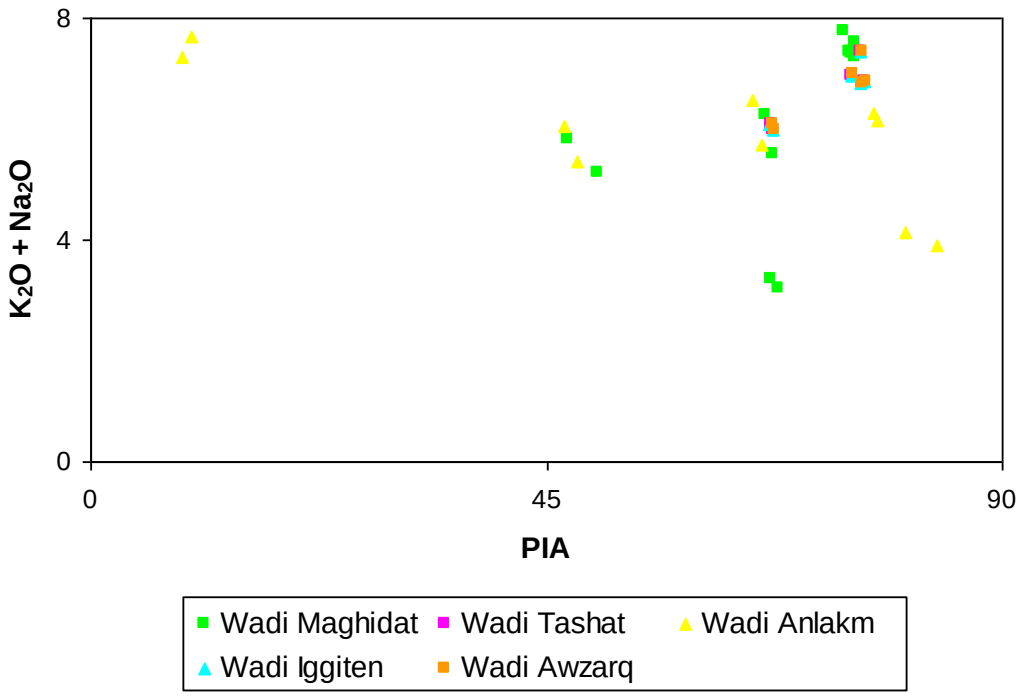

Fig. 2.12: Relationship between total alkalis ($K_2O + Na_2O$) and PIA in the studied samples

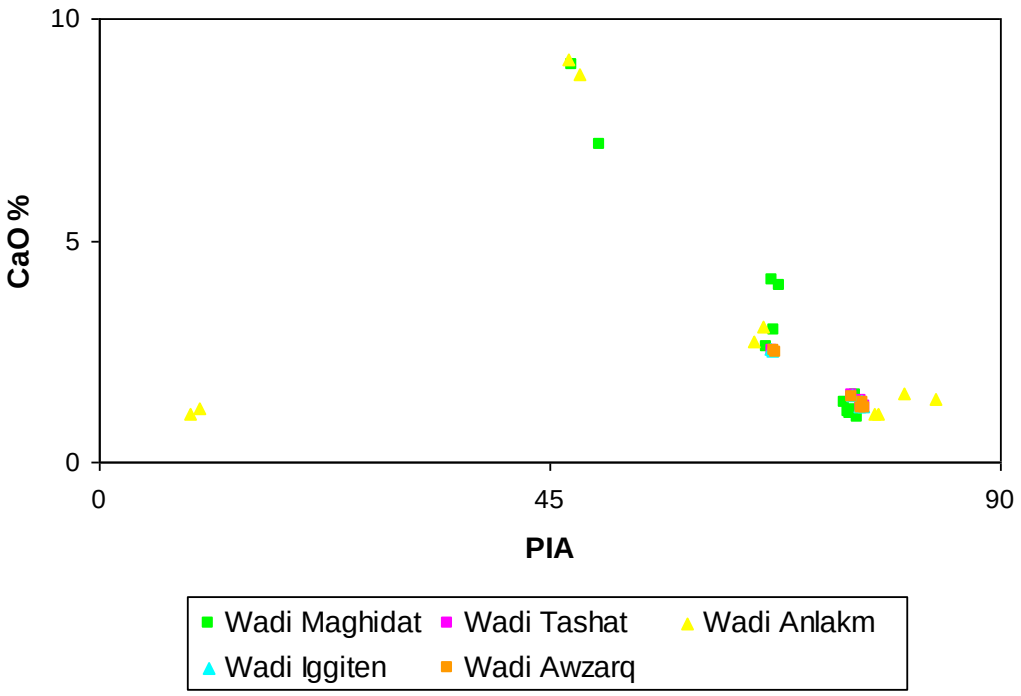

Fig. 2.13: Relationship between CaO and PIA in the studied samples

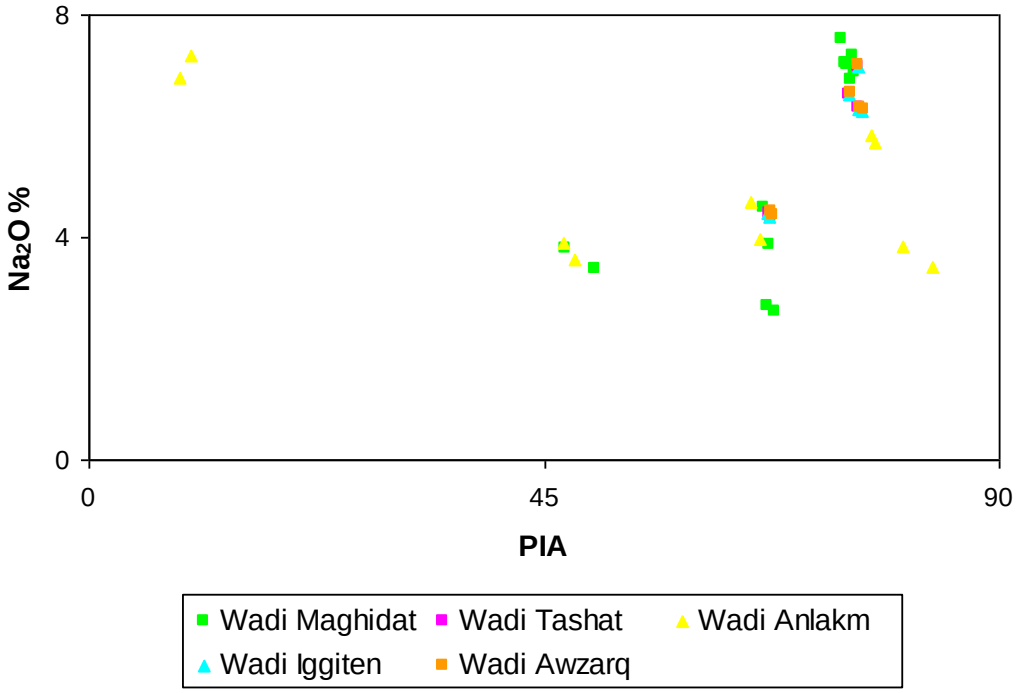

Fig. 2.14: Relationship between Na_2O and PIA in the studied samples

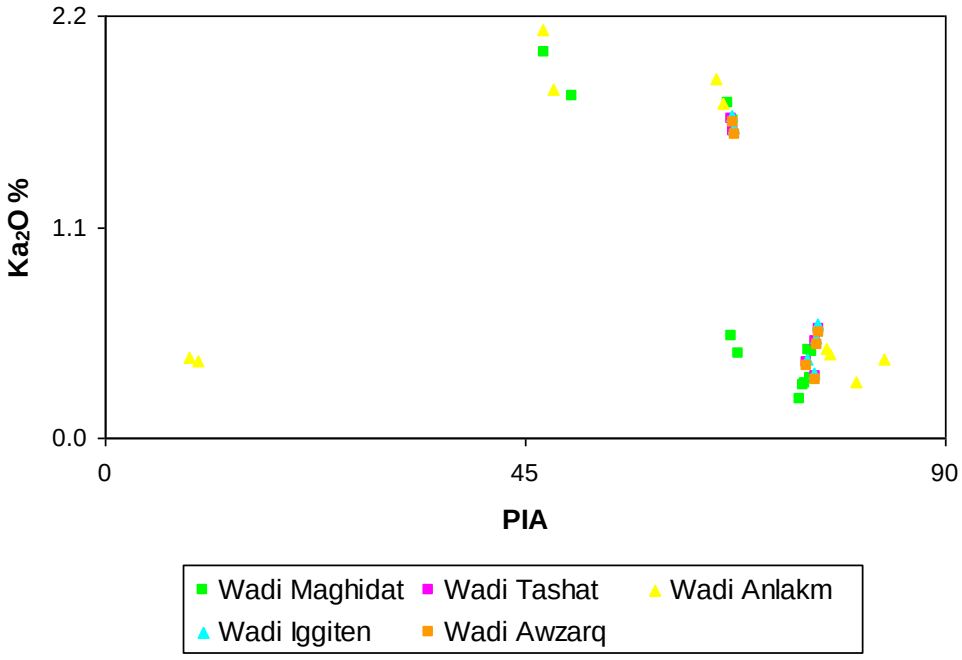

Fig. 2.15: Relationship between K_2O and PIA in the studied samples

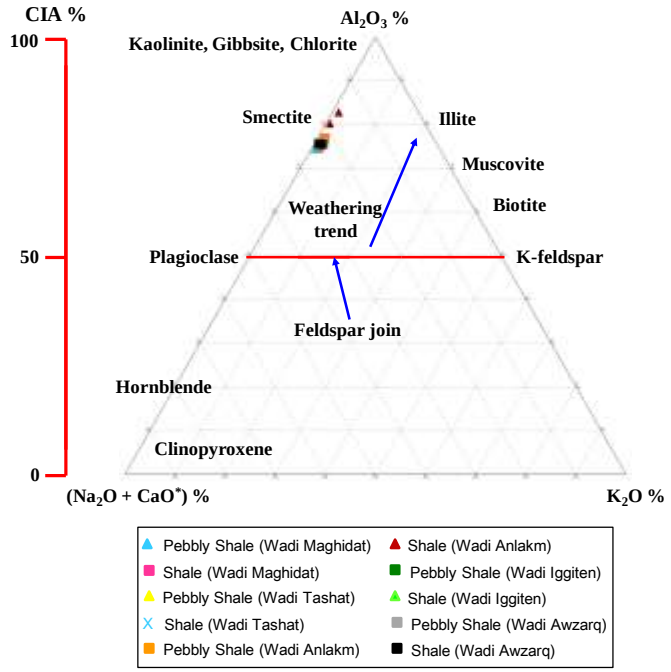

Fig. 2.16: A-CN-K ternary diagram showing the clay minerals in the shale samples (fields after Nesbitt and Young, 1982)

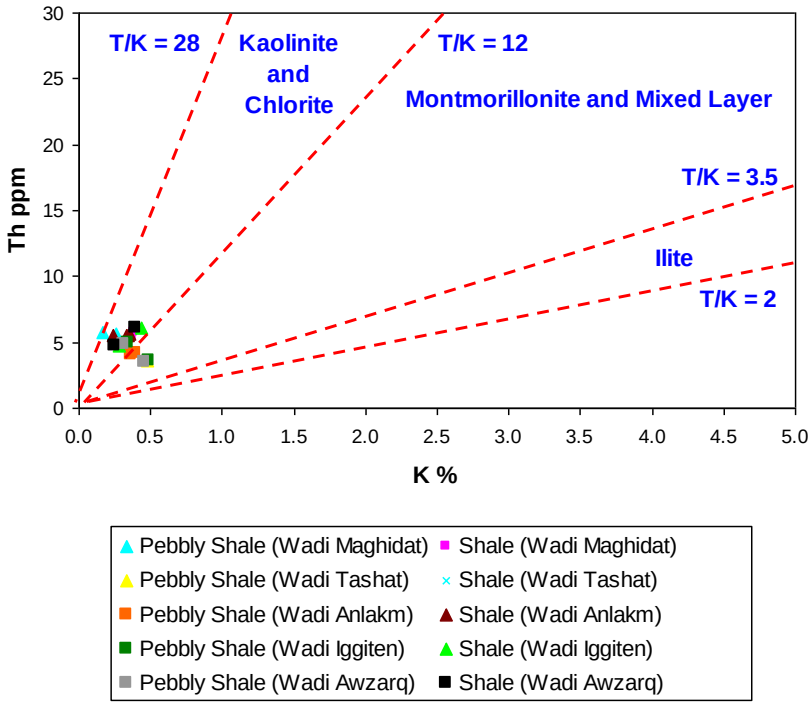

Fig. 2.17: Plot of K vs. Th showing the clay minerals in the shale samples (fields after Morgan and Heier, 1966)

2.9. Depositional Environment and Paleooxygenation Conditions

According to Bau and Alexander (2009) ratios such as Zr/Hf, Hf/Ta and Zr/Ta ratios can be used to determine the depositional environment of clastic rocks. In the marine environment, the Zr/Hf, Hf/Ta and Zr/Ta ratios range from 56 to 207, 1.3 to 2.5 and 115 to 688, respectively (Bau and Alexander, 2009). In this study, these ratios (Zr/Hf (56.59-98.59), Hf/Ta (1.49-2.54) and Zr/Ta (119.44-186.12)) indicate that the possible origin of the Bir Tlacsin Formation is the marine environment.

Many authors (e.g., Nagarajan *et al.,* 2007; Shaltami *et al.,* 2016) used the Ni/Co, V/Cr, V/Sc, V/(V+Ni) and U/Th ratios, authigenic U (AU = U – (Th/3)) and δU (δU = 2U / (U + Th/3)) to identify the paleooxygenation conditions. In oxidizing conditions, these ratios are low, while high ratios indicate reducing conditions (Table 2.10). All Ni/Co, V/Cr, V/Sc, V/(V+Ni) and U/Th ratios, authigenic U and δU are high in the Bir Tlacsin Formation, indicating deposition in anoxic conditions. This interpretation is further supported by the Ni versus V, V/Sc versus V/(V+Ni) and U/Th versus authigenic U plots (Fig. 2.18-20).

Table 2.10: Redox classification using trace element ratios (values of the Ni/Co, V/Cr, V/Sc, V/(V+Ni) and U/Th ratios, AU and δU after Jones and Manning, 1994, Kimura and Watanabe, 2001, Rimmer, 2004, Nath et al., 1997, Nagarajan et al., 2007 and Yao et al., 2017, respectively)

Ratio	Oxic conditions	Anoxic conditions
Ni/Co	<5	>5
V/Cr	<2	>2
V/Sc	<9	>9
V/(V+Ni)	<0.46	>0.46
U/Th	<1.25	>1.25
AU	<5	>5
δU	<1	>1

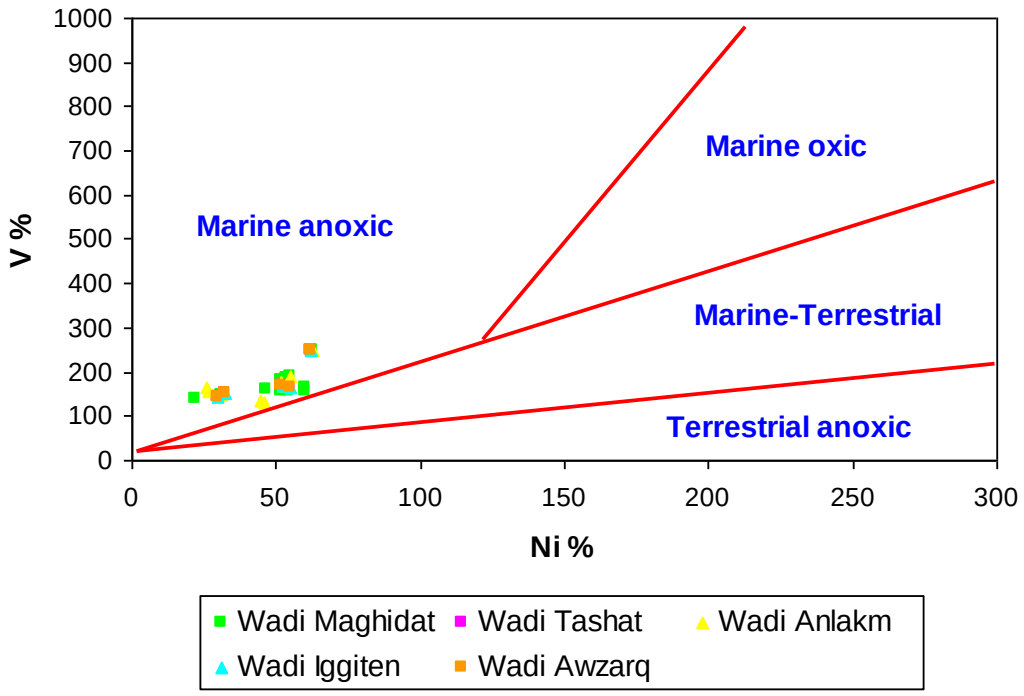

Fig. 2.18: Plot of Ni vs. V showing the paleooxygenation conditions for the Bir Tlacsin Formation (fields after Akinlua et al., 2016)

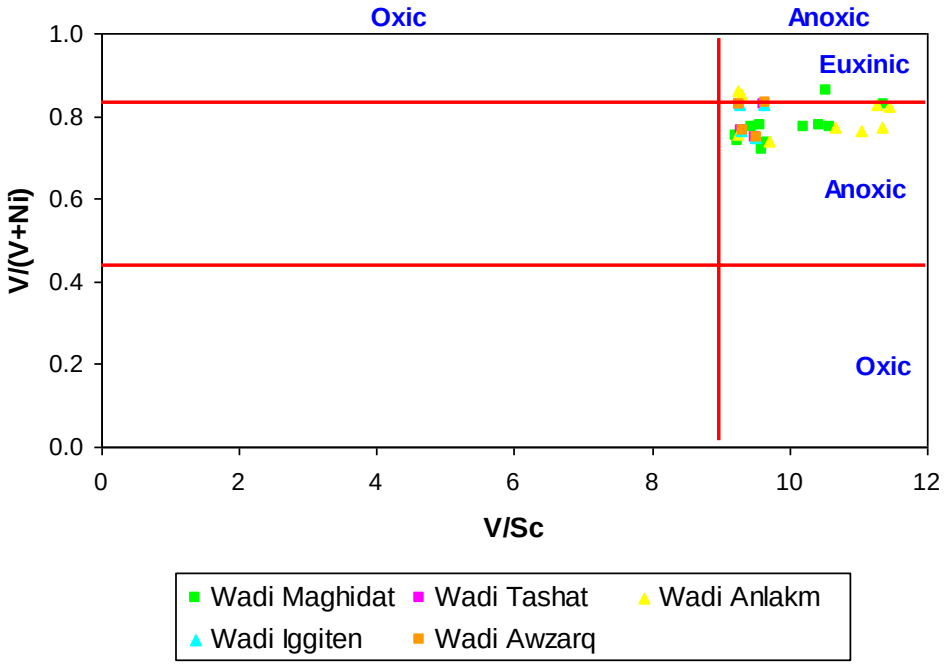

Fig. 2.19: Plot of V/Sc vs. V/(V+Ni) showing the paleooxygenation conditions for the Bir Tlacsin Formation (fields after Kimura and Watanabe, 2001 and Rimmer, 2004)

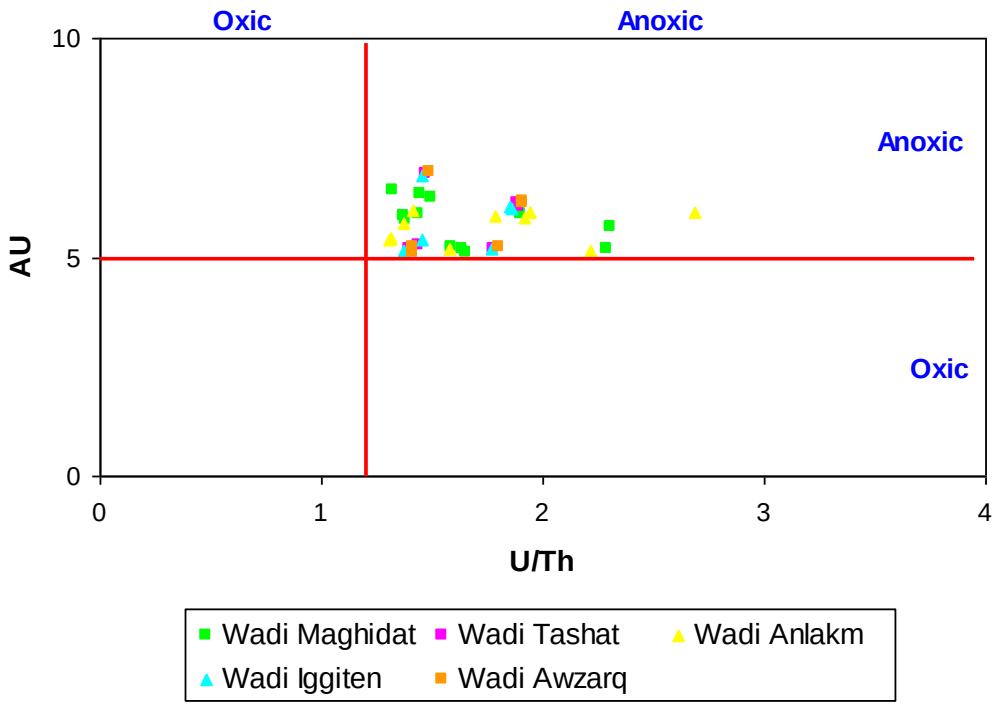

Fig. 2.20: Plot of U/Th vs. AU showing the paleooxygenation conditions for the Bir Tlacsin Formation (fields after Nath et al., 1997 and Nagarajan et al., 2007)

2.10. Paleoclimate and Maturity

The original character and maturity of sediments as well as the prevailed climatic conditions can be determined by calculating the index compositional variation (ICV) proposed by (Cox *et al.*, 1995). According to Baiyegunhi *et al.*, (2017) the ICV tends to be highest in minerals that are high in weathering intensity and decreases in more stable minerals (less weathered minerals). The ICV decreases further in the montmorillonite group clay minerals and lowest in the kaolinite group minerals (Cox *et al.*, 1995). In addition, more mature shale tends to have low ICV values (< 1). The ICV were calculated as:

$$ICV = (Fe_2O_3 + K_2O + Na_2O + CaO + MgO + MnO) / Al_2O_3$$

In this study, the ICV is low (<1) in the shales while it is high (≥1) in the sandstones, indicating the immaturity of the shales whereas the sandstones are thermally

submature to mature. There are two main models for determining the paleoclimate: the first (SiO_2 versus Al_2O_3 + K_2O + Na_2O) invented by Suttner and Dutta (1986) and the second (CIA versus K_2O/Na_2O) was designed by Goldberg and Humayun (2010). The plotted samples (Figs. 2.21-22) revealed semi-humid to semi-arid conditions for the Bir Tlacsin Formation.

2.11. Tectonic setting of the source area

(e.g., Bhatia, 1983), documented that the chemical compositions of siliciclastic sedimentary rocks are considerably controlled by plate tectonic settings of their provenances and depositional basins. Thus, siliciclastic rocks from different tectonic settings possess terrain-specific geochemical signatures. Tectonic setting discrimination diagrams give reliable results for siliciclastic rocks that have not been strongly affected by postdepositional weathering and metamorphism (McLennan *et al.*, 1993). There are four main tectonic settings, namely, Oceanic island Arc (A), continental island Arc (B), active continental margin (C) and passive continental margin (D). Figs (2.23-24) show that data of the Bir Tlacsin Formation fall in the fields of C and D. The discriminant functions are calculated as:

DF1 = -0.447SiO_2 - 0.972TiO_2 - 0.059Fe_2O_3 - 3.082MnO + 0.140MgO + 0.195CaO + 0.719Na_2O - 0.032K_2O + 7.51P_2O_5 + 0.303)

DF2 = -0.421SiO_2 +1.988TiO_2 -0.526Al_2O_3 - 2.161Fe_2O_3 + 2.720MnO + 0.881MgO - 0.907CaO - 0.177Na_2O - 1.840K_2O + 7.244P_2O_5 + 43.57)

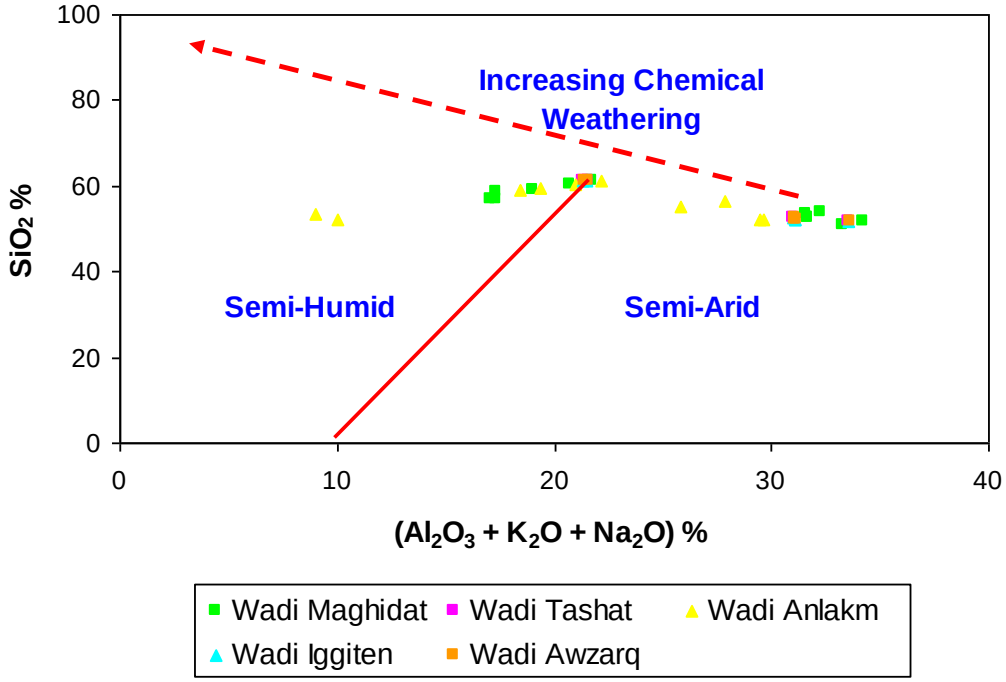

Fig. 2.21: Plot of (Al_2O_3 + K_2O + Na_2O) vs. SiO_2 showing the paleoclimate conditions for the Bir Tlacsin Formation (fields after Suttner and Dutta, 1986)

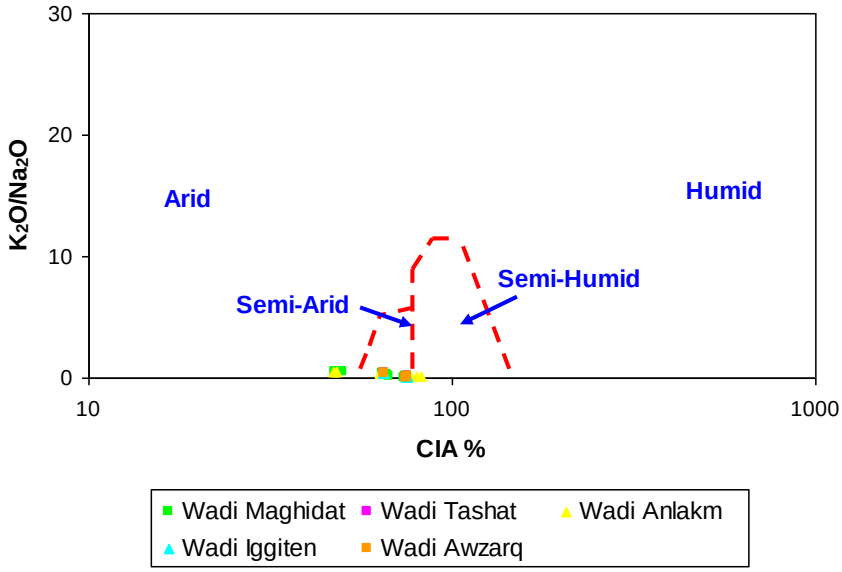

Fig. 2.22: Plot of CIA vs. K_2O/Na_2O showing the paleoclimate conditions for the Bir Tlacsin Formation (fields after Goldberg and Humayun, 2010)

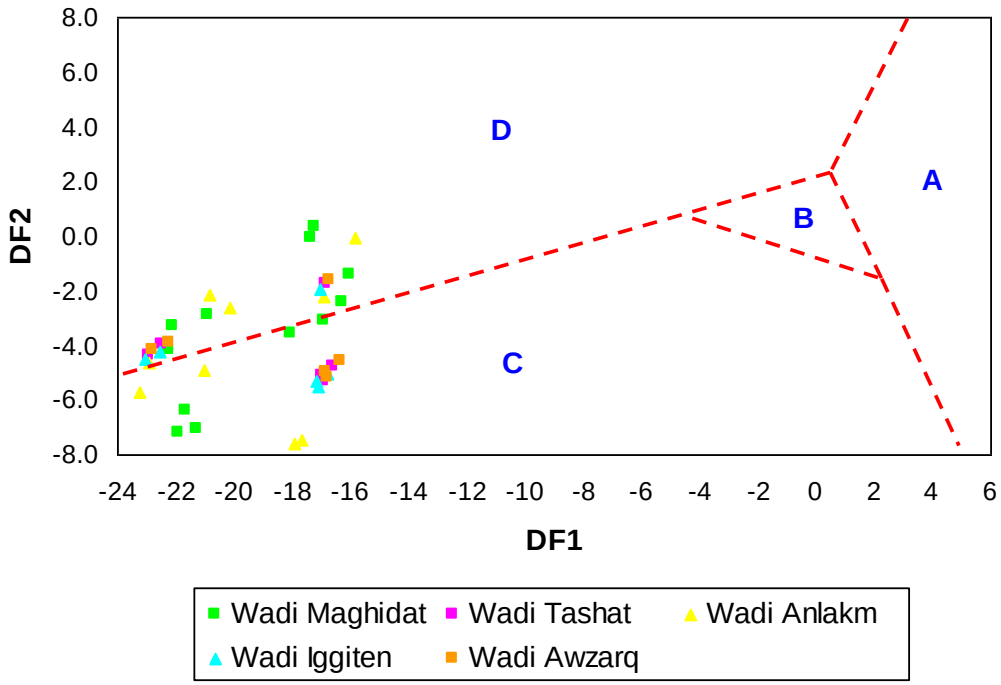

Fig. 2.23: Plot of DF1 vs. DF2 showing the tectonic setting for the Bir Tlacsin Formation (fields after Bhatia, 1983)

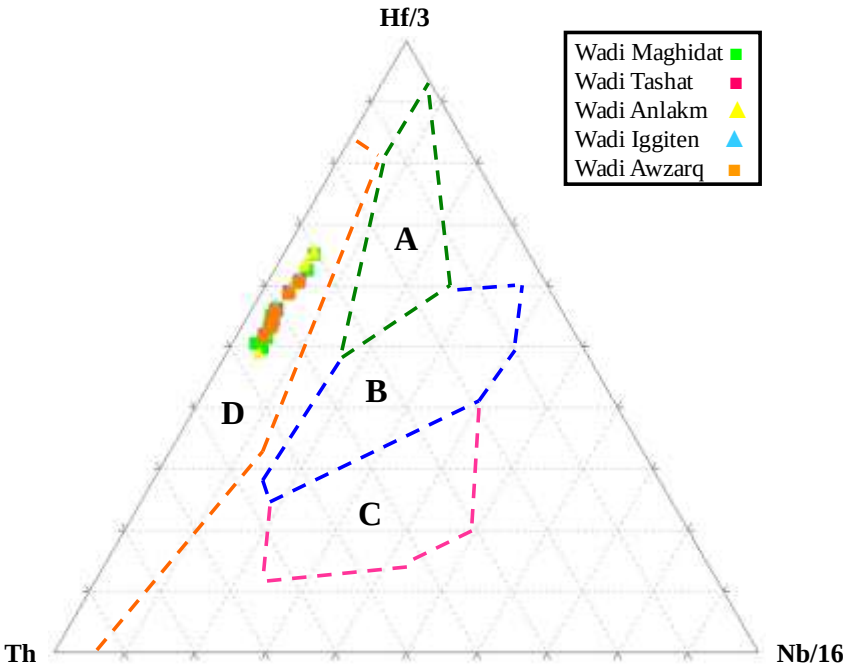

Fig. 3.24: Ternary plots of Hf/3 – Th – Nb/16 showing the tectonic setting for the Bir Tlacsin Formation (fields after Wood, 1980)

CHAPTER THREE
ORGANIC GEOCHEMISTRY

3.1. Introduction

Organic geochemistry is used as the fundamental science for understanding the properties of source rocks, productive and non productive zones, oil migration (all of which result in more efficient exploration), development of oil fields and sustainable production. The term source rock refers to an organic-rich fine-grained sedimentary rock which can produce hydrocarbons due to thermal maturation. Source rock is one of the main elements of a hydrocarbon system. Therefore, to identify a region of hydrocarbon, it is necessary to investigate the source rock and its characteristics first. Thermal maturity is the primary factor that determines whether a source rock can produce oil, gas, or condensate (Lecompte *et al.,* 2010; Gao *et al.,* 2018). In order to evaluate the source rocks various laboratory methods are used. Among these techniques, Rock-Eval pyrolysis and Gas Chromatography Mass Spectrometry (GC-MS) have been widely used in the industry as standard methods in petroleum exploration. With 44 billion barrels of oil and over 54 trillion cubic feet of natural gas, the largest proven reserves of hydrocarbons in Africa occur in Libya (Diasty *et al.,* 2017), an important founding member of the Organization of Petroleum Exporting Countries (OPEC). From the exploration perspective, the country is divided into four major basins, three of which, Ghadames, Murzuq and Al Kufra, are essentially Paleozoic basins. The fourth, Sirte, is primarily a Mesozoic-Cenozoic basin. The Ghadames Basin continues westwards into Tunisia and Algeria where it attains its greatest depth.It continues southwards into Niger, where it eventually pinches out onto basement. Libya has 29 oil fields with greater than one billion barrels of oil originally in place; 22 of these fields lie in the Sirte Basin, six in the Murzuq Basin (Hallett and Clark-Lowes, 2016) and one, Bouri, in the Sabratah Basin, offshore northwest Libya. The reserves of the Murzuq Basin are now second only to those of the Sirte Basin. A recent estimation of hydrocarbons in place for the Murzuq Basin is 6 billion barrels of oil and 1.0 trillion cubic metres of gas, which represents about 6.5% of the Libya's total production. Since oil exploration began in

1957 wildcat wells resulted in the exploitation of 11 oil fields in the basin (Rusk, 2001), several of which, including El Shararah, and El Feel (Elephant), are giant fields.

The results of Rock-Eval pyrolysis and GC-MS are shown in tables (3.1-20). The main goals of this chapter are to determine:

1) Organic matter richness
2) Kerogen type
3) Thermal maturity
4) Organic matter type
5) Organic matter input
6) Depositional environment
7) Paleooxygenation condition

Where:

TOC = total organic carbon (wt. %)

S_1 = amount of free hydrocarbons in sample (mg/g)

S_2 = amount of hydrocarbons generated through thermal cracking (mg/g) – provides the quantity of hydrocarbons that the rock has the potential to produce through diagenesis

S_3 = amount of CO_2 (mg of CO_2/g of rock) - reflects the amount of oxygen in the oxidation step

T_{max} = the temperature at which maximum rate of generation of hydrocarbons occurs

Hydrogen index: $HI = 100 * S_2 / TOC$

Oxygen index: $OI = 100 * S_3 / TOC$

Production index: $PI = S_1 / (S_1 + S_2)$

Bituminous Index: $BI = S_1 / TOC$

Semi-quantitative index: $GP = S_1 / S_2$

Ro = vitrinite reflectance (wt. %)

Pr/Ph = Pristane/Phytane

Carbon preference index: $CPI = 2(C_{23} + C_{25} + C_{27} + C_{29})/(C_{22} + 2[C_{24}+ C_{26} + C_{28}] + C_{30})$

Waxiness index: WI = $\Sigma(n\text{-}C_{21}\text{-}n\text{-}C_{31})/\Sigma(n\text{-}C_{15}\text{-}n\text{-}C_{20})$

TPP = tetracyclic polyprenoid

Table 3.1: Rock Eval analysis data of the Bir Tlacsin Formation at Wadi Maghidat

Sample No.	T5	T6	T9	T10
TOC	1.67	1.50	1.79	1.82
T_{max}	420	425	414	415
Ro	0.37	0.36	0.38	0.37
S_1	4.71	4.34	5.60	5.05
S_2	5.67	5.90	6.11	6.05
S_3	1.45	1.38	1.32	1.29
HI	339.52	393.33	341.34	332.42
OI	86.83	92.00	73.74	70.88
PI	0.45	0.42	0.48	0.45
GP	10.38	10.24	11.71	11.10
BI	2.82	2.89	3.13	2.77

Table 3.2: Rock Eval analysis data of the Bir Tlacsin Formation at Wadi Tashat

Sample No.	T15	T16	T17	T18
TOC	1.25	1.16	1.85	1.90
T_{max}	420	420	419	421
Ro	0.50	0.50	0.39	0.35
S_1	6.87	6.00	5.91	5.77
S_2	5.55	6.13	6.77	6.36
S_3	1.33	1.39	1.28	1.34
HI	444.00	528.45	365.95	334.74
OI	106.40	119.83	69.19	70.53
PI	0.55	0.49	0.47	0.48
GP	12.42	12.13	12.68	12.13
BI	5.50	5.17	3.19	3.04

Table 3.3: Rock Eval analysis data of the Bir Tlacsin Formation at Wadi Anlakm

Sample No.	T21	T22	T23	T24	T27	T28
TOC	1.09	1.11	0.65	0.80	1.65	1.80
T_{max}	425	427	395	397	426	425
Ro	0.51	0.49	0.41	0.45	0.35	0.39
S_1	5.11	5.28	2.09	2.19	6.32	6.41
S_2	5.54	5.76	2.57	2.64	6.17	6.40
S_3	1.36	1.27	1.05	1.10	1.38	1.40
HI	508.26	518.92	395.38	330.00	373.94	355.56
OI	124.77	114.41	161.54	137.50	83.64	77.78
PI	0.48	0.48	0.45	0.45	0.51	0.50
GP	10.65	11.04	4.66	4.83	12.49	12.81
BI	4.69	4.76	3.22	2.74	3.83	3.56

Table 3.4: Rock Eval analysis data of the Bir Tlacsin Formation at Wadi Iggiten

Sample No.	T31	T32	T33	T34
TOC	1.23	1.14	1.83	1.88
T_{max}	421	421	420	422
Ro	0.44	0.40	0.53	0.50
S_1	6.85	5.98	5.89	5.75
S_2	5.57	6.15	6.79	6.38
S_3	1.35	1.41	1.30	1.36
HI	452.85	539.47	371.04	339.36
OI	109.76	123.68	71.04	72.34
PI	0.55	0.49	0.46	0.47
GP	12.42	12.13	12.68	12.13
BI	5.57	5.25	3.22	3.06

Table 3.5: Rock Eval analysis data of the Bir Tlacsin Formation at Wadi Awzarq

Sample No.	T37	T38	T39	T40
TOC	1.27	1.18	1.87	1.92
T_{max}	419	420	418	420
Ro	0.48	0.43	0.52	0.51
S_1	6.89	6.00	5.93	5.79
S_2	5.53	6.11	6.75	6.34
S_3	1.31	1.37	1.26	1.32
HI	435.43	517.80	360.96	330.21
OI	103.15	116.10	67.38	68.75
PI	0.55	0.50	0.47	0.48
GP	12.42	12.11	12.68	12.13
BI	5.43	5.08	3.17	3.00

Table 3.6: Normal alkanes and isoprenoids ratios of the Bir Tlacsin Formation at Wadi Maghidat (calculated on m/z 85)

Sample No.	T5	T6	T9	T10
Pr/Ph	0.44	0.52	0.81	0.92
Pr/n-C17	0.33	0.31	0.27	0.29
Pr/n-C18	0.55	0.52	0.44	0.48
CPI	0.92	0.98	0.89	0.83

Table 3.7: Normal alkanes and isoprenoids ratios of the Bir Tlacsin Formation at Wadi Tashat (calculated on m/z 85)

Sample No.	T15	T16	T17	T18
Pr/Ph	0.71	0.55	0.92	0.94
Pr/n-C17	0.30	0.27	0.21	0.24
Pr/n-C18	0.50	0.54	0.49	0.51
CPI	0.95	0.82	0.88	0.72

Table 3.8: Normal alkanes and isoprenoids ratios of the Bir Tlacsin Formation at Wadi Anlakm (calculated on m/z 85)

Sample No.	T21	T22	T23	T24	T27	T28
Pr/Ph	0.77	0.70	0.57	0.61	0.88	0.81
Pr/n-C17	0.33	0.29	0.22	0.24	0.28	0.31
Pr/n-C18	0.55	0.54	0.40	0.43	0.44	0.47
CPI	0.74	0.66	0.51	0.57	0.80	0.77

Table 3.9: Normal alkanes and isoprenoids ratios of the Bir Tlacsin Formation at Wadi Iggiten (calculated on m/z 85)

Sample No.	T31	T32	T33	T34
Pr/Ph	0.74	0.58	0.95	0.97
Pr/n-C17	0.32	0.29	0.23	0.26
Pr/n-C18	0.48	0.52	0.47	0.49
CPI	0.93	0.80	0.86	0.70

Table 3.10: Normal alkanes and isoprenoids ratios of the Bir Tlacsin Formation at Wadi Awzarq (calculated on m/z 85)

Sample No.	T37	T38	T39	T40
Pr/Ph	0.68	0.52	0.89	0.91
Pr/n-C17	0.28	0.25	0.19	0.22
Pr/n-C18	0.52	0.56	0.51	0.53
CPI	0.97	0.84	0.90	0.74

Table 3.11: Steranes of the Bir Tlacsin Formation at Wadi Maghidat (calculated on m/z 217)

Sample No.	T5	T6	T9	T10
C_{27}	49.42	49.33	46.22	46.25
C_{28}	33.20	33.24	23.10	23.07
C_{29}	17.38	17.43	30.68	30.68
C_{29} (ßß/ßß+αα)	0.28	0.26	0.23	0.28
WI	0.89	0.83	0.90	0.93

Table 3.12: Steranes of the Bir Tlacsin Formation at Wadi Tashat (calculated on m/z 217)

Sample No.	T15	T16	T17	T18
C_{27}	49.39	49.37	49.24	49.30
C_{28}	33.22	33.27	33.20	33.18
C_{29}	17.39	17.36	17.56	17.52
C_{29} (ßß/ßß+αα)	0.23	0.21	0.21	0.26
WI	0.88	0.91	0.79	0.76

Table 3.13: Steranes of the Bir Tlacsin Formation at Wadi Anlakm (calculated on m/z 217)

Sample No.	T21	T22	T23	T24	T27	T28
C_{27}	59.35	59.27	46.09	46.14	49.35	49.38
C_{28}	33.12	33.09	32.70	32.76	33.22	33.27
C_{29}	7.53	7.64	21.21	21.10	17.43	17.35
C_{29} (ßß/ßß+αα)	0.15	0.17	0.24	0.20	0.25	0.25
WI	0.89	0.94	0.54	0.50	0.77	0.72

Table 3.14: Steranes of the Bir Tlacsin Formation at Wadi Iggiten (calculated on m/z 217)

Sample No.	T31	T32	T33	T34
C_{27}	49.34	49.32	49.19	49.25
C_{28}	33.27	33.32	33.25	33.23
C_{29}	17.34	17.31	17.51	17.47
C_{29} (ßß/ßß+αα)	0.28	0.23	0.19	0.15
WI	0.93	0.96	0.84	0.81

Table 3.15: Steranes of the Bir Tlacsin Formation at Wadi Awzarq (calculated on m/z 217)

Sample No.	T37	T38	T39	T40
C_{27}	49.44	49.42	49.29	49.35
C_{28}	33.17	33.22	33.15	33.13
C_{29}	17.44	17.41	17.61	17.57
C_{29} (ßß/ßß+αα)	0.27	0.28	0.22	0.18
WI	0.83	0.86	0.74	0.71

Table 3.16: TPP ratios of the Bir Tlacsin Formation at Wadi Maghidat (calculated on m/z 217)

Sample No.	T5	T6	T9	T10
$C_{31}R/C_{30}H$	0.53	0.57	0.47	0.40
C_{32} 22S/(22S+22R)	0.48	0.44	0.22	0.26
Hopanes/(Hopanes+∑20R steranes)	0.65	0.61	0.46	0.46
TPP ratios	0.21	0.18	0.11	0.16

Table 3.17: TPP ratios of the Bir Tlacsin Formation at Wadi Tashat (calculated on m/z 217)

Sample No.	T15	T16	T17	T18
$C_{31}R/C_{30}H$	0.43	0.44	0.36	0.34
C_{32} 22S/(22S+22R)	0.40	0.36	0.17	0.19
Hopanes/(Hopanes+∑20R steranes)	0.43	0.50	0.29	0.33
TPP ratios	0.22	0.22	0.17	0.19

Table 3.18: TPP ratios of the Bir Tlacsin Formation at Wadi Anlakm (calculated on m/z 217)

Sample No.	T21	T22	T23	T24	T27	T28
$C_{31}R/C_{30}H$	0.55	0.51	0.53	0.53	0.39	0.42
C_{32} 22S/(22S+22R)	0.22	0.21	0.21	0.16	0.48	0.41
Hopanes/(Hopanes+∑20R steranes)	0.60	0.66	0.56	0.50	0.49	0.41
TPP ratios	0.10	0.13	0.23	0.19	0.12	0.11

Table 3.19: TPP ratios of the Bir Tlacsin Formation at Wadi Iggiten (calculated on m/z 217)

Sample No.	T31	T32	T33	T34
$C_{31}R/C_{30}H$	0.38	0.33	0.56	0.58
C_{32} 22S/(22S+22R)	0.34	0.39	0.17	0.16
Hopanes/(Hopanes+∑20R steranes)	0.39	0.44	0.45	0.37
TPP ratios	0.11	0.17	0.15	0.21

Table 3.20: TPP ratios of the Bir Tlacsin Formation at Wadi Awzarq (calculated on m/z 217)

Sample No.	T37	T38	T39	T40
$C_{31}R/C_{30}H$	0.49	0.51	0.37	0.32
C_{32} 22S/(22S+22R)	0.28	0.31	0.20	0.18
Hopanes/(Hopanes+∑20R steranes)	0.61	0.54	0.38	0.33
TPP ratios	0.17	0.12	0.14	0.16

3.2. Statistical Analysis

Using the SPSS© program, different statistical methods were applied in this chapter. These methods are descriptive statistics (Table 3.21), Pearson's correlation coefficient (correlation analysis, Table 3.22 and Fig. 3.1) and factor analysis (Table 3.23). The correlation analysis (Table 3.22 and Fig. 3.1) shows a positive correlation between TOC and S_2 (r = 0.77), which indicates the contribution of S_2 from TOC. Furthermore, TOC is negatively correlated with HI, OI and PI (r = -0.62, -0.99 and -0.14, respectively), which indicates, in agreement with Edwards *et al.,* (1999) and El Nady *et al.,* (2015), that the maturity of the studied source rock is independent of the amount of organic matter. In addition, the positive correlation between S_1 and S_2 (r = 0.80) and weak correlation between T_{max} and HI (r = 0.29) indicate the immaturity of the organic matter.

Three factors explaining approximately 87.97% of the total variables are extracted (Table 3.23). The distribution of the analyzed parameters in factors 1, 2 and 3 is shown in Fig. (3.2). The following is a brief discussion of the three factors:

Factor one (F1):

It accounts for about 49.15% of the total variables. It shows positive loading for TOC, T_{max}, S_1, S_2 and S_3. This factor seems to be significant in interpreting the organic matter richness and hydrocarbon potentiality of the Bir Tlacsin Formation.

Factor two (F2):

It accounts for 27.44% of the total variables. It shows positive loading for HI, OI and PI. This factor determines the type of organic matter that characterizes the Bir Tlacsin Formation.

Factor three (F3):

It accounts for 11.32% of the total variables. It shows positive loading for Ro. This factor is of no importance.

Table 3.21: Descriptive statistics of the studied shale samples

Parameters	N	Minimum	Maximum	Mean	Std. Deviation
TOC	22	0.65	1.92	1.47	0.39
T_{max}	22	395.00	427.00	418.64	8.01
Ro	22	0.35	0.53	0.44	0.06
S_1	22	2.09	6.89	5.49	1.26
S_2	22	2.57	6.79	5.78	1.10
S_3	22	1.05	1.45	1.32	0.09
HI	22	330.00	539.47	404.95	74.56
OI	22	67.38	161.54	96.42	26.81
PI	22	0.42	0.55	0.48	0.03

Table 3.22: Correlation matrix of the studied shale samples

Parameters	TOC	T_{max}	Ro	S_1	S_2	S_3	HI	OI	PI
TOC	1.00								
T_{max}	0.46	1.00							
Ro	-0.16	0.05	1.00						
S_1	0.46	0.77	0.17	1.00					
S_2	0.77	0.83	0.04	0.80	1.00				
S_3	0.43	0.85	-0.15	0.70	0.74	1.00			
HI	-0.62	0.29	0.30	0.24	0.02	0.23	1.00		
OI	-0.99	-0.49	0.12	-0.50	-0.78	-0.42	0.60	1.00	
PI	-0.14	0.29	0.23	0.71	0.16	0.26	0.39	0.09	1.00

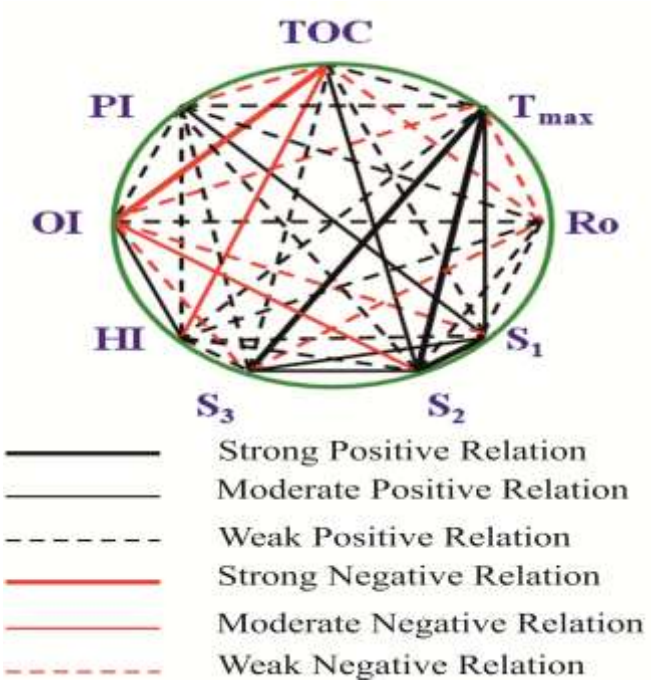

Fig. 3.1: Correlations among the analyzed parameters in the studied samples (intensity of lines corresponds to the strength of the correlation coefficient (< 0.4 to > 0.8)) (red line means inverse relation)

Table 3.23: Factor analysis of the studied shale samples

Eigenvalue	4.42	2.47	1.02
% of Variance	49.15	27.44	11.32
Cumulative %	49.15	76.60	87.92
Factor	1	2	3
TOC	0.78	-0.60	0.16
T_{max}	0.87	0.29	-0.19
Ro	-0.02	0.43	0.80
S_1	0.86	0.40	0.15
S_2	0.96	-0.02	0.02
S_3	0.82	0.23	-0.40
HI	-0.06	0.91	-0.23
OI	-0.80	0.56	-0.20
PI	0.30	0.69	0.22

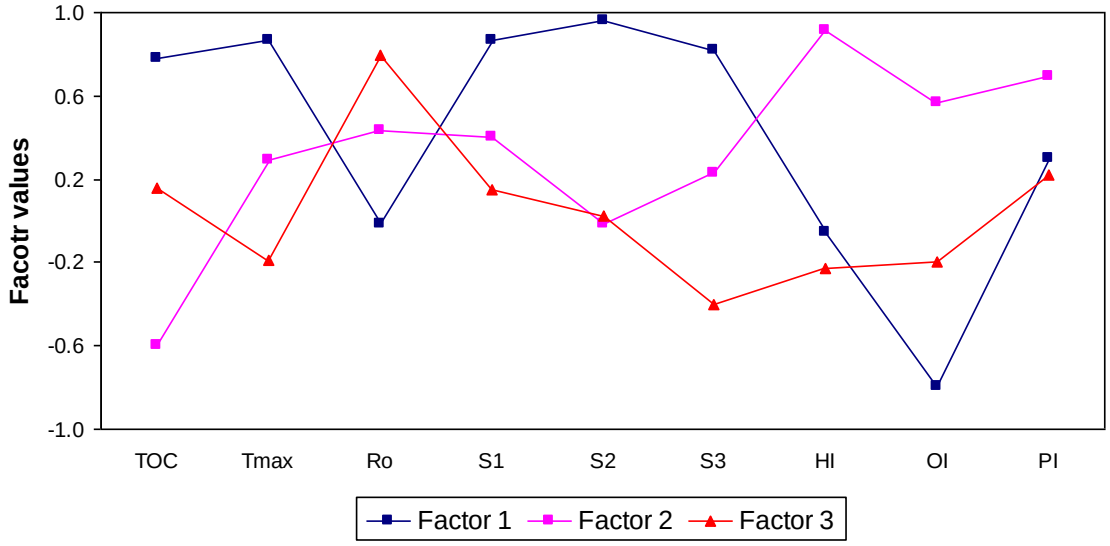

Fig. 3.2: Distribution of the analyzed parameters in factors 1, 2 and 3

3.3. Total Organic Carbon (TOC)

In this study, TOC is positively correlated with Al_2O_3 (r = 0.74, Fig. 3.3). This relationship means that clay minerals are the sole carrier of TOC. This assumption is also supported by the TOC versus Al/Si ratio plot (Fig. 3.4).

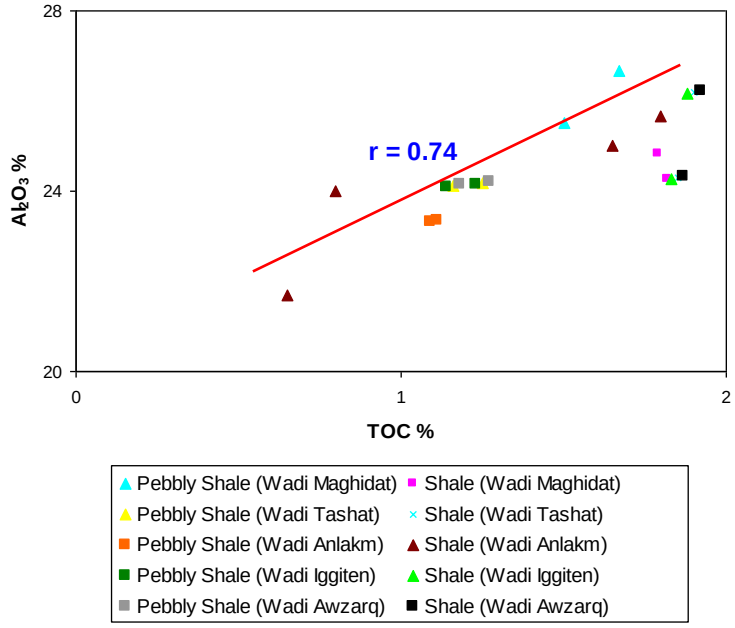

Fig. 3.3: Relationship between TOC and Al_2O_3 in the studied shale samples

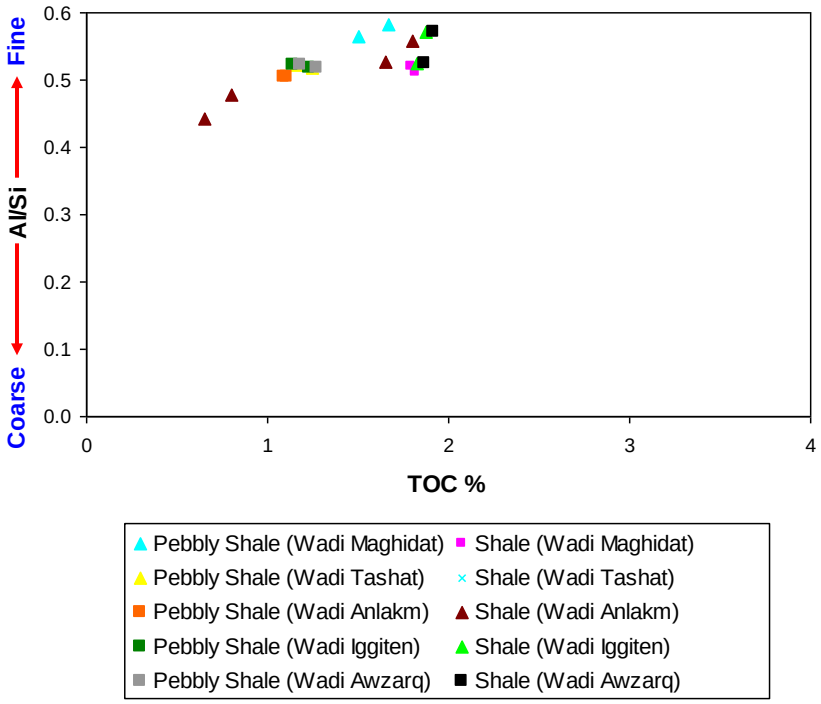

Fig. 3.4: Relationship between TOC and Al/Si ratio in the studied shale samples (fields after Sun et al., 2016)

TOC and U concentrations typically display a predictable linear relationship in black shales and thus U contents, as inferred from gamma logs, are often used as a proxy for organic richness (Spirakis, 1996). Research has shown, however, that some organic-rich shales display uncharacteristically low U concentrations despite having consistently high concentrations of organic carbon (Luning and Kolonic, 2003). In the present study, TOC is weakly correlated with U (r = 0.45, Fig. 3.5).

3.4. Organic Matter Richness and Hydrocarbon Potentiality

Tables (3.24-26) show the guidelines for interpreting source rock quantity, quality and maturation. The organic richness and potential of a rock sample is evaluated by measuring the amount of TOC in the whole rock and pyrolysis derived S_2 of the rock samples (Dembicki, 2009), while some authors (e.g., Ghori, 2002) use the TOC-GP relationship to determine the hydrocarbon potentiality. Figs (3.6-7) show that the studied shale samples are good source rocks (except for samples T23 and T24).

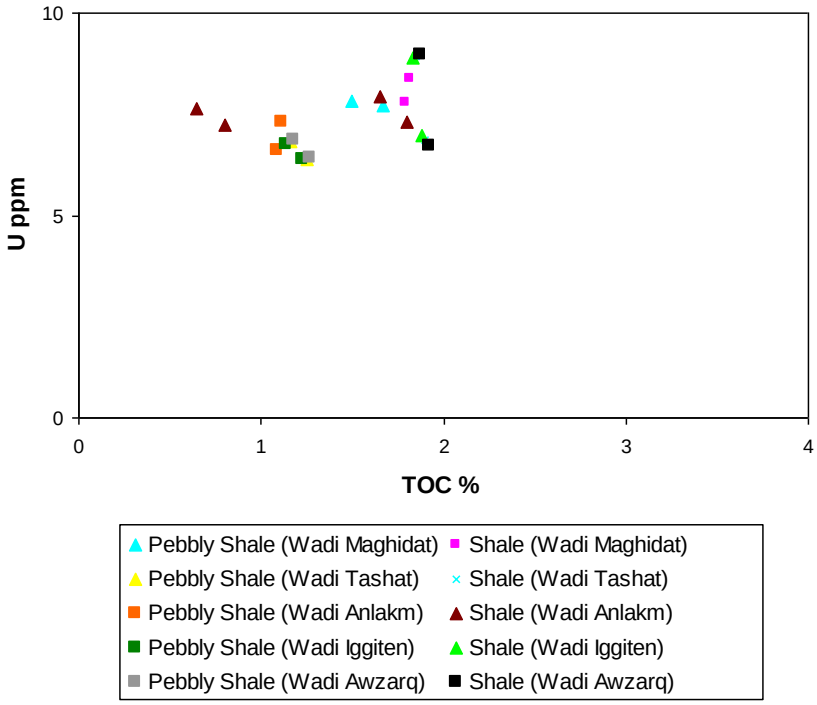

Fig. 3.5: Relationship between TOC and U in the studied shale samples

Table 3.24: Geochemical parameters describing the petroleum potential (quantity) of a source rock (after Peters and Cassa, 1994)

Quantity	TOC	S_1(mg HC/g rock)	S_2(mg HC/g rock)
Poor	<0.5	<0.5	<2.5
Fair	0.5 to 1	0.5 to 1	2.5 to 5
Good	1 to 2	1 to 2	5 to 10
Very Good	2 to 4	2 to 4	10 to 20
Excellent	>4	>4	>20

Table 3.25: Geochemical parameters describing kerogen type (quality) and the character of expelled products (after Peters and Cassa, 1994)

Quality	HI (mg HC/g TOC)	S_2/S_3	Kerogen Type
None	<50	<1	IV
Gas and Coal	50 to 200	1 to 5	III
Gas and Oil	200 to 300	5 to 10	II/III
Gas and Oil	300 to 600	10 to 15	II
Oil	>600	>15	I

Table 3.26: Geochemical parameters describing the thermal maturation (Atta-Peters and Garrey, 2014)

Maturation	Ro (%)	Tmax (^oC)
Immature	0.2 to 0.6	<435
Early Mature	0.6 to 0.65	435 to 445
Peak Mature	0.65 to 0.9	445 to 450
Late Mature	0.9 to 1.35	450 to 470
Post Mature	>1.35	>470

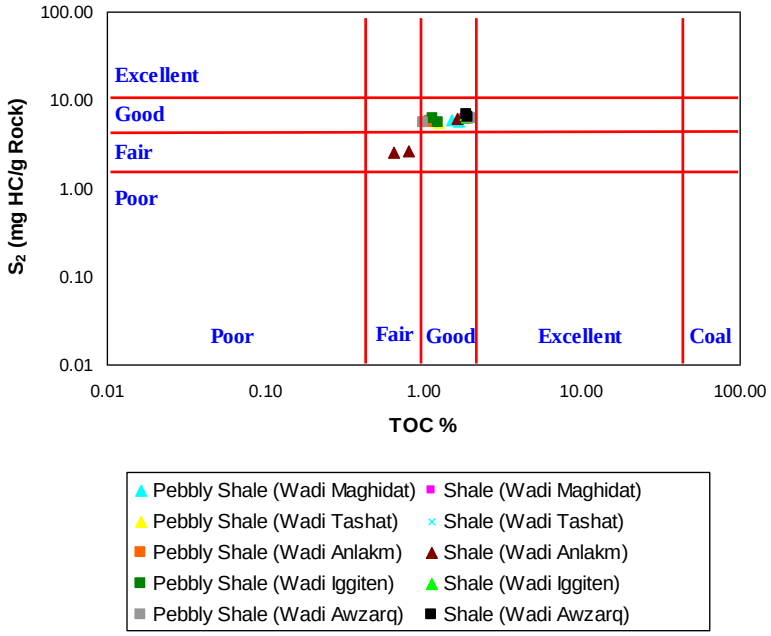

Fig. 3.6: Plot of TOC vs. S_2 showing the hydrocarbon potentialities for the Bir Tlacsin Formation (fields after Dembicki, 2009)

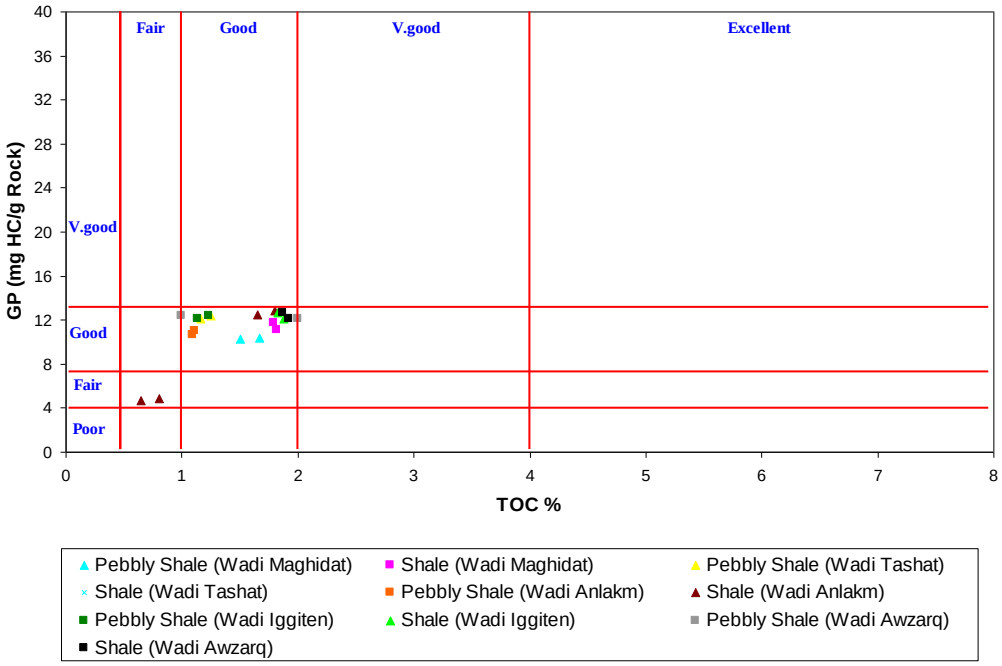

Fig. 3.7: Plot of TOC vs. GP showing the hydrocarbon potentialities for the Bir Tlacsin Formation (fields after Ghori, 2002)

3.5. Organic Matter Type

The type of organic matter completes the organic richness in evaluating the generating potential of a source rock. The organic matter in potential source rocks must be of the type that is capable of generating petroleum. The HI refers to the remaining generation potential of organic matter and T_{max} represents the temperature at the peak of hydrocarbon generation. HI versus T_{max} is commonly used to avoid influence of the OI for determining kerogen type (Hunt, 1996). Determining kerogen type using HI versus T_{max} appears to be more accurate than OI versus HI (El-Kammar *et al.*, 2015). The plot of TOC versus S_2 is the best method for analyzing the true average HI and measuring the adsorption of hydrocarbons by the rock matrix (Obaje *et al.*, 2004). In the present study, the plots of HI versus OI, TOC versus S_2 and T_{max} versus HI (Figs. 3.8-10) show that all shale samples are characterized by kerogen of type II (except for samples T23 and T24, which are characterized by mixed type II-III), which suggest, in agreement with Dahl *et al.*, (2004) and Shaltami *et al.*, (2017), that the organic matter is mostly derived from

marine algae and phytoplankton organisms which can be considered as a typical source of oil and gas.

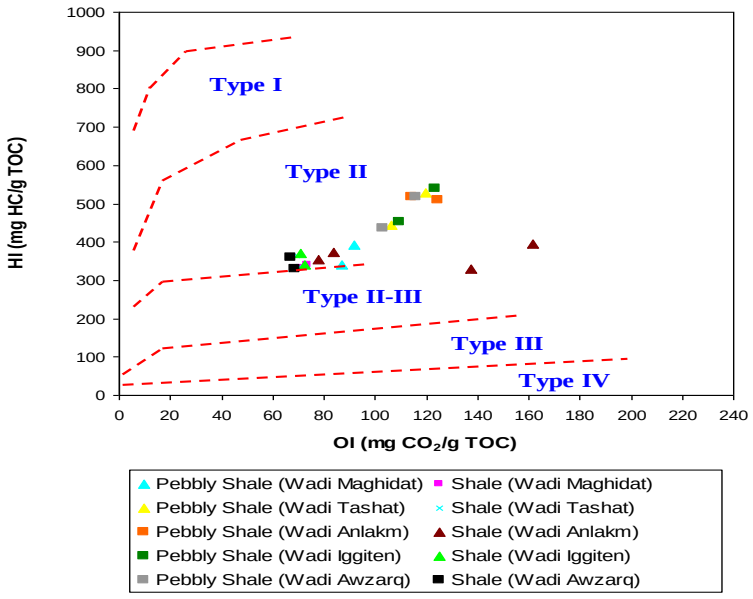

Fig. 3.8: Plot of OI vs. HI showing the kerogen type for the Bir Tlacsin Formation (fields after Van Krevelen, 1961)

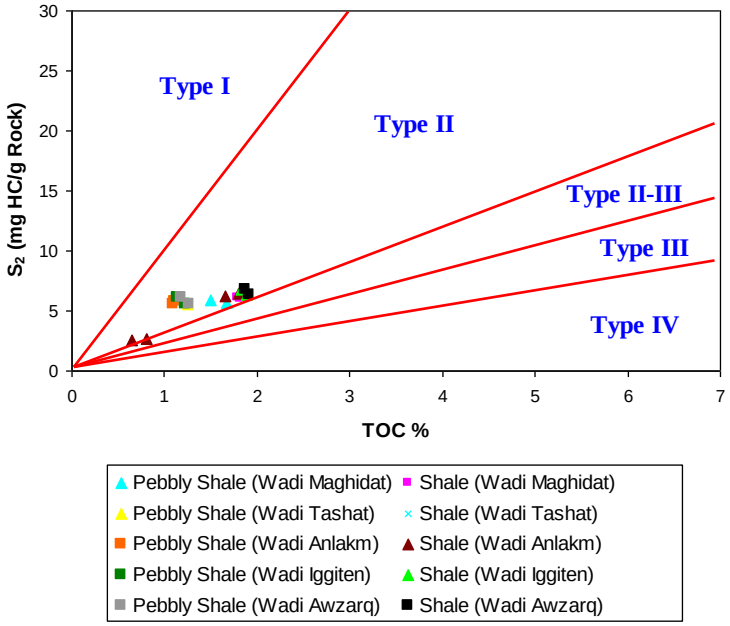

Fig. 3.9: Plot of TOC vs. S_2 showing the kerogen type for the Bir Tlacsin Formation (fields after Longford and Blanc-Valleron, 1990)

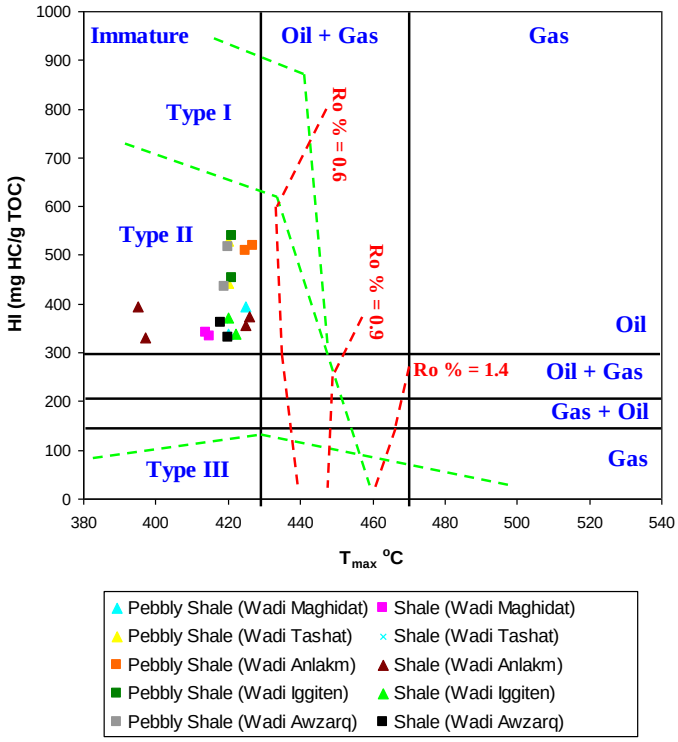

Fig. 3.10: Plot of Tmax vs. HI showing the thermal maturity and kerogen type for the Bir Tlacsin Formation (fields after Hall et al., 2016)

The plots of TOC versus S_1, PI versus T_{max} and T_{max} versus BI can differentiate between the migrated (nonindigenous) and generated (indigenous) hydrocarbons (Hunt, 1996; Hakimi *et al.*, 2010; Makky *et al.*, 2014; Ghassal *et al.*, 2018). The majority of the studied samples were shown to be migrated (nonindigenous) hydrocarbons (Figs. 3.11-13).

3.6. Thermal Maturity

The maturity levels for the oil window depend on the type of organic matter (Bacon *et al.*, 2000), and encompass a vitrinite reflectance (Ro) ranges from 0.6 to 1.4% and temperature at maximum rate of hydrocarbon generation during S_2 evolution (T_{max}) from 435 to 470°C. The PI parameter is another measure of maturity, with values ranging from 0.15 to 0.4 normally associated with oil generation.

The plots of T_{max} versus HI (Fig. 3.10), C_{32} 22S/(22S+22R) homohopane versus C_{29} (ßß/ßß+αα) sterane and T_{max} versus Ro (Figs. 3.14-15) are used to determine the level of maturation for the Bir Tlacsin Formation. In general, the studied organic matter are thermally immature.

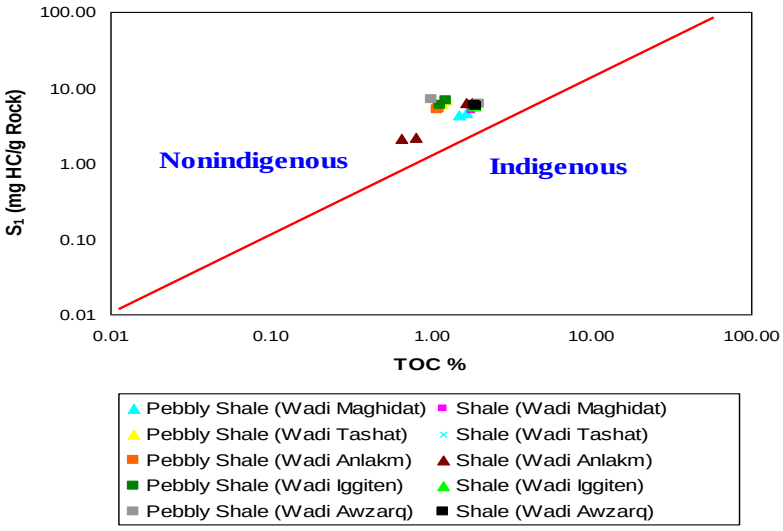

Fig. 3.11: Plot of. TOC vs. S_1 for the Bir Tlacsin Formation (fields after Hunt, 1996)

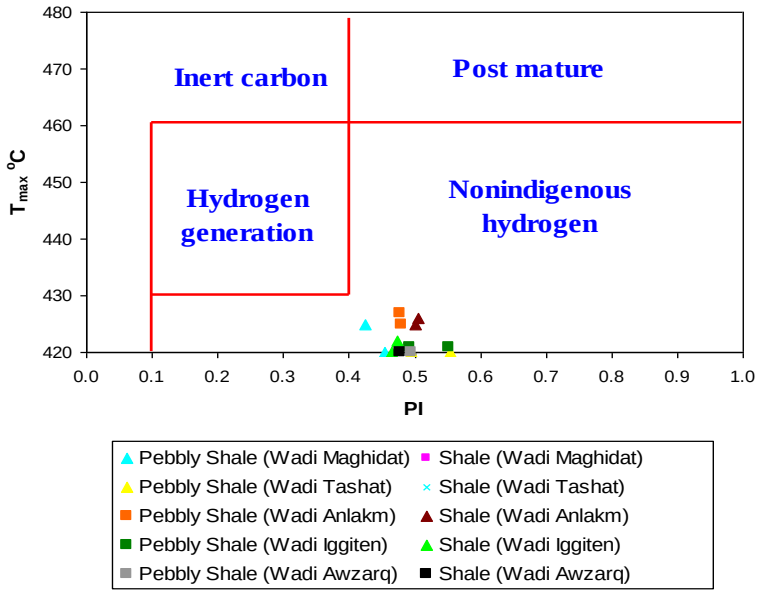

Fig. 3.12: Plot of. PI vs. T_{max} for the Bir Tlacsin Formation (fields after Hakimi et al., 2010)

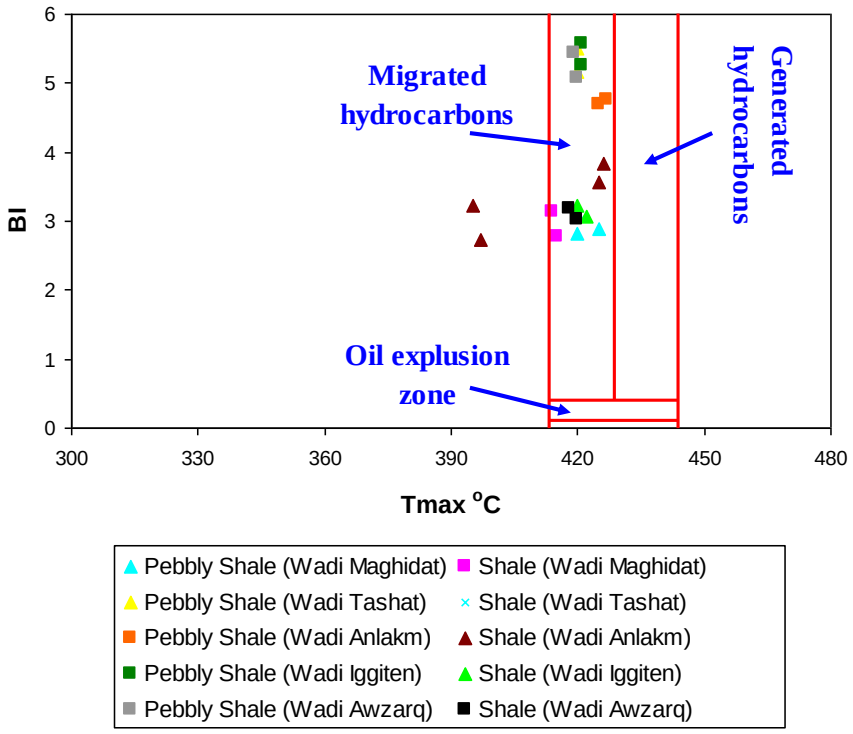

Fig. 3.13: Plot of. T_{max} vs. BI for the Bir Tlacsin Formation (fields after Makky et al., 2014)

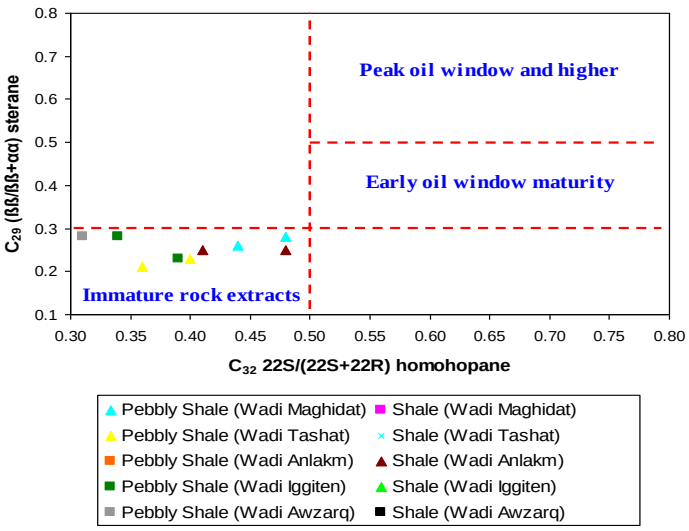

Fig. 3.14: Plot of C_{32} 22S/(22S+22R) homohopane vs. C_{29} (ββ/ββ+αα) sterane showing the thermal maturity for the Bir Tlacsin Formation (fields after Peters and Moldowan, 1993)

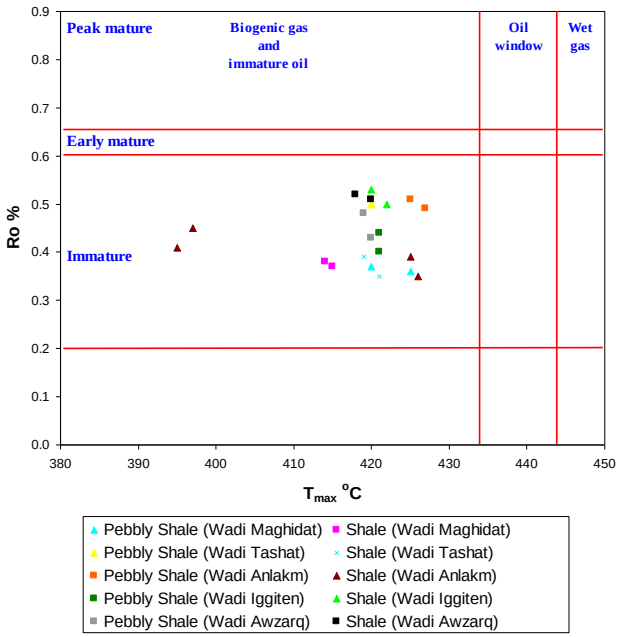

Fig. 3.15: Plot of Tmax vs. Ro showing the thermal maturity for the Bir Tlacsin Formation (fields after Atta-Peters and Garrey, 2014)

3.7. Organic Matter Origin, Depositional Environment and Paleooxygenation Conditions

The origin of the organic matter was examined based on normal alkanes, hopanoids, steroids and related compounds. The n-alkanes distribution patterns of saturated hydrocarbons can be used to define organic matter input from different producers (Brassell *et al.*, 1978). The long chain n-alkanes (>n-C_{25}) are characteristic biomarkers for higher terrestrial plants (Eglinton and Hamilton, 1967), whereas the short-chain n-alkanes (<n-C_{20}) are predominantly found in algae and microorganisms (Peters *et al.*, 2005). Waxiness index (WI) is used to determine the amount of land-derived organic matter in sediments, based on the assumption that terrigenous material contributes high molecular weight normal alkane components (Peters *et al.*, 2005). Tm (C_{27} 17α(H)- 22,29,30-trisnorhopane) and Ts (C_{27} 18α(H)-22,29,30-trisnorneohopane) are well known to be influenced by maturation, type of organic matter and lithology (Peters and Moldowan, 1993). The dominance of C_{27} sterols (steranes) indicates a preponderance of mainly planktonic/algal organic matter, while the C_{29} sterols are more

typically associated with land plants (Volkman, 1986). Grantham and Wakefield (1988) showed that the ratio of C_{28}/C_{29} regular steranes in marine environments is controlled not only by facies but also increases with increasing age. They attributed this change to evolutionary trends within living organisms. This ratio allows the oils to be dated to a first approximation.

The most widely used biomarker parameter for the assessment of redox conditions during sediment accumulation is the pristane/phytane (Pr/Ph) ratio. The idea that the ratio of these two acyclic isoprenoids alkanes is influenced by the degree of oxygenation was first voiced by Brooks *et al.,* (1969), but developed and popularized by Didyk *et al.,* (1978). According to Peters and Moldowan (1993) organic matter deposited under oxidizing conditions is expected to contain high Pr/Ph ratio of >3, while low values of Pr/Ph ratio (<1) indicate anoxic conditions, and values between 1 and 3 suggest suboxic conditions. In addition, C_{31}-22Rhopane/C_{30}-hopane ratio can be used to infer different depositional environments. This ratio is generally higher than 0.25 for marine environments whereas lower than 0.25 for lacustrine settings (Peters *et al.,* 2005).

In the present study, the ratios of CPI (0.51-0.98) and WI (0.5-0.96) indicate, in agreement with Murray and Boreham (1992) and Shaltami *et al.,* (2017), marine organic matter. In all samples, the C_{27} steranes predominate over the C_{29} steranes, reflecting a high contribution of aquatic organic matter relative to terrigenous organic matter as indicated by the regular sterane ratio ternary diagram (Fig. 3.16). This is corroborated by low C_{29}/C_{27} sterane ratios (Fig. 3.17). The low Pr/Ph ratio (0.44-0.97) is probably due to anoxic conditions at the time of source rock deposition and/or to contributions by marine source rocks during oil formation. The Pr/n-C_{17} and Ph/n-C_{18} ratios further indicate reducing conditions during deposition of the sediments (Fig. 3.18). This interpretation is further supported by the Pr/Ph versus WI and Pr/Ph versus CPI plots (Figs. 3.19-20). During oil maturation, phytane is generated more rapidly than pristane, so Pr/Ph ratios <1 could also be a response to immaturity (Shaltami *et al.,* 2017).

Echikh and Sola (2000) found that the Bir Tlacsin Formation was deposited in a marine environment. $C_{31}R/C_{30}$ hopane ratios of the shale samples are in the range of 0.32 to 0.58, suggesting that the Bir Tlacsin Formation were deposited in a marine environment (Fig. 3.21). The TPP ratios of the shale samples are relatively low, ranging from 0.1 to 0.23, supporting the deposition a marine environment. This is supported by the plot of TPP ratios against hopanes/(hopanes+Σ20R steranes) (Fig. 3.22) which also indicates a marine depositional environment.

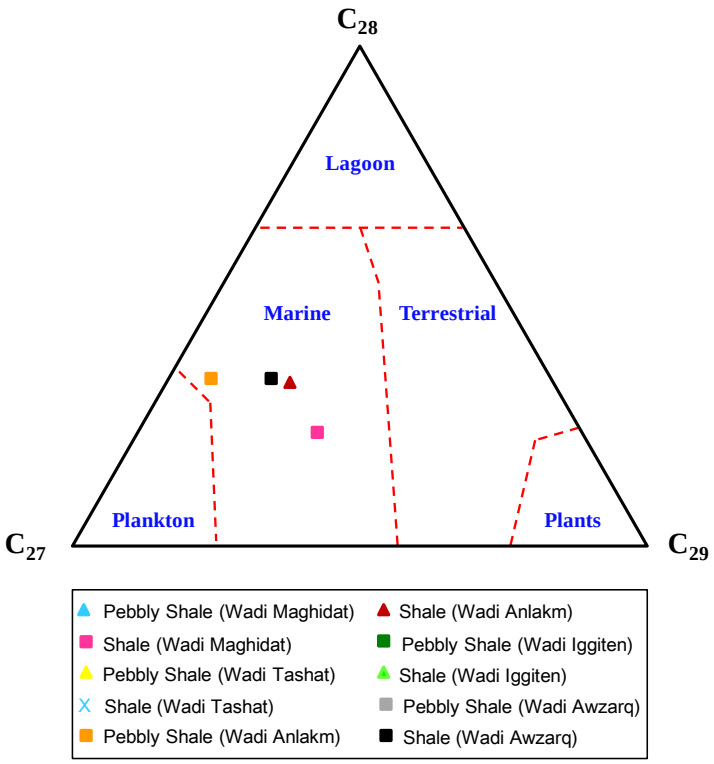

Fig. 3.16: Ternary diagram of regular steranes showing the organic matter input in the studied shale samples (fields after Huang and Meinschein, 1979)

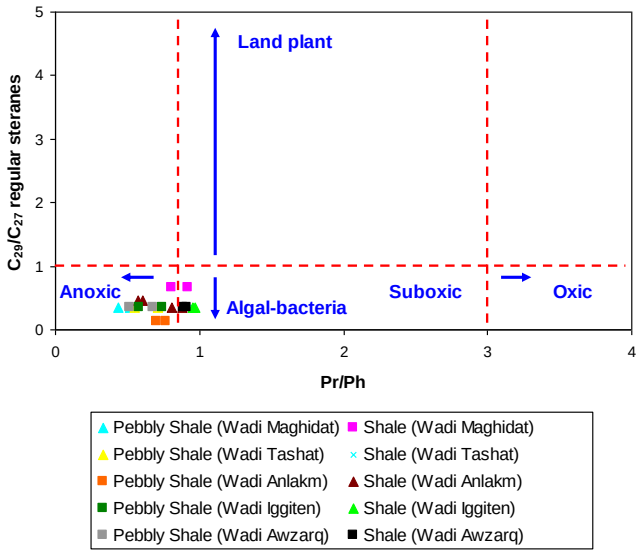

Fig. 3.17: Plot of Pr/Ph ratios vs. C_{29}/C_{27} regular steranes showing the paleooxygenation conditions and organic matter type for the Bir Tlacsin Formation (fields after Yandoka et al., 2015)

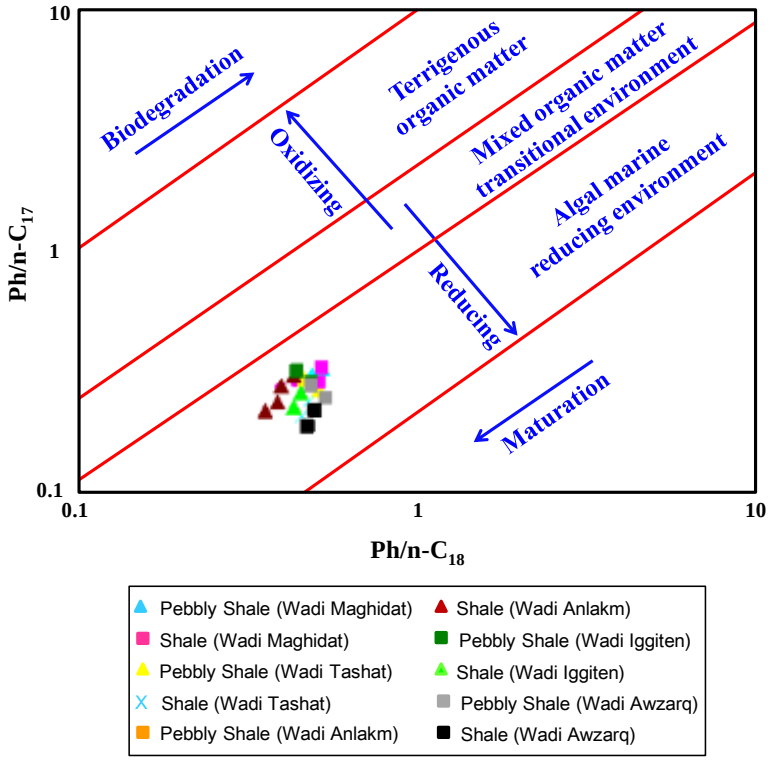

Fig. 3.18: Plot of Ph/n-C_{18} vs. Pr/n-C_{17} showing the paleooxygenation conditions and organic matter type for the Bir Tlacsin Formation (fields after Shanmugam, 1985)

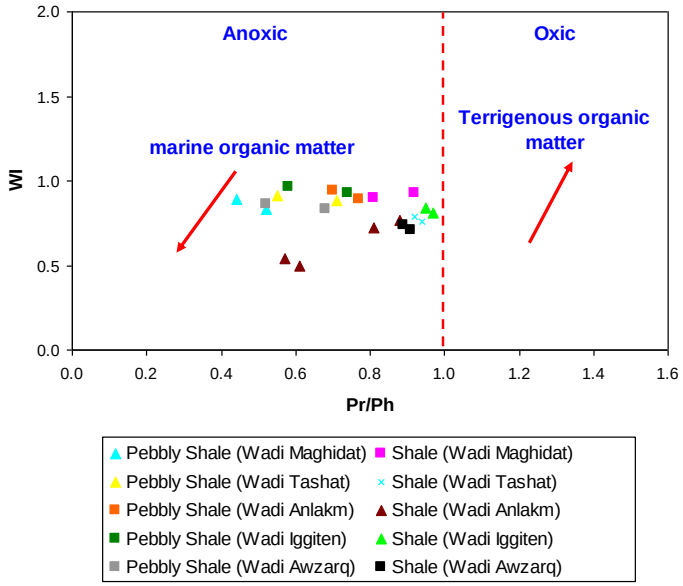

Fig. 3.19: Plot of Pr/Ph vs. WI showing the paleooxygenation conditions and organic matter type for the Bir Tlacsin Formation (fields after El Diasty and Moldowan, 2012)

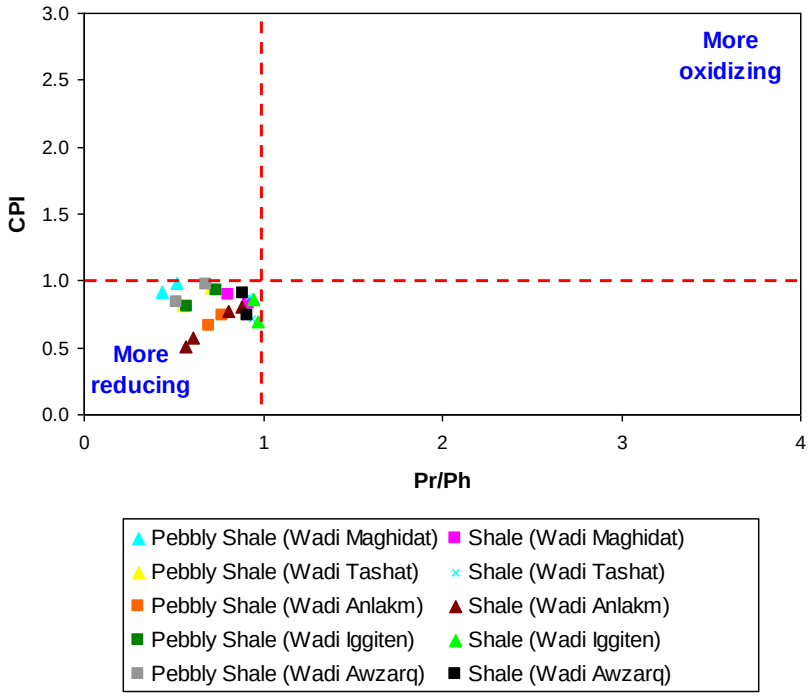

Fig. 3.20: Plot of Pr/Ph vs. CPI showing the paleooxygenation conditions of the Bir Tlacsin Formation (fields after Akinlua et al., 2007)

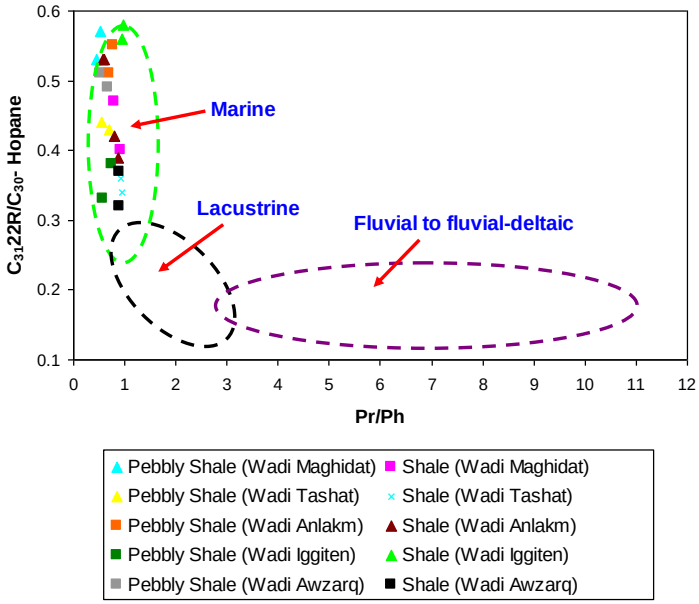

Fig. 3.21: Plot of $C_{31}R/C_{30}$ hopane ratio vs. Pr/Ph ratio showing the depositional environment of the Bir Tlacsin Formation (fields after Peters et al., 2005)

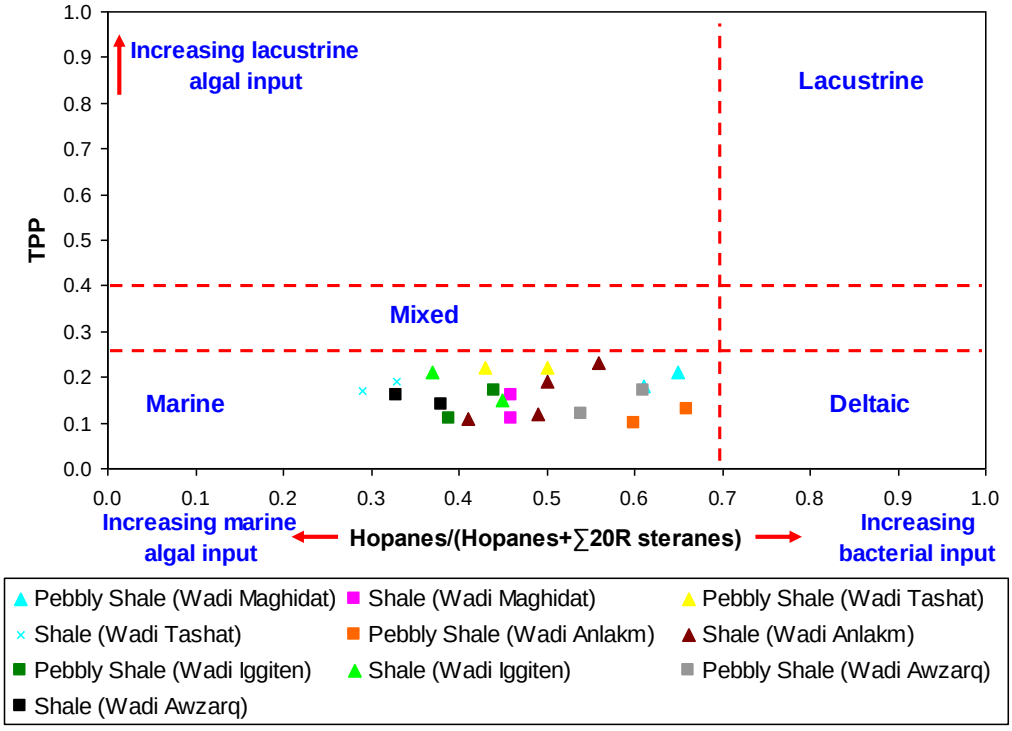

Fig. 3.22: Plot of TPP ratio vs. hopane/(hopanes+Σ20R steranes) showing the depositional environment of the Bir Tlacsin Formation (fields after Holba et al., 2003)

CHAPTER FOUR
CONCLUSIONS

The present study aims to evaluate the inorganic and organic geochemical characteristics of the Bir Tlacsin Formation at Ghat area, SW Libya. Using geochemical data, the depositional environment, paleooxygenation, paleoclimate, paleosalinity, provenance, tectonic setting, organic matter richness, kerogen types and thermal maturation of this formation were determined. About 40 samples were collected from the Bir Tlacsin Formation from 5 stations (Wadi Maghidat, Wadi Tashat, Wadi Anlakm, Wadi Iggiten, and Wadi Awzarq). The lithostratigraphic correlation between the studied sections showed that the shale units (shale and pebbly shale) are present in all sections (except for unit 5 in the Wadi Anlakm). Analysis of major oxides and trace elements was done by inductively coupled plasma-mass spectrometry (ICP-MS) technique. Rock-Eval pyrolysis was carried out on a Rock-Eval 6 instrument, while the TOC was measured on a Leco instrument. Aliphatic and aromatic fractions were analyzed by Gas Chromatography-Mass Spectrometry (GC-MS) using a Hewlett Packard (HP) 5973 mass-selective detector (MSD) interfaced to a HP6890 gas chromatograph (GC).

Regarding inorganic geochemistry, the SiO_2, TiO_2 and CaO contents in the sandstones are slightly higher than the shales, whereas, shales contain more Al_2O_3 content than the sandstones. The difference in the concentration of high field strength elements and heavy metals between sandstones and shales has no geochemical significance. The correlation matrix showed that 1) the SiO_2 occurs in both silicate and free silica modes, 2) the aluminosilicates are not the sole carrier of TiO_2 and Ga, 3) the enrichment of CaO can be attributed to the presence of diagenetic calcite cement, 4) the accessory minerals are the main carriers of trace elements and 5) each of the heavy metals and high field strength elements are definitely present in different minerals. The chemical classifications indicated that the sandstones of the Bir Tlacsin Formation are classified as greywackes. The Th/Cr, Th/Sc and Th/Co ratios and the Zr versus TiO_2 and Ni versus TiO_2 plots suggested that the granitic rocks found in the Air Mountains,

central Niger, may be the probable source of the Bir Tlacsin Formation. The Zr/Hf, Hf/Ta and Zr/Ta ratios showed that the possible origin of the studied formation is the marine environment. Moreover, the high B/Ga ratio indicated that the Bir Tlacsin Formation was deposited in a high salinity marine environment. The AU, δU, and Ni/Co, V/Cr, V/Sc, V/(V+Ni) and U/Th ratios, and the Ni versus V, V/Sc versus V/(V+Ni) and U/Th versus AU plots, suggested deposition in anoxic conditions. The CIA, CIW, PIA and CIW´ values pointed to relatively moderate to high degree of chemical weathering in the source area. The discrimination diagrams showed that the detected clay minerals in the shales are smectite, kaolinite, gibbsite and chlorite. The ICV indicated the immaturity of the shales whereas the sandstones are thermally submature to mature. The climatic discrimination diagrams showed that the semi-arid and semi-humid climate was prevalent in the source area. The tectonic discrimination diagrams indicated that the Bir Tlacsin Formation fall in the fields of active continental margin (C) and passive continental margin (D).

Regarding organic geochemistry, the correlation analysis showed that the maturity of the studied shales is independent of the amount of organic matter. The TOC versus Al_2O_3 and TOC versus Al/Si ratio plots indicated that clay minerals are the sole carrier of TOC. The TOC versus S_2 and TOC versus GP plots suggested that the shale samples are good source rocks (except for samples T23 and T24). The plots of HI versus OI, TOC versus S_2 and T_{max} versus HI showed that all shale samples are characterized by kerogen of type II (except for samples T23 and T24, which are characterized by mixed type II-III). Furthermore, the plots of TOC versus S_1, PI versus T_{max} and T_{max} versus BI showed that the hydrocarbons are mainly migrated (nonindigenous). The plots of T_{max} versus HI, C_{32} 22S/(22S+22R) homohopane versus C_{29} (ßß/ßß+αα) sterane and T_{max} versus Ro suggested that the studied organic matter are thermally immature. The CPI and WI ratios and the regular sterane ratio ternary diagram indicated marine organic matter. Moreover, the $C_{31}R/C_{30}$ hopane vs. Pr/Ph and TPP ratio vs. hopane/(hopanes+Σ20R steranes) plots indicated a marine depositional environment. The low Pr/Ph ratio and the Pr/n-C_{17} versus Ph/n-C_{18}, Pr/Ph versus WI and Pr/Ph versus CPI plots suggested reducing conditions during deposition of the sediments.

References

Abdullah, M. (2010): Petrography and facies of the Al- Mahruqah Formation in the Murzuq Basin, SW Libya. Unpublished PhD Thesis, University of Hamburg, Germany.

Abugares, Y.I. and Ramaekers, P. (1993): Short notes and guidebook on the Palaeozoic geology of the Ghat area, SW Libya. Geology of the Sirt Basin Field Guide. 1st Symposium on the Sedimentary Basins of Libya, Earth Science Society of Libya, 84 p.

Akinlua, A., Ajayi, T.R. and Adeleke, B.B. (2007): Organic and inorganic geochemistry of northwestern Niger Delta oils. Geochemical Journal; 41: 271-281.

Akinlua, A., Olise, F.S., Akomolafe, A.O. and McCrindle, R.I. (2016): Rare earth element geochemistry of petroleum source rocks from northwestern Niger Delta. Marine and Petroleum Geology; 77: 409-417.

Araujo, C.E.G., Pineo, T.R.G., Caby, R., Costa, F.G., Cavalcante, J.C., Vasconcelos, A.M. and Rodrigues, J.B. (2010): Provenance of the Novo Oriente Group, Southwestern Ceara Central Domain, Borborema Province (NE-Brazil): A dismembered segment of a magma-poor passive margin or a restricted rift-related basin. Gondwana Research; 18: 497-513.

Armstrong-Altrin, J.S. (2009): Provenance of sands from Cazones, Acapulco and Bahia Kino beaches, Mexico. Revista Mexicana de Ciencias Geologicas; 26(3): 764-782.

Armstrong-Altrin, J.S., Lee, Y.I., Verma, S.P. and Ramasamy, S. (2004): Geochemistry of sandstones from the Upper Miocene Kudankulam Formation, southern India: implication for provenance, weathering and tectonic setting. Journal of Sedimentary Research; 74: 285-297.

Atta-Peters, D. and Garrey, P. (2014): Source rock evaluation and hydrocarbon potential in the Tano basin, South Western Ghana, West Africa. International Journal of Oil, Gas and Coal Engineering; 2(5): 66-77.

Aziz, A. (2000): Stratigraphy and hydrocarbon potential of the Lower Palaeozoic succession of License NC-115, Murzuq Basin, SW Libya. In: M.A. Sola and D. Worsley (eds) Geological Exploration in Murzuq Basin. Elsevier, Amsterdam; 349-368.

Bacon, C. A., Calver, C. R., Boreham, C. J., Leaman, D. E., Morrison, K. C., Revill, A. T. and Volkman, J. K. (2000): The petroleum potential of onshore Tasmania: a review. Mineral Resources Tasmania, Geological Survey Bulletin; 71: 1-93.

Baiyegunhi, C., Liu, K. and Gwavava, O. (2017): Geochemistry of sandstones and shales from the Ecca Group, Karoo Supergroup, in the Eastern Cape Province of South Africa: Implications for provenance, weathering and tectonic setting. Open Geosciences; 9:340-360.

Bastow, T. P., van Aarssen, B.K.G. and Lang D. (2007): Rapid small-scale separation of saturate, aromatic and polar components in petroleum. Organic Geochemistry; 38: 1235-1250.

Bau, M. and Alexander, B.W. (2009): Distribution of high field strength elements (Y, Zr, REE, Hf, Ta, Th, U) in adjacent magnetite and chert bands and in reference standards FeR-3 and FeR-4 from the Temagami iron-formation, Canada, and the redox level of the Neoarchean ocean. Precambrian Research; 174: 337-346.

Beygi, M. and Jalali, M. (2018): Background levels of some trace elements in calcareous soils of the Hamedan Province, Iran. Catena; 162: 303-316.

Bhatia, M.R. (1983): Plate tectonics and geochemical composition of sandstones. Journal of Geology; 92: 181-193.

Blanpied, C., Deynoux, M., Ghienne, J.F. and Rubino, J.L. (2000): Late Ordovician glacially related depositional systems of the Gargaf uplift (Libya) and comparison with correlative deposits in the Taoudeni Basin (Mauritania). In: M.A. Sola and D. Worsley (eds) Geological exploration in Murzuq Basin. Elsevier, Amsterdam; 485-507.

Bracciali, L., Marroni, M., Pandolfi, L. and Rocchi, S. (2007): Geochemistry and petrography of Western Tethys Cretaceous sedimentary covers (Corsica and Northern Apennines): From source area to configuration of margins, in Arribas, J., Critlli, S. and Johanson, M.J., (eds.), Sedimentary provenance and petrogenesis: Perspectives from petrography and geochemistry. Geological Society of America, Special Paper; 420: 73-93.

Brassell, S.C., Eglinton, G., Maxwell, J.R. and Philp, R.P. (1978): Natural background of alkanes in the aquatic environment. In: Hutzinger, L.H., van Lelyveld, O., Zoeteman, B.C.J. (Eds.). Pergamon, Oxford; 69-86.

Brooks, J.D., Gould, K. and Smith, J.W. (1969): Isoprenoid hydrocarbons in coal and petroleum. Nature; 222: 257-259.

Condie, K.C. (1991): Another look at rare earth elements in shales. Geochimica et Cosmochimica Acta; 55: 2527-2531.

Condie, K.C. (1993): Chemical composition and evolution of the upper continental crust: contrasting results from surface samples and shales. Chemical Geology; 104: 1-37.

Condie, K.C., Lee, D. and Farmer, G.L. (2001): Tectonic setting and provenance of the Neoproterozoic Uinta Mountain and Big Cottonwood groups, northern Utah: constraints from geochemistry, Nd isotopes and detrital modes. Sedimentary Geology; 141: 443-464.

Cox, R., Low, D.R. and Cullers, R.L. (1995): The influence of sediment recycling and basement composition on evolution of mudrock chemistry in the southwestern United States. Geochimica et Cosmochimica Acta; 59: 2919-2940.

Crook K.A.W. (1974): Lithogenesis and geotectonics: The significance of compositional variation in flysch arenites (greywackes). Society of Economical, Paleontological and Mineralogical Special Publications; 19: 304-310.

Cullers, R.L. (2000): The geochemistry of shales, siltstones, and sandstones of Pennsylvanian-Permian age, Colorado, USA: implication for provenance and metamorphic studies. Lithos; 51: 181-203.

Cullers, R.L., Barrett, T., Carlson, R. and Robinson, B. (1987): Rare earth element and mineralogic changes in Holocene soil and stream sediment: a case study in the Wet Mountains, Colorado, USA. Chemical Geology; 63: 275-297.

Cullers, R.L. and Podkovyrov, V.N. (2000): Geochemistry of the Mesoproterozoic Lakhanda shales in southeastern Yakutia, Russia: implications for mineralogical and provenance control, and recycling. Precambrian Research; 104(1-2): 77-93.

Dahl, B., Bojesen-Koefoed, J., Holm, A., Justwan, H., Rasmussen, E. and Thomsen, E. (2004): A new approach to interpreting Rock-Eval S and TOC data for kerogen quality assessment. Organic Geochemistry; 35(11–12): 1461-1477.

Davidson, L., Beswethherick, S., Craig, J. Eales, M., Fisher, A., Himmali, A., Jho, J., Mejrab, B. and Smart, J. (2000): The structure, stratigraphy and petroleum geology of the Murzuq Basin, southwest Libya. In: Geological Exploration in the Murzuq Basin (Eds. M.A. Sola and D. Worsley), Elsevier, Amsterdam; 295-320.

Deepender, B. and Siddharth, D. (2015): New insight on petroleum system modeling of Ghadames basin, Libya. Journal of African Earth Sciences; 112: 111-128.

Dembicki, H.J. (2009): Three common source rock evaluation errors made by geologists during prospect or play appraisals. AAPG Bulletin; 93(3): 341-356.

Deng, H.W. and Qian, K. (1993): Sedimentary geochemistry and environment analysis. Lanzhou: Gansu Science and Technology Press.

Didyk, B.M., Simoneit, B.R.T., Brassell, S.C. and Eglinton, G. (1978): Organic geochemical indicators of paleoenvironmental conditions of sedimentation. Nature; 272: 216-222.

Echikh, K. (1992): Geology and hydrocarbon potential of Ghadamis Basin. NOC Internal Report, Tripoli.

Echikh, K. and Sola, M.A. (2000): Geology and hydrocarbon occurrences in the Murzuq Basin, SW Libya. In: M.A. Sola and D. Worsley (eds) Geological exploration in Murzuq Basin. Elsevier, Amsterdam, p. 175-222.

Edwards, D.S., Struckmeyer, H.M., Bradshaw, M.T. and Skinner, J.E. (1999): Geochemical characteristics of Australia's southern margin petroleum systems. Australian Petroleum Production and Exploration Association (APPEA); 39: 297-321.

Eglinton, G. and Hamilton, R.G. (1967): Leaf epicuticular waxes. Science; 156: 1322-1344.

El Chair, M.M. (1984): Zur Hydrogelogy, Hydrochemie und Isotopenzusammensetzung der Grundwässer des Murzuq-Beckens, Fezzan/Libyen. Unpublished Dissertation Naturwissenschaften Fakultät Universität, Tübingen, Germany, 214 p.

El Diasty, W.S., El Beialy, S.Y., Anwari, T.A., Peters, K.E. and Batten, D.J. (2017): Organic geochemistry of the Silurian Tanezzuft Formation and crude oils, NC115

Concession, Murzuq Basin, southwest Libya. Marine and Petroleum Geology; 86: 367-385.

El Diasty, W.S. and Moldowan, J.M. (2012): Application of biological markers in the recognition of the geochemical characteristics of some crude oils from Abu Gharadig Basin, north Western Desert–Egypt. Marine and Petroleum Geology; 35:28-40.

El Hawat, A.S. and Rahuma, M.M. (2008): Short notes and guidebook on the geology of Al Qarqaf area and Ghadamis Basin. 4th Symposium on Geology of Southern Libya, Tripoli.

El-Kammar, M.M., Hussein, F.S. and Sherwani, G.H. (2015): Organic petrological and geochemical evaluation of Jurassic source rocks from north Iraq. Asian Review of Environmental and Earth Sciences; 2(1): 1-8.

El Nady, M.M., Ramadan, F.S., Hammad, M.M. and Lotfy, N.M. (2015): Evaluation of organic matters, hydrocarbon potential and thermal maturity of source rocks based on geochemical and statistical methods: Case study of source rocks in Ras Gharib oilfield, central Gulf of Suez, Egypt. Egyptian Journal of Petroleum; 24: 203-211.

Fedo, C.M., Nesbitt, H.W. and Young, G.M. (1995): Unraveling the effects of potassium metasomatism in sedimentary rocks and paleosols, with implications for paleoweathering conditions and provenance. Geology; 23: 921-924.

Floyd, P.A., Winchester, J.A. and Park, R.G. (1989): Geochemistry and tectonic setting of Lewisian clastic metasediments from the Early Proterozoic Loch Maree Group of Gairloch, N.W. Scotland. Precambrian Research; 45(1-3): 203-214.

Fulai, L., Xiyu, Q. and Li, L. (2009): Depositional environment in the Northern Nei Monggol in Linxi Formation of Upper Permian. Acta Sedimentologica Sinica; 27(2): 265-272.

Furst, M. and Klitzsch, E. (1963): Late Caledonian paleogeography of the Murzuq Basin. Revue de L' Institute Français du Pétrole; 18: 1472-1484.

Gao, G., Yang, S., Zhang, W., Wang, Y., Gang, W. and Lou, G. (2018): Organic geochemistry of the lacustrine shales from the Cretaceous Taizhou Formation in the Gaoyou Sag, Northern Jiangsu Basin. Marine and Petroleum Geology; 89(3): 594-603.

Ghassal, B.I., Littke, R., El Atfy, H., Sindern, S., Scholtysik, G., El Beialy, S. and El Khoriby, E. (2018): Source rock potential and depositional environment of Upper Cretaceous sedimentary rocks, Abu Gharadig Basin, Western Desert, Egypt: An integrated palynological, organic and inorganic geochemical study. International Journal of Coal Geology; 186: 14-40.

Ghori, K.A.R. (2002): Modeling the hydrocarbon generative history of the Officer Basin, Western Australia. Journal of Philosophy of Education Society of Australasia (PESA); 29: 29-42.

Goldberg, K. and Humayun, M. (2010): The applicability of the chemical index of alteration as a paleoclimatic indicator: An example from the Permian of the Parana Basin, Brazil. Palaeogeography, Palaeoclimatology, Palaeoecology; 293: 175-183.

Grantham, P.J. and Wakefield, L.L. (1988): Variations in the sterane carbon number distributions of the marine source rock derived oils through geological time. Organic Geochemistry; 12: 61-73.

Grunert, J. (1983): Relief Boden Palaoklima. Geomorphologie der Schichtstufen am Westrand des Murzuk-Beckens (Zentrale Sahara). Gebrüder Borntraeger. Berlin, 271 p.

Hakimi, M.H., Abdulah, W.H. and Shalaby, M.R. (2010): Organic geochemistry, burial history and hydrocarbon generation modelling of the Upper Jurassic Madbi Formation, Masila Basin, Yemen.
Journal of Petroleum Geology; 33 (4): 299-318.

Hall, L.S., Boreham, C.J., Edwards, D.S., Palu, T.J., Buckler, T., Hill, A.J. and Troup, A. (2016): Cooper Basin source rock geochemistry: Regional hydrocarbon prospectivity of the Cooper Basin. Geoscience Australia, Part2; 62p.

Hallett, D. (2002): Petroleum geology of Libya. Amsterdam, Elsevier Inc., 503 p.

Hallett, D. and Clark-Lowes, D. (2016): Petroleum Geology of Libya, second ed. Elsevier, Amsterdam; 392 p.

Hayashi, K., Fujisawa, H., Holland, H. and Ohmoto, H. (1997): Geochemistry of ~1.9 Ga sedimentary rocks from northeastern Labrador, Canada. Geochimica et Cosmochimica Acta; 61(19): 4115-4137.

Herron, M.M. (1988): Geochemical classification of terrigenous sandstone and shale from core and log data. Journal of Sedimentary Petrology; 5(8): 820-829.

Holba, A.G., Dzoub, L.I., Wood, G.D., Ellisd, L., Adame, P., Schaeffere, P., Albrechte, P., Greenef, T. and Hughes, W.B. (2003): Application of tetracyclic polyprenoids as indicators of input from fresh-brackish water environments. Organic Geochemistry; 34: 441-469.
Huang, W.Y. and Meinschein, W.G. (1979): Sterols as ecological indicators. Geochimica et Cosmochimica Acta; 43: 739-745.

Hunt, J.M. (1996): Petroleum geochemistry and geology, 2nd edition, vol. 743. New York: Freeman and Company.

Jones, B. and Manning, D.C. (1994): Comparison of geochemical indices used for the interpretation of paleo-redox conditions in Ancient mudstones: Chemical Geology; 111(1-4): 111-129.

Jun, L., Bo, H., Shougang, L. and Jia, L. (2015): Langgu sag Sha 3 member and Sha4 member sedimentary environment analysis. IOSR Journal of Engineering; 5: 5-10.

Kimura, H. and Watanabe, Y. (2001): Oceanic anoxia at the Precambrian-Cambrian boundary. Geology; 29: 995-998.

Klitzsch, E. (1970): Die Strukturgeschichte der Zentralsahara. Neue Erkenntnisse zum Bau und zur Paläogeographie eins Taffellands. Geologische Rundschau; 59: 459-527.

Klitzsch, E. (2000): The structural development of the Murzuq and Kufra basins significance for oil and mineral exploration. In: Geological Exploration in the Murzuq Basin (Eds. M.A. Sola and D. Worsley), Elsevier, Amsterdam; 143-150.

Lecompte, B., Hursan, G. and Hughes, B. (2010): Quantifying source rock maturity from logs. How to get more than TOC from Delta Log R. SPE Annual Technical Conference and Exhibition, Florence, Italy; 19-22.

Lindsey, D.A. (1999): An evaluation of alternative chemical classifications of sandstones. USGS Open File Report, 23p.

Longford, F.F. and Blanc-Valleron, M.M. (1990): Interpreting Rock–Eval pyrolysis data using graphs of pyrolyzable hydrocarbons vs. total organic carbon, AAPG Bulletin; 74: 799-804.

Luning, S. and Kolonic, S. (2003): Uranium spectral gamma-ray response as a proxy for organic richness in black shales: Applicability and limitations. Journal of Petroleum Geology; 2: 153-174.

Makky, A.F., El Sayed, M.I., Abu El-Ata, A.S., Abd El-Gaied, I.M., Abdel-Fattah, M.I. and Abd-Allah, Z.M. (2014): Source rock evaluation of some Upper and Lower Cretaceous sequences, West Beni Suef Concession, Western Desert, Egypt. Egyptian Journal of Petroleum; 23: 135-149.

Mamgain (1980): The pre-Mesozoic (Precambrian to Palaeozoic) stratigraphy of Libya-A reappraisal. Industrial Research Centre, Department of Geological Researches and Mining, Tripoli, 104 p.

McCann, T. (1991): Petrological and geochemical determination of provenance in the southern Welsh Basin. In: A. C. Morton, S. P., Todd and P. D. W. Haughton (Editors), Developments in Sedimentary Provenance. Geological Society Special Publication: 57: 215-230.

McDougall, N., Quin, J.G., Vila Pont, J. and Tawengi, K. (2005): Sedimentology, sequence stratigraphy and large-scale architecture of the Upper Ordovician Mamuniyat and Melaz Shugran formations based on outcrop studies of the Gargaf area. Repsol Exploration Libya Finding Team, Madrid. Confidential Repsol Report, 95 p.

McLennan, S.M., Hemming, S., McDaniel, D.K. and Hanson, G.N. (1993): Geochemical approaches to sedimentation, provenance and tectonics. In: M.J. Johnson and A. Basu, (Eds.), Processes Controlling the Composition of Clastic Sediments. Geological Society of American Special Paper; 32, 21-40.

Miles, N.H. (2001): A palynological correlation of the Palaeozoic. Robertson Research International. Confidential ROO Report No. 6204/lb. 95 p.

Morgan, J.W. and Heier, K.S. (1966): Uranium, thorium and potassium in six U.S.G.S. standard rocks. Earth and Planetary Science Letters; 1: 158-160.

Murray, A.P. and Boreham, C.J. (1992): Organic geochemistry in petroleum exploration. Australian
Geological Survey Organization, Canberra; 230 p.
Nagarajan, R.; Madhavaraju, J.; Nagendra, R.; Armstrong-Altrin, J.S. and Moutte, J. (2007): Geochemistry of Neoproterozoic shales of the Rabanpalli Formation, Bhima Basin, Northern Karnataka, southern India: implications for provenance and paleoredox conditions. Revista Mexicana de Ciencias Geologicas; 24 (2): 150-160.

Nath, B.N., Bau, M., Ramlingeswara-Rao, B. and Rao, C.M., (1997): Trace and rare earth elemental variation in Arabian Sea sediments through a transect across the oxygen minimum zone. Geochimica et CosmochimicaActa; 61: 2375-2388.

Nesbitt, H.W., Fedo, C.M. and Young, G.M. (1997): Quartz and feldspar stability, steady and non-steady state weathering and petrogenesis of siliciclastic sands and muds. Journal of Geology; 105: 173-191.

Nesbitt, H.W. and Young, G.M. (1982): Early Proterozoic climates and plate motions inferred from major element chemistry of lutites. Nature; 299: 715-717.

Nesbitt, H.W. and Young, G.M. (1984): Prediction of some weathering trends of plutonic and volcanic rocks based upon thermodynamic and kinetic consideration. Geochimica et Cosmochimica Acta; 48: 1523-1534.

Nesbitt, H.W. and Young, G.M. (1996): Petrogenesis of sediments in the absence of chemical weathering: effects of abrasion and sorting on bulk composition and mineralogy. Sedimentology; 43: 341-358.

Obaje, N.G., Wehner, H., Scheeder, G., Abubakar, M.B., and Jauro, A. (2004): Hydrocarbon prospectively of Nigeria’s inland basins: organic geochemistry and organic petrology. American Association of Petroleum Geologists Bulletin; 88(3): 325-353.

Pachur, H.J. and Altmann, N. (2006): Die Ostsahara im Spätquartär. Ökosystemwande im größten hyperariden Raum der Erde (German Edition) Springer Verlag, 662 p.

Peters, K.E. and Cassa, M.R. (1994): Applied source rock geochemistry. In: Magoon, L.B., Dow, W.G.
(Eds.): The petroleum system from source to trap. AAPG Memorial Guidelines; 60: 93-117.

Peters, K.E. and Moldowan, J.M. (1993): The biomarker guide: Interpreting molecular fossils in petroleum and ancient sediments. Prentice-Hall, Inc, Englewood Cliffs, New Jersey.

Peters, K.E., Walters, C.C. and Moldowan, J.M. (2005): The biomarker guide: Biomarkers and isotopes in petroleum exploration and Earth history. 2nd edition, vol. 2. Cambridge University Press, Cambridge.

Pettijohn, F.J., Potter, P.E. and Siever, R. (1972): Sand and Sandstone. Plate motions inferred from major element chemistry of lutites. Precam-brian Research; 147: 124-147.

Rimmer, S.M. (2004): Geochemical paleoredox indicators in Devonian-Mississippian black shales, Central Appalachian Basin (USA). Chemistry Geology; 206: 373-391.

Roser, B.P. and Korsch, R.J. (1986): Determination of tectonic setting of sandstone-mudstone suites using SiO_2 content and K_2O/Na_2O ratio. Journal of Geology; 94: 635-650.

Rusk, D.C. (2001): Libya: petroleum potential of the underexplored basin centersda twenty-first-century challenge. In: Downey, M.W., Threet, J.C., Morgan, W.A. (Eds.), Petroleum Provinces of the Twenty-first Century. American Association of Petroleum Geologists Memoir; 74: 429-452.

Seidl, J.K. and Rohlich, P. (1984): Geological Map of Libya, 1:250000, Sheet: Sabha, NG 32-2, Explanatory Booklet. Industrial Research Centre, Tripoli-Libya, 149 p.

Shalbak, F.A. (2015): Palaeozoic petroleum systems of the Murzuq Basin, Libya. Unpublished PhD Thesis, Barcelona University, Spain.

Shaltami, O.R., Fares, F.F. and Bustany, I. (2016): Geochemistry of Mamuniyat Formation, Idri area, SW Libya. 11th International Conference and Meeting on Geology, Institute of Geosciences, University of Campinas, Brazil, Proceeding Book; pp. 88-102.

Shaltami, O.R., Fares, F.F., Elojaly, R.B., Scrimin, P.M., Maggini, M., Fabris, L. and Errishi, H. (2017): Geochemical evaluation of the Tanezzuft Formation at Murzuq Basin, SW Libya. Oil and Gas Chemistry, Perm, Russia, Proceeding Book; pp. 33-51.

Shaltami, O.R., Fares, F.F., EL Oshebi, F.M., Errishi, H., Bustany, I. and Musa, M.M. (2018): Depositional environment and absolute age of the Pliocene-early Pleistocene sediments in the Cyrenaica Basin, NE Libya. 16th Annual Conference on Isotope Geology (ACIG-16), Department of Geosciences and Natural Resource Management Faculty of Science University of Copenhagen Denmark, Proceeding Book; pp. 67-83.

Shanmugam, G. (1985): Significance of coniferous rain forests and related organic matter in generating commercial quantities of oil, Gippsland Basin, Australia. American Association of Petroleum Geologists Bulletin; 69: 1241-1254.

Singh, K.P. (2005): Non-linear estimation of aquifer parameters from surficial resistivity measurements. Hydrology and Earth System Sciences Discuss; 2: 917-938.

Spirakis, C.S. (1996): The roles of organic matter in the formation of uranium deposits in sedimentary rocks. Ore Geology Reviews; 11(1-3): 53-69.

Sun, S., Schefub E., Mulitza, S., Chiessi, C.M., Sawakuchi, A.O., Zabel, M. Baker, P.A., Hefter, J. and Mollenhauer, G. (2016): Origin and processing of terrestrial organic carbon in the Amazon system: lignin phenols in river, shelf and fan sediments. Biogeosciences Discuss., doi:10.5194/bg-2016-468.

Suttner, L.J. and Dutta, P.K. (1986): Alluvial sandstone composition and paleoclimate. Framework mineralogy. Journal of Sedimentary Petrology; 56: 326-345.

Taylor, S.R. and McLennan, S.M. (1985): The continental crust: Its composition and evolution. Blackwell Scientific Publications; 312 p.

Thiedig, F.M., Oezen, D., El-Chair, M. and Geyh, M.A. (2000): The absolute age of the Quaternary lacustrine limestone of the Al Mahruqah Formation-Murzuq Basin, Libya. In: Geological Exploration in Murzuq Basin (Eds. M.A. Sola, and D. Worsley), Elsevier Science, Amsterdam; 89-16.

Toulkeridis, T., Clauer, N., Kröner, A., Reimer, T. and Todt, W. (1999): Characterization, provenance, and tectonic setting of Fig Tree greywackes from the Archaen Barberton Greenstone Belt, South Africa. Sedimentary Geology; 124: 113-129.

Van Krevelen, D.W. (1961): Coal: typology-chemistry-physics-constitution: Elsevier Science, Amsterdam; 514 p.

Volkman, J.K. (1986): A review of sterol biomarkers for marine and terrigenous organic matter. Organic Geochemistry; 9: 83-89.

Wei, G.J., Liu, Y., Li, X.H., Shao, L. and Fang, D. (2004): Major and trace element variations of the sediments at ODP Site 1144, South China Sea, during the last 230ka and their paleoclimate implications. Palaeogeography, Palaeoclimatology, Palaeoecology; 212: 331-342.

Wood, D.A. (1980): The application of the Th-Hf-Ta diagram to problems of tectonomagmatic classification and establishing the nature of crustal contamination of Basaltic Lava of the British Tertiary Volcanic Province. Earth and Planetary Science; Letters: 50: 11-30.

Wronkiewicz, D.J. and Condie, K.C. (1987): Geochemistry of Archean shales from the Witwatersrand Supergroup, South Africa: source-area weathering and provenance. Geochim. Cosmochim. Acta; 51: 2401-2416.

Wronkiewicz, D.J. and Condie, K.C. (1990): Geochemistry and mineralogy of sediments from the Ventersdorp and Transvaal Supergroups, South Africa: cratonic evolution during the early Proterozoic. Geochimica et Cosmochimica Acta; 54: 343-354.

Yan, Y., Xia, B., Lin, G., Cui, X., Hu, X., Yan, P. and Zhang, F. (2007): Geochemistry of the sedimentary rocks from the Nanxiong Basin, South China and implications for provenance, paleoenvironment and paleoclimate at the K/T boundary. Sedimentary Geology; 197: 127-140.

Yandoka, B.M.S., Abdullah, W.H., Abubakar, M.B., Hakimi, M.H. and Adegoke, A.K. (2015): Geochemical characterisation of Early Cretaceous lacustrine sediments of Bima Formation, Yola Sub-basin, Northern Benue Trough, NE Nigeria: Organic matter input, preservation, paleoenvironment and
palaeoclimatic conditions. Marine and Petroleum Geology; 61: 82-94.

Yao, C., Guo, W., Liu, J. and Li, H. (2017): Multiple proxies on the paleoenvironment of the Early Cambrian marine black rock series in the Tarim Basin, NW China: Molybdenum isotope and trace element evidence. International Journal of Geosciences; 8: 965-983.

التقييم الجيوكيميائي لتكوين بئر تلاسين في منطقة غات ،حوض مرزق ،جنوب غرب ليبيا

اعداد

يوسف مفتاح بوخريص

المشرف

اسامة رحيل الشلطامي

الملخص

الهدف من هذه الدراسة هو التقييم الجيوكيميائي لتشكيل بير تلاكسين في منطقة غات ، جنوب ليبيا. يشمل هذا التقييم البيئة الترسيبية ، والأكسجين القديم ، والمناخ القديم ، والقدرات القديمة ، والأصل ، والوضع التكتوني ، وثراء المواد العضوية ، ونوع الكيروجين والنضج الحراري. شملت الرحلات الميدانية خمسة أقسام سطحية لتشكيل (وادي مجيدات ووادي تساح ووادي عنلاك ووادي إيجيتين ووادي أوزرق). يتكون هذا التكوين من الحجر الرملي ووحدات الصخر الزيتي. الحجر الرملي هي أساسا greywackes. المعادن الطينية المرصودة في الصخور المدروسة هي السميكتايت ، والكاولينايت ، و gibbsite ، والكلوريت. هذه المعادن هي الناقل الرئيسي ل TOC. تشير نسب Th / Cr و Th / Sc و Th / Co ومخططات التمييز في المنشأ إلى أن الصخور (الجرانيتية) الموجودة في جبال إير ، في وسط النيجر ، قد تكون المصدر المحتمل لتكوين Bir Tlacsin. استناداً إلى قيم ICV ، تكون الصخور غير ناضجة حرارياً في حين أن الأحجار الرملية هي ناضجة حرارياً حتى تنضج. علاوة على ذلك ، أظهرت البيانات الجيوكيميائية العضوية أن المادة العضوية غير ناضجة حراريا. المادة العضوية هي أساسا من أصل بحري. تشير نسب Zr / Hf و Hf / Ta و Zr / Ta و B / Ga إلى أن تكوين Bir Tlacsin قد تم ترسيبه في بيئة بحرية عالية الملوحة. استناداً إلى عنصر التتبع ، نسب Pr / Ph، Pr / n-C17 و Ph / n-C18 كانت الظروف الأكسجين السائدة أثناء الترسب. كانت البيئة القديمة السائدة في منطقة المصدر شبه شبه قاحلة وشبه رطبة. البيئة التكتونية هي في الأساس قارية (الهامش القاري النشط (C)

والهامش القاري السلبي (D)). عموما ، الصخور هي الصخور مصدر جيد. أظهرت مخططات التمييز أن النوع الثاني من الكيروجين هو النوع الأساسي في عينات الصخر الزيتي. يتم هيدروكربون بشكل رئيسي (غير أصلي).

التقييم الجيوكيميائي لتكوين بئر تلاسين في منطقة غات ،حوض مرزق ،جنوب غرب ليبيا

قدمت من قبل:

يوسف مفتاح بوخريص العشيبي

تحت اشراف :

د.اسامة رحيل الشلطامي

قدمت هده الرسالة استكمالا لمتطلبات الحصول علي درجة الماجستير في الجيولوجيا

جامعة بنغازي

كلية العلوم

مايو 2018